UNIVERSITÉ DU QUÉBEC

THÈSE
PRÉSENTÉE À
L'UNIVERSITÉ DU QUÉBEC À CHICOUTIMI

POUR L'OBTENTION
DU DOCTORAT RESSOURCES MINÉRALES

PAR

DIJIANG GUO

CARACTÉRISTIQUES STRUCTURALES DE LA ZONE DE CISAILLEMENT DE WULONG ET DE LA MINÉRALISATION RELATIVE D'OR DANS LE CAMP D'OR DE WULONG, PROVINCE DU SUD-EST DE LIAONING, CHINE

JUILLET 18, 2001

Bibliothèque
Paul-Émile-Boulet

UQAC
Université du Québec
à Chicoutimi

Mise en garde/Advice

Afin de rendre accessible au plus grand nombre le résultat des travaux de recherche menés par ses étudiants gradués et dans l'esprit des règles qui régissent le dépôt et la diffusion des mémoires et thèses produits dans cette Institution, **l'Université du Québec à Chicoutimi (UQAC)** est fière de rendre accessible une version complète et gratuite de cette œuvre.

Motivated by a desire to make the results of its graduate students' research accessible to all, and in accordance with the rules governing the acceptation and diffusion of dissertations and theses in this Institution, the **Université du Québec à Chicoutimi (UQAC)** is proud to make a complete version of this work available at no cost to the reader.

L'auteur conserve néanmoins la propriété du droit d'auteur qui protège ce mémoire ou cette thèse. Ni le mémoire ou la thèse ni des extraits substantiels de ceux-ci ne peuvent être imprimés ou autrement reproduits sans son autorisation.

The author retains ownership of the copyright of this dissertation or thesis. Neither the dissertation or thesis, nor substantial extracts from it, may be printed or otherwise reproduced without the author's permission.

Résumé

La zone de cisaillement de Wulong est principalement formée de failles parallèles à pendage NNE, elle traverse différents types de roches allant de gneiss du protérozoïque inférieur à des sédiments du Mésozoïque supérieur. Cette zone présente différents types de déformations traversant plusieurs variétés de roches hôtes. Le camp aurifère de Wulong est contrôlé structurellement par la zone de cisaillement de même nom. Elle est localisée près de la ville de Dandong, au sud-est de la Province de Liaoning, Chine. Le camp aurifère comporte trois mines: les mines d'or de Wulong et Sidaogou et la mine de cuivre-or de Jielishu.

Dans la région de la mine Wulong, la zone de cisaillement s'est développée dans des gneiss archéens supérieurs. La déformation ductile est soulignée par des grains de quarts allongés, des gains de micas en forme de « poissons » et des zones de pressions. La mesure des contraintes indique que le cisaillement de la région de la mine Wulong est de type ellipsoïdal. Les mesures paléopiézométriques donnent des valeurs de contraintes différentielles variant de 81.5 MPa à 144.6 MPa dans la mine Wulong et un taux de contrainte allant de 9.428×10^{-23} à 4.284×10^{-21} sec^{-1}.

Dans la mine d'or de Sidaogou, la zone de cisaillement Wulong s'est développée durant le Protérozoïque inférieur dans les grès métamorphisés du groupe Liaohe. La zonation des tectoniques n'y est pas bien développée. Les structures de déformations ductiles développées dans cette région inclues des foliations mylonitiques, des linéations de glissement, des plis, des lentilles et des boudinages intrafoliés. Les mesures de contraintes (finies) suggèrent une déformation proche de celle d'un ellipsoïde de contraintes normales. Les mesures de pression différentielle dans la région de la mine Sidaogou sont de 71.5 MPa, correspondant à un taux de contrainte de $4.026 * 10^{-23} sec^{-1}$.

Dans la région de la mine Jielishu, La zone de cisaillement Wulong traverse le groupe de marbre Liaohe datant du Protérozoïque moyen et du Protérozoïque supérieur. Les marbres mylonitiques et les lentilles sont tous deux biens développés dans cette zone de cisaillement. Les mesures des contraintes finies donnent une valeur de 1.03 au paramètre de Flinn (k). Dans l'intrusion de Sanguliu, la valeur paléopiézométriques obtenue est faible, de l'ordre de 61,1 MPa, elle correspond à un taux de contrainte de $1.449 * 10^{-23} sec^{-1}$.

Indépendamment des emplacements structuraux choisis dans la zone de cisaillement de Wulong, les critères de cisaillement, que ce soit à l'échelle macroscopique ou microscopique indiquent un mouvement senestre. Le calcul du bilan de masse montre que les gains et pertes de masse dépendent du type des roches hôtes et les variations suggèrent que d'intenses réactions eau/roche aient eu lieu durant la phase de migration des fluides dans la zone de cisaillement.

Les âges chronologiques donnés par les isotopes et les fossiles indiquent que l'évolution de la zone de cisaillement Wulong s'est étendue sur une longue période de temps, elle aurait débutée vers 156 Ma et était encore active vers 73 Ma.

Chaque dépôt du camp aurifère de Wulong montre des caractéristiques géologiques et minéralogiques différentes en fonction des différentes roches hôtes et des structures particulières à chacune des mines.

Le gisement aurifère de Wulong, situé dans des gneiss granitiques, est composé d'une série de filons de quartz aurifères ayant un pendage NE-E. Ces filons sont exclusivement situés dans les gneiss. La minéralisation est composée de pyrite, pyrrhotine, chalcopyrite, arsénopyrite, bismuthinite, de galène en quantité mineure, de sphalérite et d'or natif. L'or se retrouve principalement dans le quart, la bismuthinite, la pyrite et la pyrrhotine. Les analyses des éléments traces et mineurs des minéraux porteurs de l'or et, de quartz de différentes générations indiquent que le quartz formé lors du second épisode dans le dépôt de Wulong, l'ont été sous un rapport élevé Au/Ag. En général, les minéraux associés à une minéralisation aurifère ont un rapport Au/Ag élevé.

Le gisement d'or de Sidaogou se retrouve dans des métagrès. L'assemblage minéralogique retrouvé est simple. La pyrite représente 95% des sulfures et est accompagnée de chalcopyrite et pyrrhotine en faible quantité. La pyrite est le principal minerais hôte de l'or, le quartz en est le second. À la différence du dépôt de Wulong, l'or natif de la minéralisation de Sidaogou a un rapport Ag/Au élevé.

Dans la mine de Jielishu, l'or et le cuivre sont économiquement valables. Le dépôt est situé dans un marbre. Les sulfures observés dans le dépôt de Jeilishu sont : pyrite, chalcopyrite, chalcocite, malachite et en faible quantité de la sphalérite et de la galène. De l'or natif y est fréquemment observé dans la chalcopyrite et la pyrite. Le dépôt de cuivre-or de Jielishu est caractérisé par des cavités (vacuoles) développées dans la zone minéralisée. Cette structure n'est pas observée dan les deux autres dépôts. La concentration en or a une relation directe avec la valeur de Bi dans ces dépôts.

Diverses techniques géochimiques ont été appliquées à ces trois dépôts. Les signatures des « REE » suggèrent que les minéralisations développées dans le camp aurifère de Wulong aient des sources similaires. Les isotopes de plomb indiquent que les minéraux associés à la minéralisation proviennent de la croûte supérieure. Les isotopes de souffre de la minéralisation souligne une origine probablement magmatique des sulfures (+1.55‰~+2.5‰), par contre les réactions roches/fluides contribuent à un accroissement de la quantité des sulfures minéralisés dans le dépôt de Sidaogou (environ +11.33‰). L'analyse des isotopes d'hydrogène et d'oxygène ne donnent aucune information additionnelle au sujet des fluides minéralisateurs pourtant la compilation des données montre des valeurs se situant à l'extérieur des domaines définis par les fluides « sources ». Cependant, les isotopes de carbone provenant des veines de calcite suggèrent une source de carbone magmatique (-5.51‰~-1.21‰).

Les études des inclusions fluides révèlent que, dans le fluide minéralisateur, l'ébullition est un phénomène omniprésent dans les dépôts aurifères de Wulong et Sidaogou. Le dépôt de Wulong montre des températures homogènes beaucoup plus élevées (T=360 °C) que celles du dépôt de Sidaogou (T=175 °C). Une seule mesure microthermométrique a été effectuée dans le dépôt de Jielishu, donnant une valeur de 108 °C.

Les résultats de l'étude des inclusions fluides indiquent également que la minéralisation en or a une salinité faible de l'ordre de 2,4 % à 6.1 % poids NaCl (équivalent). Les pressions moyennes des fluides capturés sont de l'ordre de 65 MPa dans le dépôt aurifère de Wulong et de 51 MPa dans celui de Sidaogou. La composition

moyenne des fluides extrait des inclusions indique que les fluides contiennent généralement du CO_2, CH_4, CO, N_2, H_2 sous forme gazeuse, Na^+, K^+ sous forme de cations et des anions F^-, Cl^-, $SO4^{2-}$. Les fluides du dépôt de Sidaogou contiennent visiblement plus de Ca^{2+} que le dépôt de Wulong.

Une des caractéristiques omniprésentes du camp aurifère de Wulong est la relation spatiale et temporelle entre les filons aurifères de quartz et les différents dykes. Les signatures des « REE », du rapport isotopique K-Ar, des éléments traces de la minéralisation, des roches hôtes et des différents dykes suggèrent que les dykes et la minéralisation soient probablement issus du même « matériel source » ou de processus géologiques identiques, ils ont aussi des âges géologiques similaires.

En se basant sur les caractéristiques géologiques et géochimiques de ces trois dépôts aurifères, l'auteur propose que ceux-ci aient été contrôlés par la structure de la zone de cisaillement de Wulong, et que la minéralisation d'or est génétiquement reliée avec l'intrusion de Sanguliu. Une modélisation de la mise en place, de la minéralisation aurifère et de l'intrusion magmatique; et de la formation de la zone de cisaillement de Wulong est proposée.

Abstract

The Wulong shear zone is composed of approximately parallel NNE striking faults and it traverses different rock types, varying from early Proterozoic gneiss to late Mesozoic sediments. The shear zone demonstrates different deformation features in different host rocks. The Wulong gold camp, structurally controlled by the Wulong shear zone, is located near the Dandong City, southeastern Liaoning province, China. This gold camp is composed of three gold mines: the Wulong gold mine, the Sidaogou gold mine and the Jielishu gold-copper mine.

In the Wulong mine area, the Wulong shear zone is developed in late Archean gneiss. Ductile deformation is demonstrated by elongated quartz grains, mica-fish and pressure shadow. Finite strain measurement indicates that the shear is flattened ellipsoid type in the Wulong mine area. Paleopiezometer measurements indicate that differential stress in shear zone ranges from 81.5 MPa to 144.6 MPa in the Wulong mine, and strain rates vary from $9.428x10^{-23}$ to $4.284x10^{-21}$ sec^{-1}.

In the Sidaogou gold mine, The Wulong shear zone is developed in the early Proterozoic Liaohe group metamorphosed sandstone rocks. Zonation of tectonites is not well developed in this area. Ductile deformation structures developed in the Sidaogou area include mylonite foliation, gliding lineation, intrafolial folds, lenses and boudinages. Finite strain measurements suggest that deformation type is near plain-strain ellipsoid, differential stress measured in Sidaogou mine area is 71.5 MPa, corresponding to a strain rate of $4.026*10^{-23}sec^{-1}$.

The Wulong shear zone is distributed in middle to late Proterozoic Liaohe group marble in the Jielishu mine area. Both marble mylonites and lenses are well developed in the shear zone. Finite strain measurements indicate that the Flinn parameter (k) is 1.03. A low paleopiezometer value (61.1Mpa) was obtained in mylonite developed in the Sanguliu intrusion and corresponding strain rate is $1.449*10^{-23}sec^{-1}$.

Regardless of the structural locations selected in the Wulong shear zone, all macroscale and microscale shear criteria indicate a sinistral movement of the shear zone. Mass balance calculations indicate mass gains and losses occurring in the shear zone were dependent on types of host rocks and these variations suggest that intense water/rock reactions took place during fluid migration in the shear zone.

Isotopic and fossil chronological ages indicate that evolution of the Wulong shear zone experienced a long geological history. The shear zone was probably initiated at 156 Ma, and it was still active at as late as 73 Ma.

Each deposit in the Wulong gold camp shows different geological and mineralogical characteristics because of the different host rocks and structural features in individual mine.

The Wulong gold deposit, hosted in granitic gneiss, is composed of a series of NEE striking auriferous quartz lodes. These lodes are exclusively hosted in gneiss. Predominant ore minerals include pyrite, pyrrhotite, chalcopyrite, arsenopyrite, bismuthinite and minor galena, sphalerite as well as free gold. Quartz, bismuthinite, pyrite, pyrrhotite are the main gold-bearing minerals. Trace and minor element analyses of gold-bearing minerals and

different generation of quartz indicate that quartz formed at second stage generally has high Au/Ag ratios in the Wulong deposit. Gold-bearing minerals generally have high Au/Ag ratios.

The Sidaogou gold deposit is hosted by metasandstone. Mineral assemblages are quite simple. Pyrite accounts for 95% of total sulfides in ores with minor chalcopyrite and pyrrhotite. Pyrite is the predominant gold-bearing mineral and quartz takes the second place in the Sidaogou gold deposit. Unlike the Wulong deposit, free gold in Sidaogou deposit has high Ag/Au ratios.

In the Jielishu mine, both gold and copper are economically valuable. The deposit is hosted in marble. Observed sulfides in the Jielishu deposit include pyrite, chalcopyrite, chalcocite, malachite and minor sphalerite and galena. Free gold was frequently observed in chalcopyrite and pyrite. The Jielishu gold-copper deposit is characterized by vug structure developed in ore bodies, which was not observed in the other two deposits. Au contents have intimate relationships with Bi contents in these deposits,

Various geochemical techniques were applied to the three gold deposits. REE signatures suggest that ores developed in the Wulong gold camp have similar sources. Pb isotope data indicate that the ore materials were obtained from upper crust. Sulfur isotope data of ores suggest that sulfur was probably of magmatic origin (+1.55‰~+2.5‰), but host rock/fluid reactions contributed additional sulfur to ores of the Sidaogou deposit (+11.33‰). H, O isotope data of ores did not give much useful information about the source of ore-bearing fluids since plots of ores fall outside of the origin-known fluid source domains. However, carbon isotope data from calcite veins suggest magmatic carbon source (-5.51‰~-1.21‰).

Fluid inclusion studies revealed that in ore-bearing fluids, boiling is a ubiquitous phenomenon in the Wulong and Sidaogou gold deposits. The Wulong deposit has much higher homogeneous temperature (Th=360 °C) than that of the Sidaogou deposit (Th =175 °C). Only one Th datum was measured in the Jielishu deposit, which is 108 °C.

Fluid inclusion study results also indicate that gold-bearing ores have low salinity values ranging from 2.4 wt.% NaCl to 6.1 wt% NaCl (equiv.). Estimated average entrapment pressures of fluids is 65 MPa in the Wulong gold deposit and 51 MPa in the Sidaogou deposit. Bulk composition analysis of fluids extracted from fluid inclusions indicate that fluids generally contain CO_2, CH_4, CO, N_2, H_2 gaseous components, Na^+, K^+ cations and F^-, Cl^-, $SO4^{2-}$ anions. Fluids in the Sidaogou deposit contain obviously higher Ca^{2+} contents than that of the Wulong gold deposit.

One of the ubiquitous features in the Wulong gold camp is the intimate spatial and temporal relationships of auriferous quartz lodes and various dykes. Signatures from REE, K-Ar isotope and trace elements of ores, host rocks and various dykes suggest that dykes and ores were probably from the same material source or experienced similar geological processes, and they have similar geological ages.

Based on geological and geochemical features in the three gold deposits, the author proposes that the three gold deposits are structurally controlled by the Wulong shear zone. and the gold deposit is genetically related with the Sanguliu intrusion and a descriptive model of gold mineralization, magmatic intrusion and the Wulong shear zone is proposed.

Acknowledgements

I would like to thank Professor Huanzhang Lu who accepts me as his Ph D. student that I have pursued and dreamed about for many years. I also would like to thank the committee members of my graduate program—Professor Guy Archambault and Professor Jayanta Guha for their direction during my graduate study at Université du Québec à Chicoutimi. Professor Guha's fruitful suggestions and critical comments make this thesis in a more logical organization. Professor Archambault's patient proof reading of the first draft and comments on chapter three.

I gratefully acknowledge the financial assistance from NSRNC and FUQAC (to professor Lu) and the Society of Economic Geologists (USA) for the graduate research grants (for Dijiang Guo, 1999, 2000). Without these financial supports, my graduate study would have been impossible. Same kind of thanks also go to the Chinese National Natural Science Foundation (to professor Lu) for financial assistance during my field work in the Wulong gold camp, China.

Warm and unsolicited thanks go to Mr. Chunfu Yang, a geologist of the Geological Survey of the Wulong Gold Mine, for his generous help during my field work in the Wulong gold camp and his assistance to access unpublished data and samples of the mine. I also benefited from discussion with Mr. Junhao Wei, an assistant professor at China university of Geoscience, during my field work. Mr. Liu, a technician at the laboratory of the Yichang Institute of Geology, Chinese Academy of Earth Science, helped to prepare all the thin sections. Chemical and isotope analyses were also conducted in this institute. Mr. Denis Cote helped me to access the photographic equipments at the laboratory of science de la terre, UQAC. I want to thank my dear friend and also my classmate, here in UQAC, Mr. Tangfu Xiao for his kind and prompt help to print my thesis when I was in difficult situation, without his generous help, my thesis would probably have been postponed.

I am particularly indebted to my wife, Ms. Xiaohong Hou; it was she who had taken care of me during my busiest days in thesis writing, although she was pregnant then. Her encouragement made me to focus my mind on my thesis when I was in financial difficulty.

Finally, thanks go to my little son, Eric Guo, his coming to this family brings us great enjoyment and new inspiration when I was writing my thesis.

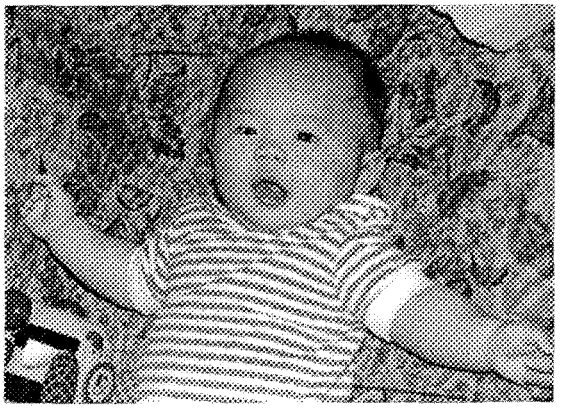

(Eric Guo, at his 100 days in Montreal)

TABLE OF CONTENTS

List of figures

List of table:

List of Plates:

Chapter I

Introduction

Shear zones have long been recognized as important precipitating sites of economically valuable deposits of Au, Ag, Pb, Zn, Cu, U etc., (McKinstry 1948). Shear zone hosted gold deposits are also commonly referred to as "mesothermal gold deposits", "greenstone gold deposits" or "lode gold deposits" (Roberts, 1987). This type of gold deposits accounts for a large proportion of the world's gold production.

Shear zone, in the early stage of structural geological study, was termed as "breaks" in geological literatures to denote the conjunction of gradients in lithology, strain intensity, magmatism, and metamorphic grade (e.g. Gunning and Ambrose 1937). Many of the shear zone structures are considered to have been pre-existed mineralization, subsequently acting as conduits for upward migrating fluids, or to have been responsible for tectonically "remobilizing" a pre-existing ore deposit. Recently the significance of shear zone structures on the formation of gold deposits and geodynamic environments of such structural systems has been increasingly emphasized (Sibson et al., 1988, Kerrich and Wyman 1990, Groves 1993).

Numerous researchers have documented that shear zone hosted gold-bearing quartz vein systems of all ages, from Archean to Cenozoic, are characterized by similar geodynamic environments, local structure features, mineral paragenesis, metal budgets, P-

T-t paths, geochemistry, fluid dynamics and isotopic properties, which collectively imply a singular hydrothermal process. The features of deformation, magmatism, regional metamorphism and uplift indicate that gold-bearing shear zone systems are defined in accretionary boundaries such as closure of back-arc basins and arc-continent or continent-continent collisions (Kerrich, 1989). Examples of such gold-bearing shear zone systems include the Abitibi gold camp, Quebec, Canada (Archean); the Norseman Wiluna belt, Yilgarn block Western Australia (Archean); Kolar schist belt, India (Archean); Foothills Metamorphic belt, California, USA (Mesozoic) (Kerrich 1989), the Alaska Cordillera, USA (Mesozoic) (Goldfarb et al., 1986) and the Cenozoic Monte Rosa district, Western Italian Alps (Curti, 1987).

Though greenschist facies is a ubiquitous metamorphic facies related to gold-bearing shear zone system, geologists realized that gold-bearing shear zone system may also occur in intermediate to high grade metamorphic facies such as amphibolite facies or lower granulite facies and even in sub-greenschist facies metamorphic rocks (Burlinson 1991). Based on these evidences, Groves (1993) proposed a crustal continuum model for the shear zone hosted gold deposit (Fig 1-1). In his model, a deeply sourced primary ore fluid, maybe either derived from the lower crust and/or mantle and equilibrated with older felsic crust below the greenstone, or derived from anotectonic granitoids that were derived from such crust, is assumed, and such fluids precipitate over at least 15 km crustal profile at PT conditions ranging from 180 ^{o}C at less 1kbar to 700 ^{o}C at 5 kbar. From this crustal continuum model, fluid movement, and changes in the chemistry of the ore fluids as they rise along crustal-scale hydrothermal systems would be inevitable, when P-T change, ore-

bearing fluids become saturated in ore and gangue minerals, fluids react with host rocks, and ore minerals precipitate as geochemical conditions changed.

In recent years, a new group of gold deposit-intrusion related gold deposit, has been suggested to compromise a distinct class of magmatic-hydrothermal system (Lang and Baker 2001). Recent research results (Lang et al, 1997, Thompson et al., 1999, Goldfarb et al., 2000, Lang et al., 2000, Newberry 2000) indicate that this group of gold deposit collectively share several features common to most intrusion-related gold deposit and provinces, one of the distinct feature is that gold grade is proportional to Bi, As contents. In addition, this group of gold deposit is featured by low sulfide mineral contents (mostly <5%) with a reduced ore mineral assemblage that typically comprises arsenopyrite, pyrrhotite, and pyrite, enrich of CO_2 phase in fluid inclusions and typical tectonic settings, which is closely related to convergent plate boundaries, where continental magmatism commonly contains coeval intrusions.

In China, shear zone hosted gold deposits account for about 70% in the total explored gold reserves in the whole national gold production (Nie, 1997). These gold bearing shear zone systems are mainly distributed in three major tectonic belts: the transcontinental Tancheng-Lujiang shear zone; the Qingling orogeny, and the northern rim of the North China craton (Fig.1-2). Unlike shear zone hosted gold provinces in the rest of the world, many shear zone hosted gold provinces in China, especially in northern China, gold provinces are characterized by the older host rocks (usually Archean) with much younger metallogenic ages (Mesozoic is common). It is this large time gap that causes confusing conclusions regarding the emplacement mechanism and ages of these gold deposits. For

example, some researchers suggested that shear zone hosted gold deposits in north China were formed during the Archean time and were reformed during the Mesozoic Yanshanian orogeny and these gold deposits are metamorphic derivatives (Nie, 1997a). The critical evidence that these researchers hold is that most of these gold deposits are hosted in the Archean metamorphic rocks. Other workers proposed that the shear zone hosted gold deposits are the results of the Mesozoic Yanshanian orogeny, and the gold deposits resulted from the magmatism formed during that period, and the gold deposits are of magmatic hydrothermal origin (Wu and Nie 1995). The critical consideration for this school of thought is that these gold deposits have younger ages coinciding with the Mesozoic magmatism and, in addition, many Mesozoic intrusives, especially the various dikes, do have close spatial relationships with them. Others considered that the shear zone hosted gold deposits are the results of structural (tectonic) deformation (especially the shear zone) (Wang 1990, Ru 1993). In this hypothesis, the gold was thought to be originally deposited in the Archean sedimentary rocks, which experienced high-grade metamorphism in the Archean time. The shear zone related metamorphism remobilized the gold from the host rocks and gold re-deposited in the shear zones. These researchers consider that occurrences of gold deposits exclusively restricted to shear zones are convincing arguments. The debate as to the genesis of theses deposits is still continuing and is the principal motive for choosing the Wulong gold camp as a thesis project.

The Wulong gold camp is part of the north China gold province. The gold camp consists of three gold deposits (namely Wulong, Sidaogou and Jielishu) hosted by metamorphic rocks with different metamorphic grades. The Wulong gold deposit is located

in the late Archean gneiss. The Sidaogou deposit is situated in early Proterozoic metamorphic sandstone, while the Jielishu gold deposit is in the middle Proterozoic marble. The latter two deposits are hosted by rocks showing greenschist facies assemblages. Though the wide age gaps of the host metamorphic rocks, the three gold deposits are spatially shear zone controlled. A ubiquitous phenomenon is that Mesozoic intrusives have intimate relations with gold lodes and the three deposits share many similarities and differences in metallogenic features. These similarities and differences are behind the disputes and arguments regarding the genetic relations of gold deposits developed in the Wulong gold camp. Moreover, till date, the possible genetic relations of gold deposits, dykes and the Wulong shear zone have not been touched in previous researches on the gold camp.

Regarding the genesis of the gold mineralization in this region, like its counterparts nationwide, many disputing on their genesis hypotheses have been proposed. There are three principal ideas: an early genetic model based on a sedimentary-metamorphic approaches was proposed by Zhang (1985). In this model, gold sources were assumed to be originally deposited in the Archean sedimentary rocks, and gold was concentrated during successive regional metamorphism. The second hypothesis was based on the fact that gold deposits have an intimate spatial relationship with diverse dikes introduced during the Mesozoic tectonism, during which the predominant mineralization resulted. Accordingly, it was suggested that the gold deposits were the results of massive magmatism during the Mesozoic and the gold deposit should be of magmatic hydrothermal derivative (Ni and Xu 1993, Li et al., 1987, Peng et al., 1988). The third proposal was not developed

until the recognition of the existence of the Wulong shear zone in this region. In late 1980's, Wang et al. (1989) identified a large-scale shear zone in the Wulong region. This shear zone was recognized as the Wulong shear zone and it structurally controlled the gold mineralization. These workers suggested that the Wulong shear zone played a critical role in gold mineralization (remobilizing gold from the hosting rocks), although whether or not the energy released through shear activity could be high enough to remobilize minerals from host rocks and concentrate them to economic level is still in doubt. Actually, how these gold deposits are genetically related is still a puzzle and needs to be resolved.

As gold resources are quite low in the Wulong gold camp, only several tons of gold reserves are left. Targeting potential gold exploration is on the top agenda of the Wulong gold mining camp administration. A question to be asked is that: is there any possibility to find other exploration targets in the Wulong gold camp or the mining camp is dying out?

Since so many academic and economic problems need to be answered, it was important to carry out this project. The objectives of this project will be mainly focused on the following two aspects:

1). The structural characteristics of the Wulong shear zone, and its role in gold mineralization in the Wulong region, especially the relationship between the tectonic evolution of the shear zone and the evolution of ore-bearing hydrothermal fluid within it.

2). The relationships between the intrusions, gold lodes and the Wulong shear zone, especially their possible genetic relations of the gold deposits developed in the Wulong mining camp.

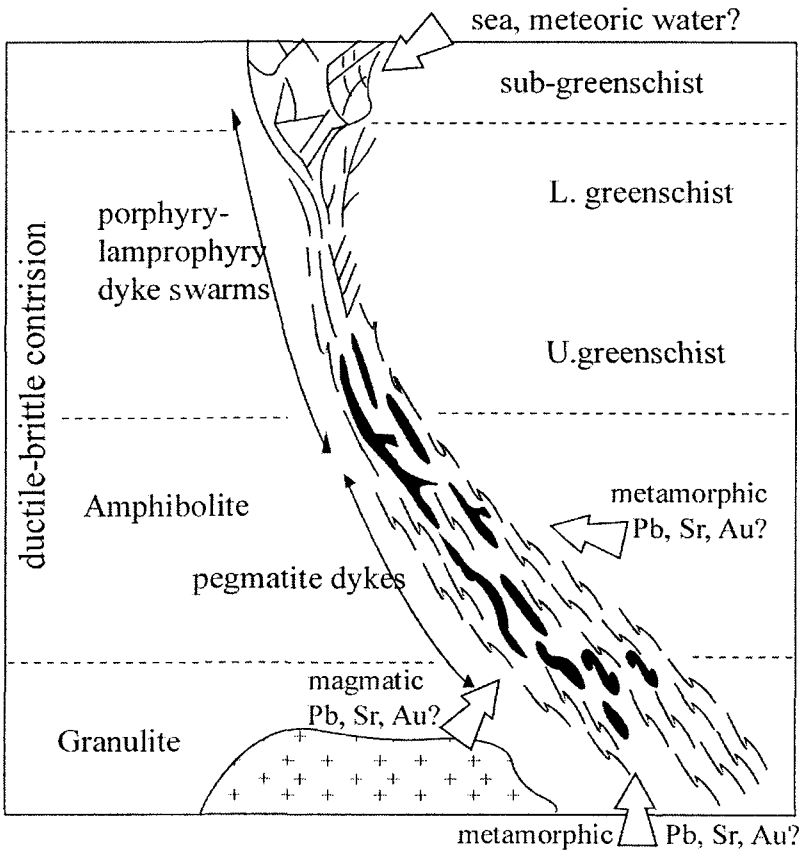

Figure 1-1 Schematic crustal section showing possible fluid and material sources and spatial deposition of gold deposits (modified from Groves, 1993)

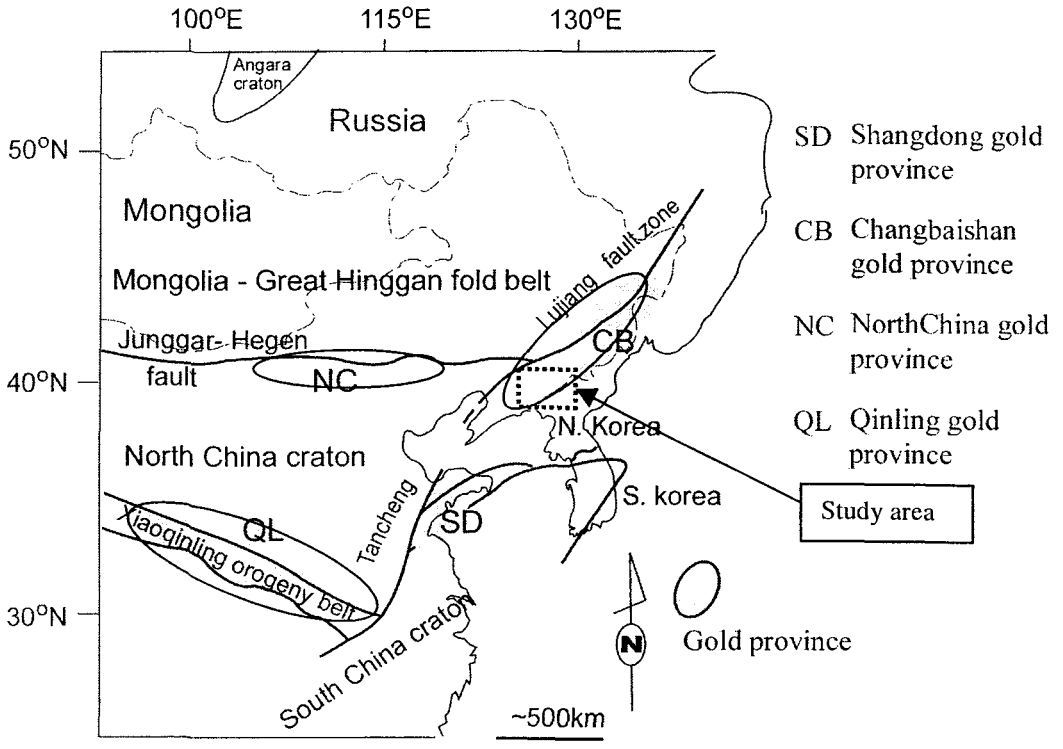

Figure 1-2 Spatial relationship of major gold provinces and orogenic belt at the NE Asian continental margin

(modified from Miller et al. 1998)

Chapter II

Regional geology and tectonic evolution

Introduction

The study area is located at southwest Dandong city, SE Liaoning province, NE China (Fig.2-1). The SE Liaoning province is one of the major gold producers in China, and the gold reserves in this region accounts for 40%-50% of the total gold resources of the province (Cui et al., 1995). In this region, active gold mines include three large scale gold deposits (gold reserves exceeding 50 tons), and several tens of middle scale deposits (reserves of less than 20 tons) and occurrences.

Tectonically, this region is located at the NE margin of the North China craton, commonly referred to as the Sino-Korean platform or craton. On a local scale, this region is located on the south margin of the EW striking YingKou-Kuandian subuplift (Wang 1990, Yao et al., 1988). The whole region experienced deformation and metamorphism as early as the Archean time and the later structural deformation and magmatic intrusion occurred during the Mesozoic age.

2.1 Lithostratigraphy and metamorphic rocks

Regional lithostratigraphy is dominated by the Precambrian metamorphic rocks. The Archean metamorphic rocks are mainly distributed in the Anshan area to the north and in

the southwest area. The early Proterozoic metamorphic rocks, generally striking EW, are the predominant rocks and mainly developed in the central part of the region. The post-Precambrian strata are absent and only minor Jurassic clastic-sedimentary rocks and pyroclastic rocks are sporadically developed in the Mesozoic pull-apart basins in the Wulong area. The regional lithostratigraphy is summarized in table 2-1.

2.1.1 Classification of metamorphic rocks

Based on the formation, petrological and geochemical features, the metamorphic rocks can be classified into two metamorphic complexes in this region: the Archean Anshan-type amphibolite metamorphic formation and the early Proterozoic tourmaline-mica metamorphic formation.

The common metamorphic rock units are classified into five types:

① Schist: mainly mica-quartz schist, quartz schist and sillimanite-mica schist.

② Gneiss: the common gneissic rocks include garnet-sillimanite gneiss, mica gneiss and amphibole-mica gneiss.

③ Granulite: this type includes mica granulite, tourmaline granulite, amphibole granulite, and tourmaline-magnetite-bearing leucoleptite.

④ Marble: mainly occurs as dolomite marble.

⑤ Quartzite: dominated by mica quartzite.

2.1.2 Stratigraphic sequences of metamorphic rocks

2.1.2.1 The Archean Anshan group

The Archean layered metamorphic rocks are developed in the south and north margin of the region and they generally strike EW. Such metamorphic rocks mainly occur as remnants in the Archean TTG series (Cui et al.,1995). Generally, the Anshan Group can be divided into two formations from bottom to top according to Cui et al., 1987 and Li 1988:

The Chengzitan formation:

Total thickness of this formation is about 22,160 meters. The major lithological assemblages include (from the bottom to top of the formation): eclogite-amphibolite-plagiogneiss, amphibolite assemblages; amphibolite-mica-granulite, leucoleptite, gneiss and hornblendite assemblages; hornblende-mica gneiss with the mixed layers of amphibolite, mica-hornblende granulite and magnetite quartzite assemblages.

The Dongjiagou formation:

Total thickness of this formation is about 6,150 meters. The lithological variation from bottom to top shows the following mineral assemblage sequences: hornblende-bearing mica gneiss, mica granulite, leucoleptite and the mixed layers of amphibolite assemblages; mica-hornblende schist or gneiss assemblages; to the mica-plagiogneiss with layered hornblende-mica schist and two-mica schist assemblages at the top.

2.1.2.2 The Proterozoic Liaohe Group

The Liaohe Group can be classified into five litho-units from bottom to top: the Langzishan Formation, the Lieryu Formation, the Gaojiayu Formation, the Dashiqiao Formation and the Gaixian Formation.

The Langzishan Formation:

This formation overlies the Anshan Group with an angular unconformity. The dominant lithological units include chlorite-sericite schist, phyllite, two-mica schist, two-mica granulite and marble, locally with quartzite and conglomerate in the bottom. The major metamorphic facies is greenschist, with local epidote-amphibolite facies. Total thickness ranges from 206 to 2005 meters.

The Lieryu Formation:

This formation conformably lies over the Langzishan formation, but in the south and eastern part of the region, it directly overlies the Archean TTG series with an angular unconformity. The major petrological units include leucoleptite, tourmaline granulite, schist marble and metamorphic rhyolite and tuff. Dominated metamorphic facies includes greenschist, epidote-hornblende facies and almandite-hornblende facies. Thickness ranges from 830 to 1,884 meters.

The Gaojiayu Formation:

Basically, this formation has similar spatial distribution as the Lieryu Formation. It shows conformable contact with both the over-lying and the underlay formations. The petrochemistry of this formation is characterized by the existence of carbon (graphite).

Major lithological associations include schist, slate, and granulite with overlapping marble, sebesite-diopside and amphibolite. greenschist and epidote-hornblende facies are the dominant metamorphic facies.

The Dashiqiao Formation:

The Dashiqiao formation is characterized by the thick marble and the occurrence of magnesite deposit. Conformable contact with both the overlying and the underlay formations indicates a relatively stable sedimentary environment during the development of the sedimentary formation. The major lithologic units include dolomitic marble, calcitic marble, and tremolite-diopsidite with overlapping schist and granulite assemblages. Total thickness of the formation ranges from tens of meters to 4,000 meters.

The Gaixian Formation:

This formation has the widest spatial distribution in this region. It may directly overlay the Archean granitic gneiss to the south part of the region. Dominated litho-units are characterized by the staurolite-sillimanite-bearing mica schist and gneiss. Total thickness of this formation ranges from 1750 to 4969 meters.

2.1.3 Protolith identification of metamorphic rock units

Though metamorphism involves complex geochemical processes, a fundamental assumption is that the lithochemical compositions are supposed to be constant during metamorphism (Niggli 1954). Many protolith restoration methods were proposed (i.e. Kohler and Raaz, 1951, Simonen, A. 1953, Niggli 1954, Opletal 1971). Most of the

methods are based on the lithochemical compositions of the metamorphic rocks through the major element approaches. Discrimination of different protolith rocks can be realized by means of diagrams (i.e. the diagram of K_2O+Na_2O vs. SiO_2, or Na_2O+K_2O vs. K_2O/Na_2O) or characteristic values such as the Niggli's values (al, fm, c, alk, mg, k, si etc.,) recalculated through the major elements. And all of the protolith restoration methods are based on the assumption that metamorphism occurs in a relatively closed system.

Previous works show that relatively simple diagram of the ratios of oxides may express excellent criteria for protolith discrimination. For example, Na_2O/K_2O ratio may express the differentiation trend of metamorphosed sediments (inverse ratios of alkalies) and metavolcanics (increase of potassium content in the differentiation series at constant sodium content, which is characteristic of the given assemblage) (Suk 1983). Miyashiro (1975) characterized the changes in chemical composition in metamorphism by means of diagrams, with $Na_2O +K_2O$ plotted on the X-axis and the Na_2O/K_2O ratio on the Y-axis.

Besides the major element parameters, Niggli's values are also reliable and are parameters frequently used in protolith identification. In general, the Niggli values are expressed as: al = Al_2O_3; fm = FeO + MgO + MnO; c = CaO; alk = $Na_2O + K_2O$; mg = MgO/(FeO + MnO + MgO); theoretically, Σ(al + fm + c + alk) = 100. All the variables are in weight percentage. These Niggli's values (parameters) may be used either in Niggli's diagrams (SI on the X axis, and the remaining ones on the Y axis), which have been proved adequate particularly for metavolcanic rocks (Suk 1983), or in several specific diagrams. The most widely used diagram is SI vs. (al+fm)-(c+alk). The ratio of these two values expresses mainly the fundamental trend of sedimentary differentiation and makes it

possible to distinguish between sedimentogenic and volcanogenic metamorphic rocks. According to Peltola (1960), the value of al – (c+alk) strictly distinguishes the field of sediments from that of igneous and the formula (alk+al) - (fm+c) is a good instrument to the study of metabasites in discriminating between metamorphic equivalents of igneous and sedimentary rocks. The recalculation method of Kohler and Raaz (1951) is usually applied in identification of metamorphosed volcanic rocks. Since each of the restoration method was proposed on a specific lithologic type, its application on strongly metamorphosed lithologic units is accordingly limited. To minimize the uncertainty of protolith discrimination, several different identification methods are used and choose the most frequently identified rock types as the final acceptable discrimination results. The following combination of methods is used during the protolith identification in this region:

Discrimination formula (Peltola, 1960)

(al-alk) vs C diagram (Niggli. 1951)

SiO_2 vs (Na_2O+K_2O) diagram (Kuno, 1968)

(al+fm)-(c+alk) vs Si diagram (Simonen 1953)

106 sample data were chosen for the calculation. Parts of the discrimination results are plotted on the figure 2-2. The discrimination results are summarized as following:

The upper subgroup of the Liaohe group includes the Gaixian, Dashiqiao and the Gaojiayu formations are predominated by quartz schist, two-mica schist, garnet-sillimanite-bearing mica gneiss, mica granulite, mica-bearing tremolite-diopsidite and marble with minor amphibolite. On the (al+fm)-(c+alk) vs Si diagram, these rock units plots in the

domain of clay, sand and calcareous sediments (Fig.2-2). The plots of amphibolite are located in the magmatic area.

The Lieryu Formation and the Langzishan Formation of Liaohe group are mainly composed of the tourmaline-hornblende-mica granulite, hornblende-tourmaline-magnetite leucoleptite, mica gneiss, and amphibolite with dolomitic marble and boron-bearing layers. Various calculation results and discrimination methods indicate that the protoliths of the Lieryu Formation and the Langzishan Formation are volcanic rocks with overlapping clay, sand and chemical sediments or pyroclastic rocks (Fig. 2-2).

The Dongjiagou formation of the Anshan group includes hornblende granulite, mica-hornblende gneiss, mica schist, mica-gneiss with overlapping amphibolite are the dominant litho-units. Sample data plots from this formation fall in the volcanic rock area (Fig.2-2). Lithochemical calculation results indicate metamorphic rocks were evolved from magmatic rocks.

The Chengzitan formation of the Anshan group is mainly composed of mica-hornblende granulite and mica-hornblende gneiss as well as mica-hornblende leucoleptite with minor amphibolite and magnetite quartzite. Sample data plots of this formation are mainly located in the area of intermediate-basic volcanic rock or tuff, only the magnetite quartzite plots falls in the area of sediments (Fig.2-2). Like its overlying neighbor, lithochemical parameter calculation of the Chengzitan formation indicates that the metamorphic rocks were derived from magmatic rocks.

2.2 Magmatism

The area of the outcropped intrusive rocks in this region is about 12000 km^2, which accounts for about one third of the total area of the SE Liaoning region (Peng et al., 1988). These intrusions are dominantly formed during Mesozoic ages (the Indo-Chinese epoch (P2-J1) and the Yanshanian epoch (J2-K2)). Intrusive rocks formed during the Mesozoic ages are characterized by their intimate spatial and temporal relationship with gold mineralization. This is why many researchers suggested that the Mesozoic intrusions are the sources of gold mineralization (Cui et al.,1995). Since the Precambrian magmatic rocks are mostly metamorphosed and have large geological time age gaps with gold mineralization, and they are generally considered with no genetic relation with gold mineralization in this region (Cui et al., 1995). This section will focus on the Mesozoic intrusions.

2.2.1 The Mesozoic intrusive rocks

2.2.1.1 Geological characteristics

Outcrops of intrusions in theSE Liaoning province are dominated by granites, which accounts for 80% of the total area of the intrusives in the region (Peng et al. 1988). The major rock types are diorite followed by alkali complexes.

Based on the spatial relationships of these intrusions and geochronological ages, about 20 intrusives were formed at the early Mesozoic according to Peng (1988), the

representative intrusives include the Huanglingzi, Zhoujiabaozi and the Wujiashan. Most of the intrusives were formed at the middle Mesozoic period, and about 25% of the granites formed at this stage are batholiths, the representatives being Youyan, Wulongbei and the Sanguliu intrusives.

Exposed magmatic rocks formed at the Yanshanian epoch are about 2000 km^2. Individual intrusion usually ranges from n~n*10 km^2. In the southeast part of the region, such magmatism occurred as volcanic eruption. Late Jurassic to early Cretaceous volcanic sediments or tuffs are common in some small pull-apart basins.

2.2.1.2 Petrological characteristics

Intrusives formed at early Indo-China epoch are dominated by quartz diorite, quartz monzonite, diorite and pyroxene diorite. Major minerals include plagioclase, quartz, mica, amphibole and pyroxene. Intrusives formed at the middle Indo-China epochs are dominated by monzonitic granite with minor granodiorite. The Youyan, Wulongbei and Sanguliu intrusions are represent the intrusives formed at this stage.

The Youyan intrusion: This is the largest batholith (about 2,533 km^2) developed in this region (Peng et al. 1985). Many dykes are developed in this batholith. Identified dykes include pegmatite, granoporphyry, granitic porphyry, granodiorite porphyry, quartz diorite, and lamprophyres. These are also quartz veins. Inspite of the large size of the batholith, phase zonation is not obvious in the batholith.

The Wulongbei intrusion*:* This *intrusion* occupies an area of about 1200 km^2 (Peng et al., 1985). It intruded the Liaohe group and the early Mesozoic diorite. Xenoliths of metamorphosed rocks observed in this intrusion are common, so as the late stage fine-grained granite dikes. Dominant rock types of this intrusion are monzonite followed by granodiorite. Major minerals are quartz (26%, average values, thereafter), k-feldspar (29%), plagioclase (35%), and mica (6.6%). Plagioclase is commonly replaced by k-feldspar and micas are mostly chloritized.

The Sanguliu intrusion: Though it is a stock, with an outcrop area of 11.4 km^2, a marginal phase and central phase are clearly recognizable in the Sanguliu stock. The marginal phase is composed of granodiorite, while the central phase consists of monzonitic granite. Major minerals include k-feldspar (23%), plagioclase (36%), quartz (22%) and minor mica and hornblende.

In general, granites formed at late Indo-China epoch are characterized by the fine-granular texture, small size, and usually occur as dykes. Quartz (30%), K-feldspar (25%), plagioclase (40%), mica (<5%), white mica (<5%) are the dominant minerals.

Granites formed at the Yanshanian epoch (late Mesozoic) are clustered at two periods—the early stage and the late stage. Granite formed at early stage are mainly monzonitic granite, in which k-feldspar occupies a percentage of 24-40, plagioclase accounts for 35-40%, quartz ranges 20-25% and mica is about 5%. Granite, perthitic granite and granodiorite are the major rock types formed at the late stage. The Fenhuangshan intrusive is a representative of this type and is composed of perthite (60%), quartz (35%), and mica (+ hornblende) (<5%).

2.2.1.3 Petrogeochemical characteristics

Major element analysis results of representative intrusions were used to compare the petrochemical features of the rock types formed during the Mesozoic age. The partly re-grouped analysis data are listed in table 2-2. From the table, we know that, regardless of the scales of the intrusions, there are no sensible differences in major element contents among the three intrusives.

2.2.1.4 Trace and rare earth element features

Generally, concentrations of trace elements in intrusions are low in this region. Contents of the iron-group elements (Cr, Ni, Co, V) in the Mesozoic granites are roughly twice of those in the gneiss. Contents of F and Cl^- are 770 ppm, 260 ppm, respectively.

Table 2-3 shows several major REE parameters of the three intrusions. Generally, contents of REE in granites are relatively high with a variation ranging from 134.00ppm to 301.00 ppm. The three intrusives show enriched LREE signature and intermediate depletion of Eu, and δEu values range from 0.62 to 0.73. On the normalized REE pattern plots, they have similar distribution patterns and slopes to the right (Fig.2-3).

2.2.1.5 Isotopic characteristics

Several isotope data from magmatic rocks in this region were collected during this study. The U-Th-Pb Isotope data are listed in table 2-4, and the K-Ar dating data are listed

in table 2-5. The results of isotope data from this study demonstrate the similar features as previous done in this region, as shown in the two tables, isotopic ages of the magmatic rocks are quite variable. Many geologists suggested that the isotopic age variations in this region are probably the result of strong post-magmatism tectonic activities occurred in this region.(Li et al., 1987, Zhang 1992).

One widely accepted argument regarding to geological time in this region is that the granites intruded both the Liaohe Group and the late Archean gneiss, but the upper bound of geological ages of the intrusion events is still argued. Most of the Mesozoic granites have ages ranging from 100 Ma to 200 Ma. These data are in accordance with the evidence that the Mesozoic magma intruded the Cretaceous and Permian strata. From these data, it's obvious that the ages of the zircon and monazite have discordant ages, and when the contents of common lead are low, the difference of the discordant ages is low. So far, we have not enough information to discuss the causes that how and why these discordant ages were formed, since Zircon and monazite have usually quite steady isotope ages. The fact that, in the northeastern China, geological units usually have quite variable geological ages due to the disturbance of tectonic and magmatic events occurred during the Mesozoic period may provides certain explanations for the variable isotope ages defined in the magmatic rocks. The Fenghuanshan intrusive has an average U-Th-Pb age of 120 Ma (the 255Ma datum was excluded during average age calculation since the Fenghuangshan intrudes the Sanguliu intrusion and it is believed to be the latest intrusion in the Wulong area). It's reasonable that the Mesozoic magma series were formed at early Yanshanian epoch, the age range varies from 140 to 180 Ma. The isotope ages of the Liaohe group are

set to 1100 – 1500 Ma based on the K-Ar age dating method. Considering the post-magmatism tectonic disturbance, and considering the U-Th-Pb ages of the gneiss, it's geologically reasonable to assume that the gneissic rocks were reformed at about 260 – 300Ma, the 100 – 130 Ma ages identified in the gneiss rocks are mostly probably the imprint of the tectonic-magmatic thermal event occurred during the Mesozoic Period.

In summary, granites developed in the SE Liaoning region can be divided into three periods of formation based on their isotope ages. The much younger ages of the gneiss we get in this study were probably caused by late magmatic thermal disturbance since these thermal events were very frequently happed in this region from Proterozoic to Mesozoic ages. Granites were mainly formed during 140 –180 Ma (early Yanshanian epoch). The latest intrusions were formed at 120 Ma (late Yanshanian epoch).

2.2.2 Dykes

Four major types of dykes are recognized in the SE Liaoning province. These dykes, with quite variable scales, cover a quite wide range of compositions (Tab. 2-6). Based on previous works on the various dykes (Peng et al., 1988), the dykes developed in the SE Liaoning region can be grouped into three geologic ages:

Proterozoic dykes: These dykes are dominated by metamorphosed mafic species, such as metalamprophyres, metagabro, pyroxene and amphibolite. These dykes mainly strike EW.

Early Mesozoic dykes: Dykes formed at this stage are not very common, they are dominated by dioritic porphyry, fine-grained diorite and minor pyroxenite.

Late Mesozoic dykes: This group of dykes is widely developed in this region. The major rock types include fine diorite, granitic porphyry, granophyre, granodioritic porphyry, fine granite, lamprophyre, andesite, rhyolite, diabase, pegmatite and quartz veins. These swarms mainly strike NNE and NW. Scales of the dykes are quite variable and have a range from 30 to 1000 meters in length and 2 to 30 meters in width. Generally, the andesite, rhyolite, diabase and granodioritic porphyry dykes are assumed to be the latest products of the dyke generation.

Most of the dykes are hosted in gneiss. Though they are made up different mineral associations, the REE patterns of the dykes are quite similar to the gneiss and stocks hosting these dykes (Li et al., 1988).

2.3 Tectonic setting and tectonic evolution

Tectonically, the SE Liaoning region is located at the northeastern margin of the Sino-Korea plate. A general consensus exists that the Pacific Ocean Plate subducted the Sino-Korea plate during the Yanshanian movement (about 180 – 80 Ma), and triggered the massive magmatism along the convergent margin (Yin and Nie, 1993, Xu and Zhu, 1994). This collision also established the basic tectonic framework of China and resulted in the metallogenic provinces in northeastern China (Xu and Zhu, 1994, Kumarapeli et al., 1990). As one of the products of tectonic plate subduction event, the NEE striking continental Tancheng –Lujiang wrench shear zone played an important role in the metallogeny in NE China (Zhang 1992).

Numerous works revealed that the continental scale Tancheng – Lujiang shear zone, 3600 km in length and 50 km in width, is the first order structure which controls gold metallogenic provinces in NE China (Zhang 1992, Mueller et al., 1991). Though the formation mechanism, kinematic characteristics and geochronologic ages of the shear zone system are still debated, it is generally accepted that the Tancheng – Lujiang shear zone was quite active during the Yanshanian orogeny. This continental shear zone controlled the gold clusters in northeastern China, for example, the Jiaodong gold cluster in Shandong province, the Jiapigou gold province in Jilin province, and the Wulong gold camp in Liaoning province (refer to Fig. 1-2).

Previous study on regional tectonics revealed that the whole SE Liaoning region was submitted to multiple episodes of structural deformation (Liu, 1982, Yang, 1984). These deformation events together with regional metamorphism and magmatism shaped the complex image of the regional structural feature of the SE Liaoning region. The multi-stage regional tectonic events can be classified into four tectonic episodes (Yang 1984):

D1 tectonic episode:

This episode is characterized by the formation of a series of ESE striking folds. This tectonic event, developed at the Archean ages, had a wide and strong influence in this region, established the regional structural trend and contributed the regional metamorphism in this region. The Hupiyu antiformal anticlinoria and the Gaixian-Youyan synclinoria were the products of this tectonic episode. The lithographic unites involved in this tectonic event are the Anshan Group.

The synkenimatic granites and the host rocks were involved in the D1 tectonic deformation. The synkenimatic granite and the host rocks show concordant contact. The synkenimatic granites have an average isotope age of 2060 Ma (U-Pb method) according to Yao et al., (1988). According to Yang (1984) and Yao (1988), the first regional metamorphism was formed in the D1 episode.

D2 tectonic episode:

Medium to large scale NS striking folds are the products of this episode. The D2 tectonic episode was not well developed in the SE Liaoning region. The representative structures formed in that event are the Buyunshan fold belt and the Zhuanyou structural zone. both the Anshan Group and the Liaohe Group were involved in this event. Isotope data suggests that this episode occurred at 1800 –1900 Ma (Wang 1990).

D3 tectonic episode:

The D3 tectonic event is the weakest of all the tectonic events occurred in this region. Only small-scale folds were formed in this event, and these fold system were mainly developed on the limbs of the D1 fold system. The D3 fold system overlapped the D1 fold system. Magmatism was not active in this event.

D4 tectonic episode:

Tectonic features occurred during the D4 episode were quite different. Tectonic features were characterized by the development of shear zones of various scales and the introduction of massive magmatic intrusions. The Wulong shear zone was one of the structures of the D4 event. The structural characteristics of the Wulong shear zone will be detailed in the following chapter.

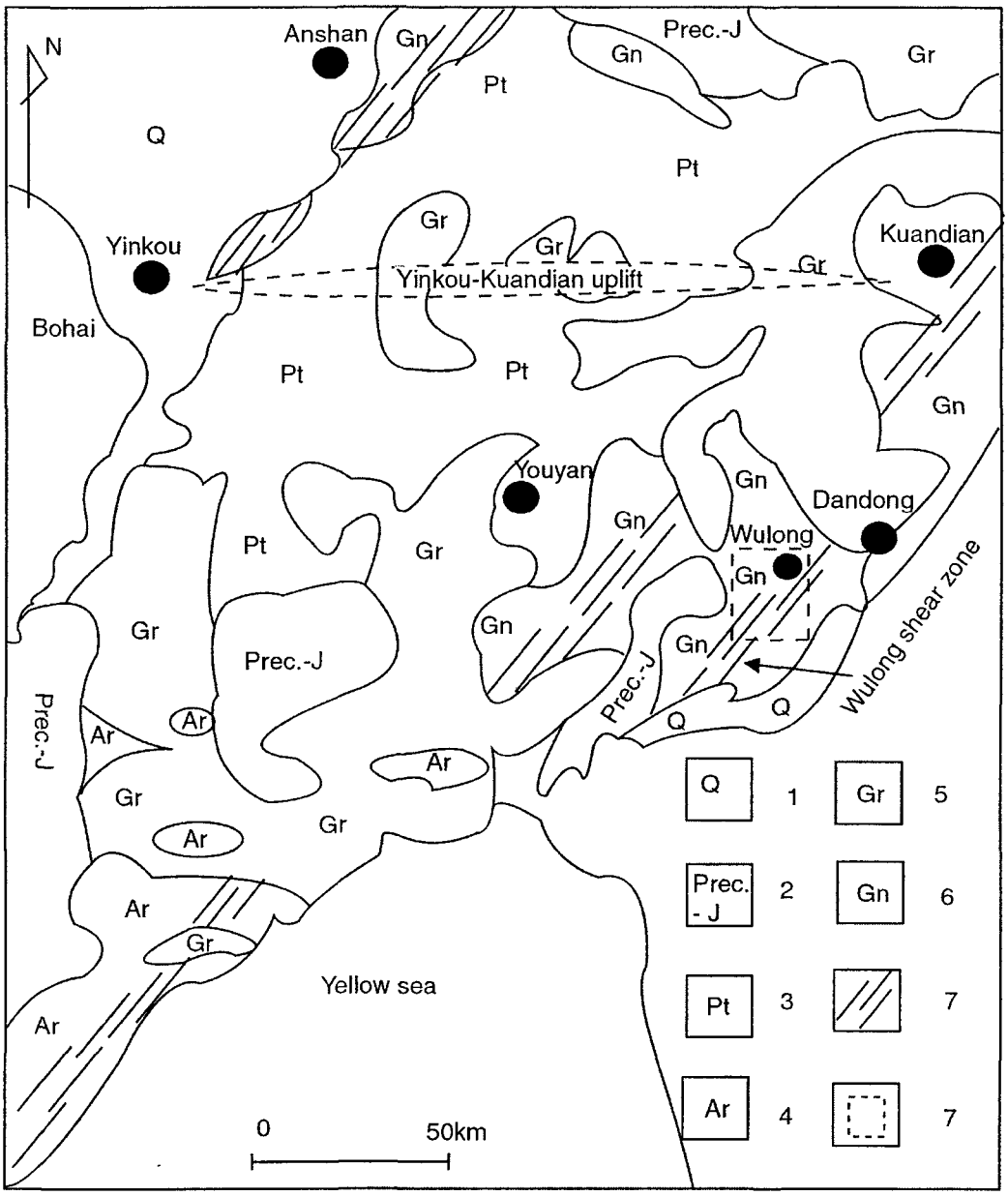

1. Quaternary; 2. Mesozoic sedimentary rocks; 3. Proterozoic metamorphic rocks;
4. Archean (Anshan Group); 5. Mesozoic granites; 6 late Archean gneiss; 7. Shear zone,
8. location of the study area

Figure 2-1 Simplified geological map of the SE Liaoning province, China
(cited from Liu 1993)

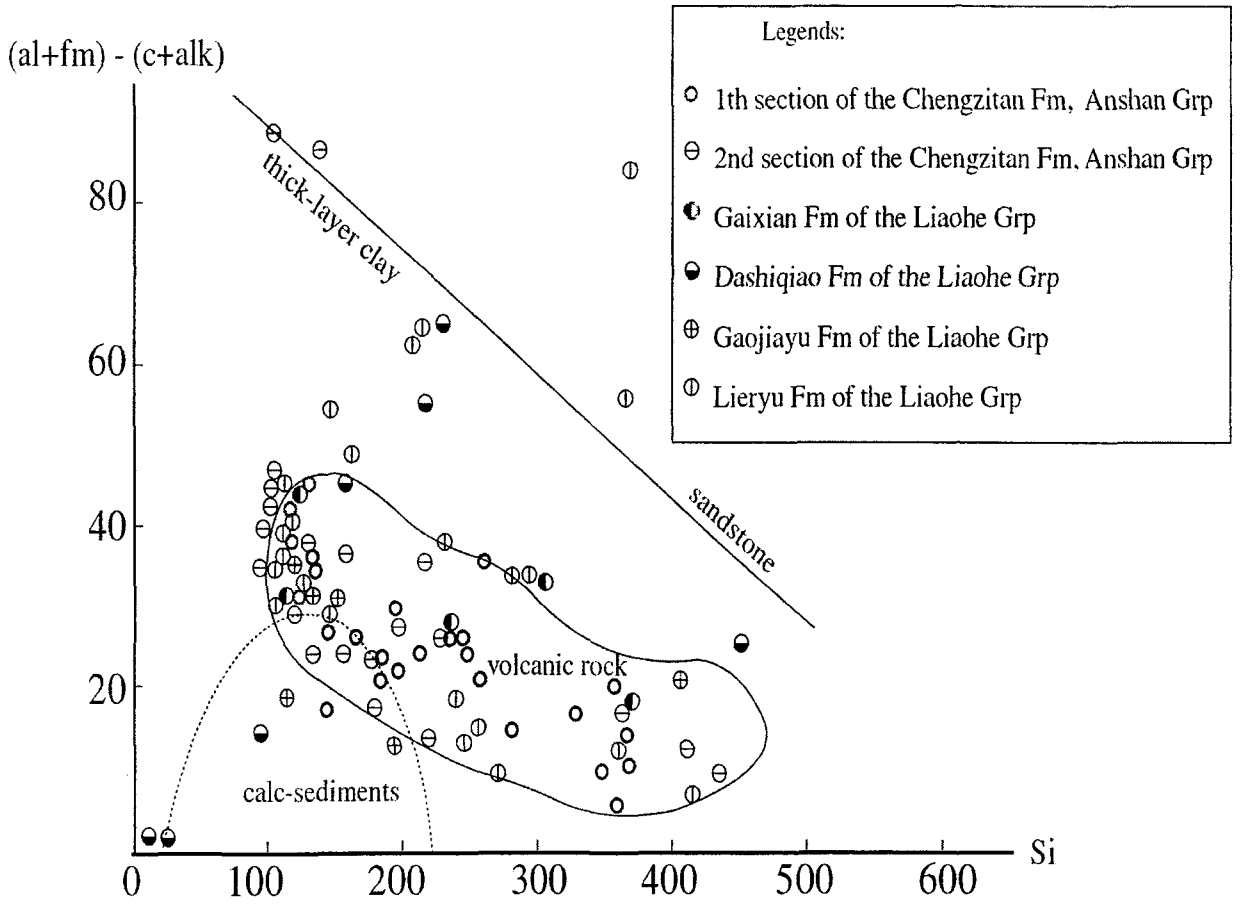

Figure 2-2 Si vs. (al-fm)-(C+alk) diagram of metamorphic rocks in the SE Liaoning province (according to Liu 1993)

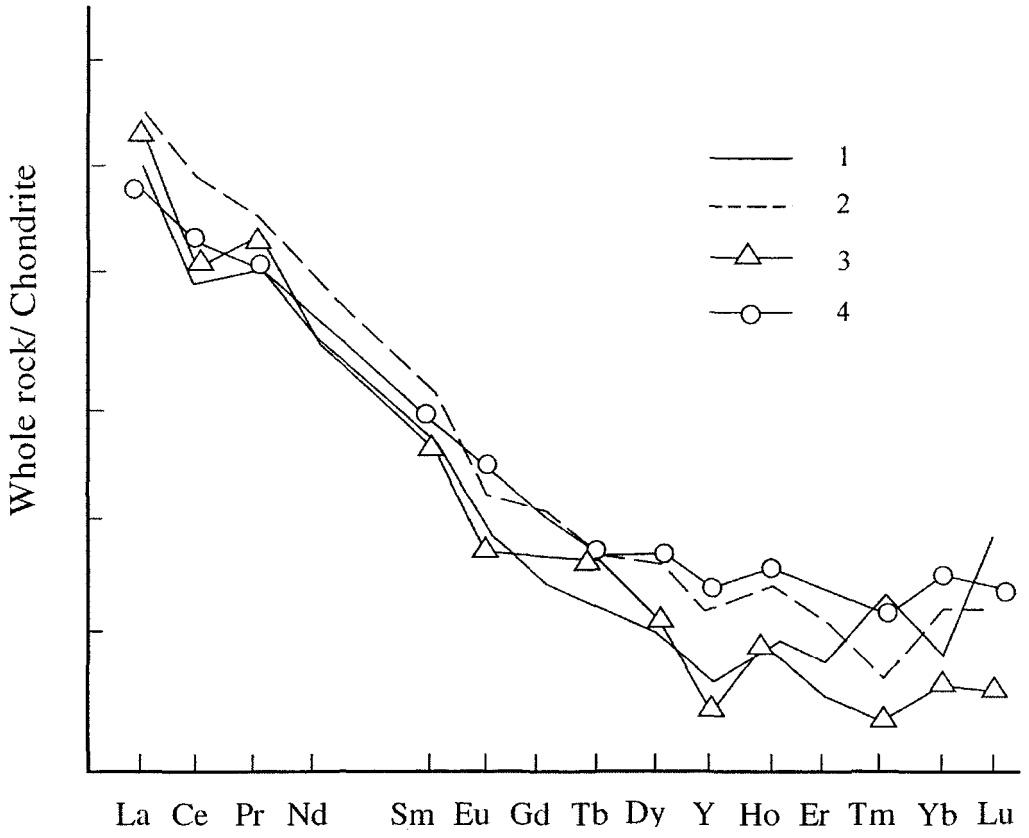

Figure 2-3 REE patterns of different granites in the Wulong region

1. Wulongbei intrusion; 2. Sanguliu intrusion; 3.Fine grained diorite; 4. Gneiss. (according to Liu 1987)

Table 2-1 : Regional stratigraphic sequence and lithologies of the SE Liaoning province, China (complied from the source of Li 1987, Liu 1982)

Era		Litho-group (formation)		Major Rock type	Protolith formation	Metamorphic facies
Mesozoic				Andesite basalt, Andesite, tuff, tuff-breccia and siltstone.	Sediments, volcanic rocks,	Unmetamor-phosed
Proterozoic	Upper Pt	Sinian system		Marble, Phyllite (Jielishu deposit)	Terrian clastic rock formation	Greenschist facies
	Lower Pt	Liaohe Group	Gaixian Formation	Phyllite, two-mica schist, slate,	Clay rock formation	Greenschist facies
			Dashiqiao Formation	Marble, schist, granulite. Quartzose sandstone (Sidaogou deposit)	Carbonate formation	
			Gaojiayu Formation	Schist, slate, biotite-granulite.	Carbonaceous shale	Amphibolite facies
			Lieryu Formation	Metamorphosed volcanic rock, granulite, schist, marble, metamorphosed sendimentary rocks	Alkaline-volcanic rock formation	
			Langzishan Formation	Phyllite, schist, two-mica granulite,	Terrigenous clastic-clay rock formation	
Archean		Anshan Group	Dongjiagou Formation	Gneiss, amphibolite (Wulong deposit)	Greenschist formation	Amphibolite facies
			Chengzitan Formation			

Table 2-2 Comparison of major chemical composition characteristics of the three representative intrusions (data are sourced from Ru 1993)

Intrusion	SiO_2	K_2O+ Na_2O	K_2O /Na_2O	TFe+MgO +MnO	CaO	Serial index (σ)	
						Variation	average
Youyan	68.23	8.04	1.00	4.32	1.97	1.85--3.01	2.47
Wulongbei	72.14	7.80	1.35	3.01	0.79	1.03 – 3.33	2.10
Sanguliu	68.60	7.70	1.23	4.54	2.34	1.04 – 2.46	2.70

Table 2-3 Major REE characteristics of the three Mesozoic intrusives of the SE Liaoning province

Intrusions	∑REE	LREE/HREE	δEu
Youyan (9)*	301.00	10.90	0.73
Wulongbei (11)	134.00	8.17	0.62
Sanguliu (6)	197.00	8.23	0.70

* number in the bracket is the sample numbers analyzed

(data are cited from Cui et al., 1988)

Table 2-4 U-Th-Pb dating of zircon (monazite) of magmatic rocks of the SE Liaoning province

Sample No.	Locality	Mineral And rock	U(%)	Th (%)	Pb(%)	Pb compositions (%)				Ages (Ma)				references
						204	206	207	208	206/238	207/235	207/206	208/232	
Pao-2	Wulong	Zircon (Gneiss)	0.1892	0.0278	0.0129	0.749	53.346	14.579	31.326	198	266	916	286	III
Pao-2-1	Wulong	Monazite (gneiss)	0.2060	3.4000	0.0268	0.072	11.790	1.640	86.498	100	101	109	148	III
Pao-1	Wulong	Zircon (granite)	0.0659	0.0566	0.0029	0.712	47.484	13.075	38.729	114	125	347	135	I
Dj3	Baijialin	Zircon (granite)	0.1560	0.1780	0.0055	0.680	51.980	12.430	34.910	104	101	-	61	II
Dj4	Heigou	Zircon (granite)	0.0817	0.1090	0.0029	0.680	49.670	12.510	37.110	98	103	48	66	II
Laogg-3	Dinqishi	Zircon (granite)	0.1120	0.0823	0.0327	0.337	60.505	7.970	31.185	117	117	115	117	I
Dj8	Fenghs	Zircon (granite)	0.1042	0.2137	0.0104	0.960	35.080	16.920	47.040	130	255	115	130	II

* I : Scientific research report of the metamorphic rocks of the Liaoning province by the Bureau of the Geology and Mineral Resource of Liaoning and Changchun college of Geology (1982); II : Isotope age compiling by Shengyang Institute of Geology (1983); III : No. 3 Institute of nuclear energy (1985).

Table 2-5 K-Ar dating of granitic gneiss and the Liaohe group in the Wulong gold camp

Location	Rock type	analyzed Mineral	K(%)*	$^{40}Ar*10^{-6}$ (g/g)	^{Ar}air (%)	$^{40}Ar/^{40}K$	Ages (Ma)
Wulong	Pegmatite (dyke)	Mica	8.290	0.09486	19.0	0.009590	157
Wulong	Pegmatite (dyke)	Mica	8.340	0.07530	27.7	0.007565	125
Caomigu	Pegmatite (dyke)	Mica	8.240	0.06875	41.4	0.006993	116
Heigou	Gneiss	Biotite	7.585	0.08839	28.9	0.009768	360
Sidaogou	Mica schist (Liaohe Group)	Mica	5.110	0.52540	4.4	0.086200	1083
Wudaogu	Granulite (Liaohe Group)	Hornblende	0.800	0.13160	5.5	0.133800	1516

*Data are cited from Yao et al., (1988)

Table 2-6 Dyke types identified in the SE Liaoning province

Acid – intermediate acidic dyke	Intermediate – acidic dyke	Mafic-ultramafic dyke	Lamprophyre
Rhyolite	Diorite	Diabase	Camptovogesite
Granitic porphyry	Fine diorite	Basalt	Minette
Eurite	Dioritic porphyry	Gabrro	Odinite
Granophyry	Andesite	Proxenite	
Granodioritic porphyry		serpentinite	
Syenite porphyry			

(according to Peng 1988)

Chapter III

The Wulong shear zone

Introduction

Identified in the 1980's (Liu 1982, Wang. 1990), the Wulong shear zone is a substructure of the Tancheng – Lujiang shear zone system, and it controls the Wulong gold camp and various intrusions (Ru 1993). Researchers have proposed several different genetic models for the gold deposits because these gold deposits are hosted by different lithologic units. Numerous papers have discussed the relationships among the Wulong shear zone, intrusions and gold deposits, but few discussed the possible genetic relationships of the shear zone, magmatism and gold mineralization in this region. In this chapter, the structural characteristics, the geochemical processes that occurred in the Wulong shear zone and its evolution will be highlighted.

3.1 Structural characteristics of the Wulong shear zone

3.1.1 Geometry of the Wulong shear zone

The Wulong shear zone is composed of approximately parallel ENE striking fault zones (Fig. 2-1). This shear zone cuts through different lithologic units such as the late Proterozoic marble, middle-late Proterozoic metamorphosed sandstone, and the late Archean gneiss (Fig. 3-1). It's approximately 50 km in length and 12 km in width. Due to the various lithology of the host rocks, the Wulong shear zone demonstrates different

structural patterns and structural characteristics at different locations. For this reason, three different structural sections were selected to study the shear zone during field investigation. The three structural section sites were selected at the Wulong gold deposit, the Sidaogou gold deposit and the Jielishu gold-copper deposit, since the three gold deposits are also located in related sections of the shear zone. The lithologic rocks of three sections are gneiss, metamorphosed sandstone, and marble, respectively (refer to Tab. 2-1).

3.1.2 Tectonite types and zonation in the Wulong shear zone

3.1.2.1 The Wulong mine area

The Wulong mine is located in the west of the Wulong gold deposit (Photo 3-1). The host rock involved in the shear zone is the late Archean gneiss. Mineral associations of the original gneiss is mainly composed of plagioclase (35 – 45%), k-feldspar (25 –35%), quartz (25%), mica (3%), white mica (<2%) and other minor minerals (<2%). Schistosity is well developed, and the sheet mica and elongated quartz shape the fabric. Quartz grains usually show wavy extinction and banded texture. Based on the deformation features of the rocks involved in the shear zone, the tectonized rocks can be classified into three types:

① Gneissic proto-mylonite

The gneissic proto-mylonite consists of plagioclase phenocryst and matrix. Phenocryst-matrix ratio is around 50 – 60%. The phenocrysts usually show rounded and rotated eye-shape or lens form (Photo 3-2). The matrix is dominated by quartz, mica,

and minor muscovite, and they are usually distributed around the phenocrysts and show banded orientation. Quartz grains show elongated form.

② Gneissic mylonite

S-C fabrics are well developed in the gneissic mylonite. Phenocryst/matrix ratio decreases to 30 – 40%. Components of the matrix are quartz, mica and chlorite. Quartz shows ductile deformation. White mica is deformed and occurs as "mica-fish" (Photo 3-3). In addition, other ductile deformation textures formed in quartz grains include the core-mantle texture and subgrains texture (Photo 3-4). On macroscale, the phenocryst or the clasts of the brecciated rocks also demonstrate ductile deformation during shear strain (Fig.3-1).

③ Gneissic ultralmylonite

Such ultra-mylonite usually occurs within the gneissic mylonite and is 2 – 10 cm in width. The ultra-mylonite is characterized by the laminated structure of the deformed rocks. The phenocryst / matrix ratio is less than 3%. Matrix components are quartz, mica, and minor chlorite. Grain size is less than 0.01 mm, and rocks show obvious mylonite texture (Photo 3-5).

The rock types described above show certain regular spatial distribution pattern and demonstrate zonation from the undisturbed gneiss to the ultra-mylonite. The zonation occurs in the following order: mica gneiss in the undeformed country rock → gneissic proto-mylonite → gneissic mylonite → gneissic ultra-mylonite in the extremely deformed central part of the shear zone.

3.1.2.2 The Sidaogou mine area

The metasandstone of the Gaixian Formation of the Liaohe Group developed in the Sidaogou area occurs as large lenses or irregular massive blocks. Apart from the shear zone, no fabric is developed in the metamorphosed sandstone. Major minerals are dominated by quartz (55 –60 %), plagioclase (35 – 40%), and minor white mica (5%). Quartz and plagioclase occur as rounded grains with size ranging from 0.3 – 1mm. Three types of tectonite are identified.

① mylonitized metasandstone

Formed as narrow bands on the edges of weakly deformed or undeformed metasandstone blocks, the mylonitized sandstone is composed of quartz, plagioclase and white mica. These minerals generally show spatial orientation. Wavy extinction is common in quartz grains.

② sericite-quartz mylonite

The sericite-quartz mylonite is the most commonly developed tectonites in the metamorphosed sandstone. Though the dominant minerals are still the same as in the mylonitized metamorphosed sandstone, contents of plagioclase are obviously decreased. The S – C fabrics are common. Quartz grains or quartz aggregation usually form the phenocrysts, white mica and sericites distribute around the quartz phenocrysts and form the so-called "rock-bar" structure in the area, such "rock-bar" usually occurs as round, eye-shape or hook-like shapes (Fig.3-2). These rock bars may account for 30% in the deformed rocks. On microscope, deformation is mainly demonstrated by the elongated grains, kink belts deformation in minerals.

③ sericite quartz ultra-mylonite

This banded narrow ultramylonite is developed within the sericite quartz mylonite, and it is characterized by dark color, fine grain size of the ultramylonite.

Because of its dark color, this ultramylonite was once mistakenly called graphite schist in previous literatures*. Microscope observation indicates that the ultramylonite is dominantly composed of mylonitized quartz and sericite with grain size less than 0.01mm.

Occasionally quartz phenocrysts are observed with grain size varying from 0.01 to 0.05 mm. Chemical analysis results indicate the "graphite Schist" is compositionally quartz dominated (Tab.3-1). In fact, there are not much petrochemical composition differences between the ultramylonite and mylonite, the obvious difference is the phenocryst / matrix ratio which reflects that the ultramylonite is more strained during progressive shear in the shear zone.

Zonation of tectonites is not well developed in the metamorphosed rocks. But a zonation trend varying from metamorphosed arkose quartz sandstone → mylonitized metamorphosed sandstone → sericite quartz mylonite → ultramylonite is still recognizable. This zonation represents progressive deformation of weak deformation → strong deformation → extremely strong deformation processes.

3.1.2.3 The Jielishu area

This site is located at 0.5 km NE of the Jielishu gold-copper deposit. The Proterozoic silicified marble of the Liaohe group is well developed in this area. Generally, the silicified marble occurs as lenses with light gray color and massive structure. Dominant rock-forming minerals include calcite (60 – 70%), dolomite (25 - 35%) and minor quartz and sericite.

* Scientific Report of Tianjin Institute of Geology, 1991

Microscopic observation indicates that calcite shows *e* twin, while dolomite shows *f* twin, quartz demonstrates wavy or band extinction. Tectonites developed in the marble can be classified into the following five types:

① mylonitized marble

The mylonitized marble is distributed along the edges of weakly deformed or undeformed silicified marble lenses. Microscopic observation revealed that phenocrysts are dominated by calcite, dolomite and minor quartz. 1 – 3 groups of *e* twin bands are developed in calcite with 3 – 4^{th} order of interference color. The interference color bands are oblique or perpendicular to the orientation of matrix minerals. The oriented matrix minerals form the mylonite fabric. The mylonitized rocks show both mylonite and granular blastic texture.

② Marble mylonite

Marble mylonites distributed within the high strain domain. S – C fabrics are well developed. Residual phenocrysts are mainly calcite and quartz, dolomite phenocryst is minor. Phenocrysts occur as round or lens shape. The interference color bands of the *e* twin of calcite are usually nearly parallel to the orientation of elongated minerals.

The shear zone is composed of high strain domains and low strain domains. In the high strain domains, mylonite is well developed, and the mylonite usually have length of several hundred meters to several kilometers, with width of several tens of centimeters to several meters, while the weakly deformed domains usually preserve the original structure features of marbles. Ratios of matrix-phenocryst are higher than those of the mylonitized marble. Compared with the mylonitized marble, the marble mylonites have darker color and finer grain size and, in addition, dolomite phenocrysts

are obviously decreased, more *e* twins formed in calcite and they are mostly parallel to the orientation of minerals.

③ Marble ultramylonite

Characterized by gray-black color, the marble ultra-mylonite is developed within the marble mylonite zone, and it represents the strongest shear strain in marble. Residual phenocrysts are rare, rock-forming minerals are mainly composed of fine calcite, quartz, dolomite, sericite, and talc. No *e* twin is observed. Mylonite fabrics are well developed.

④ Marble blastomylonite

This type of rock has the same compositions as the silicified marble except the increased contents of dolomite. The difference is that the marble blastomylonite has much smaller mineral grain size and show equal-granular blastic texture. Sutured grain boundary is common and such boundary usually shows preferred orientation.

⑤ Marble cataclasite

Marble cataclasites are gray colored and show cataclastic texture. The cataclastic breccia takes irregular forms, and mainly show sharp-edge and round shapes. Grain size of breccia ranges from 0.2 mm to several centimeters. Under the microscope the abnormal interference color of the *e* twins in calcite is visible, when calcite is positioned at extinction, part of the twins show dark band, while the rest part show the $3 - 4^{th}$ order interference color. *f* twins are visible in dolomite, but no obvious grain boundary gliding and rotating were noticed. The matrix has the same compositions as the breccia and grain size is around 0.2 mm. No recrystallization and no oriented mineral arrangement are observed.

Marble tectonites described above usually demonstrate temporal sequence with the progressive shear strain and periodic change of stress field. A typical variation of tectonite types in spatial section occurs as in the following order: silicified marble → mylonitized marble → marble mylonite → marble ultramylonite → marble blastomylonite → marble cataclastite. This tectonite zonation in the section not only represents the spatial variation of tectonic strain, but also the dynamic evolution of the shear zone. With the evolution of the shear zone, tectonites in this section also show the following features: ① rock types changes from the weakly deformed silicified marble in the country rocks to the narrow strong strain belt in the shear zone. ② colors of rock changes from light gray to dark gray to light gray again in the ultramylonite zone. ③ contents of calcite change from major to minor, dolomite from minor to major. ④matrix-phenocryst ratio changes from low to high. ⑤ oriented flow structures changes from faint to clear, and the mylonite fabrics show the same trend. ⑥ recrystallization in rocks changes from non to complete recrystallization. The tectonite variation of the section in marble is illustrated in Figure 3-3.

3.1.2.4 The Sanguliu intrusion area

Shear zones developed in Mesozoic granites are characterized by their relatively small scales. Such shear zone is usually several to several tens of centimeters in width and several tens to hundreds of meters in length. The dominant rock-forming minerals include quartz (26%), k-feldspar (28%), plagioclase (32%), mica (5%), and hornblende (9%) as well as minor pyroxene.

Microscope observation revealed that all the rock-forming minerals involved in the shear zone were deformed in certain degree. Quartz and mica mainly demonstrate ductile deformation and wavy extinction. Subgrain, elongated quartz and mica fish are easily observed in thin sections. Plagioclase usually show brittle deformation and quartz subgrain formed in the microfractures of plagioclase (Photo 3-6).

Ductile deformation is limited in a very narrow domain, and in the high strain domains, elongated quartz grains and mica show obvious orientation. Plagioclase usually takes round shape in high strain domain.

Zonation of tectonites in the shear zone developed in granite is faint because of the small Scales of the shear zone. Generally, deformed rocks show mylonite texture, rock type is dominated by the mylonitized granite.

3.2 Characteristics of structural elements of the Wulong shear zone

On microscope scale, recognizable structural elements in the Wulong shear zone include planar fabrics, stretching lineation, kink belt, core-mantle texture of deformed quartz, pressure shadow, and subgrain. Study of structural elements has been proved an effective approach for regional stress field recovery and evaluation of the evolution of shear zone (Ramsay 1980, Simpson and Schmid, 1983). Development of these structural elements is different due to the different protoliths and strain conditions in which the Wulong shear zone is developed, and the description of structural elements will accordingly be based on individual study area.

3.2.1 The Wulong mine area

3.2.1.1 Ductile structures

Planar fabrics:

Identified planar structures in the Wulong mine area are mainly the S and C fabrics. According to Bursnall (1989), the formation mechanism of S-C fabrics can be illustrated in

Figure 3-4.

The S fabric is a kind of pervasive surface developed in ductile shear zone. C fabrics is a series of shear planes parallel to the boundary of the shear zone. The C surfaces are usually parallel to the orientation of elongated or sheet minerals such as mica and hornblende, and they are mainly developed within high strain domains and their orientations generally represent the strike of the shear zone (Fig. 3-4b). Gliding and stretching lineations are common on the surfaces of C planes, these lineations are also usually parallel to shear direction. Orientation of these lineations represents the maximum stretching direction of the strain ellipsoid.

S-C fabrics are common in the granitic mylonite in the Wulong mine area, and these fabrics are shaped by the oriented "eye-shape" plagioclase porphyroclast, elongated quartz grains and sheet micas. In general, the maximum stretching direction of the residual porphyroclasts represents the S fabric, and the direction of "tails" of deformed quartz and mica represents the C plane. Under microscope, the maximum strain plane of the "mica fish" is parallel to the S fabric, and this plane is oblique to C shear plane defined by the orientation of elongated felsic minerals.

Measurements were conducted on 59 representative S – C fabrics of the Wulong shear zone in the Wulong area. The measured data were processed and plotted on

stereonet (Fig. 3-5-c-1). The high-density area represents the preferred direction of the C fabric that strikes 120 ° and dips 45° SE. This state roughly represents the spatial position of the shear zone in the Wulong mine area.

Lineation structure:

Besides the planar fabrics, lineation fabrics were also developed on the mylonite fabrics, the most common lineation fabrics are mineral growth lineations and gliding lineations. These lineation fabrics are represented by the compressed, elongated minerals or the oriented needle-shaped minerals. 52 sets of data on lineation fabrics were measured, and the data were plotted on the Lm fabric diagram (Fig.3-5-c-2).

The results plotted on the diagram indicate that the lineation fabrics generally strike SE – NW, strike of these lineation fabrics represents the maximum stretching axis of the strain ellipsoid (X). Results of mylonite fabrics and stretching lineations plotting on the lower stereosphere show similar stress field feature (Fig. 3-6). This result suggests that the mylonite fabric and stretching lineation were formed in similar structural strain conditions.

3.2.1.2 Brittle – ductile structures

The formation of the brittle – ductile structural elements is represented by various fractures and veins developed in shear zone. The formation mechanism of the brittle-ductile fractures is well-described in literatures (Roberts, 1987, Ramsay and Huber, 1987). In the Wulong mine area, brittle-ductile deformation is characterized by the non-pervasive widely

spaced brittle-ductile shear planes and the accompaning veins. Formation of these veins can be explained by a model (Fig. 3-7) proposed by Roberts (1987). In this model, the low angle (R) and its conjugate (R') Riedel shear planes were first formed during deformation, followed by the thrust shear planes (P and P'). The principal shear fracture (D), which is usually located at the center of the shear and parallel to the shear zone boundary , is formed after the thrust shear fractures (P and P'). In the Wulong mine, the well developed brittle-ductile fractures are the C, R shears and T fractures.

The C shear:

The C shears, which define the domain of the Wulong shear zone, strike NE and are approximately equally spaced in the Wulong mine area. Examples of the C shears include the Heigou fault, the Jixingou fault and the Youpangou fault (as shown in Fig.4-2). These faults inherited the early mylonite fabric or cut the fabric with small acute-angle and show multiple-stage activities. In these shear belts, gneissic mylonite and brecciated dykes as well as fault gouges were observed. Rocks (or dykes) close to the C shears usually show passive deformation and demonstrate obvious brittle – ductile deformation features.

The R shear:

The R shears are developed within the shear zone boundaries. They are composed of a series of NNE striking and step dipping shear fractures. These fractures are equally spaced on plane and show sinistral offset .

The T fracture:

The T fractures show extension features and strike NW, dip to SW, with angle ranging from 30^{o} to 75^{o}. The T fractures usually co-exist with the R fractures. The syntectonic dykes and lodes filled the R shears and formed swarms. In haulage drift of

the Wulong mine, quartz veins hosting fractures are this type of structures and they show ductile-brittle shear deformation features.

3.2.1.3 Microscale structures

Most of the microstructure observations were based on samples collected from the Wulong gold mine. The frequently recognizable microstructures developed in gneissic mylonite include microfractures, wavy and band extinction, elongated grain (quartz), pressure shadow, subgrain, and mica-fish.

① Microfractures: microfractures are readily observed on residual plagioclase phenocryst. In some cases, the microscale sliding fractures, which distribute along twin boundaries, were filled with quartz subgrains, and these fractures can be used to analyze shear sense (Photo 3- 6).

② Wavy and band extinction of quartz or mica are probably the most common feature visible in samples. These optical features indicate that these minerals suffered ductile deformation during shear (Photo 3-7, 3-8).

③ Pressure shadows: such microstructures are not very common, but is significant in shear sense determination. In most cases, the phenocryst core was plagioclase, the shadow is either elongated quartz or rotated mica (Photo 3-9).

④ subgrain and elongated quartz grain: ductile deformation of quartz is shown in several ways. Besides its special extinction feature, the other two noticeable ductile deformation behaviors are the formation of subgrains and elongated grains. Formation of subgrain resulted from migration recrystallization of grain boundaries or rotation crystallization during shear process (Poirier and Nicholas, 1975, Poirier and Guillope,

1978). The ratio of extension axis to shortening axis of elongated quartz grain can reach 10:1 or more (Photo 3-7).

3.2.2 The Sidaogou area

Structural elements of the Wulong shear zone developed in metasandstone in the Sidaogou area can be classified into ductile deformation structures and brittle-ductile deformation structures based on their formation sequences and deformation features.

3.2.2.1 Ductile structures

Ductile deformation structures include mylonite fabric, mineral lineation, gliding lineation, passive fold, lenses, and boudinage.

S – C fabrics:

The planar structures developed in the Sidaogou area are mainly composed of oriented lenses and sheet minerals. On outcrop scale, the S fabrics are outlined by planes of the maximum flattening lenses and the "S" shaped mylonite fabrics. The tail trace of lenses usually represents the direction of C shear (Fig. 3-8). The S – C fabrics are usually developed in relatively small-scale shear zone in the metamorphosed sandstone in the Sidaogou area.

Under microscope, mica-fish is common in mylonite. The S fabrics are outlined by the elongation direction of the mica-fish, while the C fabrics are defined by the microscale high strain domains (refer to Photo 3-3). In addition, the elongated quartz grains can also be used to define the S – C fabrics (Photo 3-10). The S – C fabrics

developed in the metamorphosed sandstone of the Liaohe group are much similar to the second type of S – C fabrics described by Lister (1984). 115 sample data of the S – C fabrics were measured on outcrops at the Sidaogou area. On the stereonet diagram, the representative preferred direction of C is 45 / 125 (dip angle / striking direction, thereafter) (Fig.3-5-b-1).

Lineation: Lm

Gliding and mineral lineations dominate the lineation structures. Mineral lineations are mainly developed on the surfaces of the pervasive S planes, and are outlined by the oriented sericite fabrics. The gliding lineations mainly occur on the mylonite fabric (C surface). On the lineation fabric diagram, the preferred direction of lineation is 30 / 160 (Fig. 3-5-b-2) This direction roughly represents the shear movement of the Wulong shear zone.

Boudinage:

The boudinage structures are mainly developed in the sericite quartz mylonite. They occur as necked "quartz bar", eye-shape or pinch-and-swell structures(Fig.3-2). The maximum extension direction of boudinages represents the principal extension axis of the strain ellipsoid, and this direction is also in agreement with the orientation of gliding lineations.

Lenses:

The lenses are unique structures developed in the metamorphosed sandstone in the Sidaogou area. The lenses are dominated by metamorphosed sandstone and syntectonic quartz veins, and their scale varies from field mapping scale to hand sample or even microscale. Figure 3-8 is an example illustrating the ductile deformed lenses. The plane of maximum flattening coincide with the S plane. On steorographic projection diagram,

the lenses (and accordingly the S fabric) have a preferred orientation of 35/150 (Fig.3-9).

Intrafolial fold : Fm

The intrafolial folds were mainly developed in high strain domain of the shear zone. The deformed rock types are dominated by sericite quartzite. Fold forms are various, such as homocline tight fold, recumbent fold and "Ω" shaped fold were observed during field investigation (Fig. 3-10, Fig. 3-11). Scales of such fold are quite variable and mostly on centimeter scales. This kind of fold was probably formed during shear processes and the fold "layers" formed the S and C fabrics.

3.2.2.2 Brittle-ductile structures

Similar to the Wulong mine area, the brittle-ductile deformation structures are predominated by the C, R and T fractures.

C shear:

The C shears are series of NNE striking narrow compressive schistosities and cataclasite zones. These schistosities are mainly parallel to (but occasionally cut through with acute angles) the C fabrics formed in early mylonites. But development of the C is variable and depends on the lithological features of the host rocks. For example, in high strain domain, C shears are well developed, while in the weakly deformed metasandstone or in quartzite, the C shears are poorly developed.

R shear:

The R shears are composed of series of NNE striking shear planes dipping NW and cutting through mylonite fabric with an angle ranging $10^{\circ} - 15^{\circ}$.

T fractures:

The T structures strike NW and occur as series of extension fractures with intermediate angle dipping NE. The T fractures cut mylonite fabrics with obtuse angles. Microstructure in metasandstone mylonite is not well developed. In high strain domains, rocks were usually "ground" so fine that many workers mistakenly considered them as graphite, while in the relatively low strain domains, rocks were weakly deformed and tectonites are mainly lenses and boudinages.

3.2.3 The Jielishu area

3.2.3.1 Ductile structures

S – C fabrics:

In the marble dominant Jielishu area, the S – C fabrics are outlined by oriented marble lenses and fabrics. The maximum extension direction of marble lenses represents the S direction, and the trace of the lenses tails points to the orientation of C fabrics (Fig. 3-12).

75 measurements were taken in the field on the C fabric. On the stereonet diagram, the preferred direction is read as 45 / 140. (Fig. 3-5-a-1).

Lineation structure: Lm

The lineation structures are mainly developed in marble mylonite, and they occur as clusters of gliding lineations formed on the C planes. 45 measurements were taken in the Jielishu area on lineations. On the fabric diagram, the preferred direction is read as 30 / 140(Fig. 3-5-a-2). The dip of lineations is in agreement with that of the C fabrics.

Lenses:

Structural lenses on various scales are well developed in the shear zone in the Jielishu area. The extension axis of the lenses is in accord with the gliding lineations. Unlike the boudinages observed in the shear zone in the Sidaogou area, the boudinages "stick" each other at both ends (Fig. 3-13).

3.2.3.2 Brittle structures

Brittle fractures developed in the Jielishu area are common. The C structures developed in this area have similar deformation features as those in the Sidaogou area..

R shears:

Striking 20 – 50° and dipping NW at dipping angle of 50°, the R shears are composed of series of shear fractures.

T fractures:

T fractures are recognized in this area, which strikes NW and demonstrate extensional feature.

It's worth to note that auriferous quartz lodes are located in the R shears and T fractures in the Jielishu area, and both gold and copper occur at economic levels.

From the above description and analysis of the tectonite structures developed at the three structural sites, it is clearly shown that both ductile and brittle structures are well developed in the Wulong shear zone, the shear zone is generally striking NE and dips to NW with dipping angle ranging from 40° to55°, the shear zone shows certain reverse movement on the section direction.

3.3 Finite strain measurements of the Wulong shear zone

Ductile shear zone offers a unique opportunity to study the progressive development of mylonite microstructures and fabrics with increasing strain. They also provide, through the study of these features, an insight into the deformation processes and kinetics associated with the development of the shear zone. Shear zones, in general, are expected to form when the plastic threshold of the host materials has been exceeded (White, 1979).

3.3.1 Determination of the principal strain axis and axial strain measurements

Finite strain measurement is a method using parameters such as shape, distribution and properties of strain markers to determine the strain state during deformation processes. Finite strain measurement of deformed rocks is of significance in interpreting the deformation processes and strain mechanism.

Field investigation and microscope observation revealed that the deformed lenses, boudinages and elongated mineral grains can be used to measure the finite strain in the Wulong shear zone. Strain measurement follows the method proposed by Ramsay (1967). Once the principal axes are set to a specific strain object, the lengths of the three principal axes can be measured ($X \geq Y \geq Z$).

The Flinn parameter (K) can be used to measure the strain states and mechanism. According to Flinn (1962), the calculation of the K value can be expressed as:

$$K = X(Z-Y)/Y(Y-X)$$

X, Y, Z, are principal strain axes

Different K values represent different strain mechanism and strain ellipsoid.

$$K = \begin{cases} 0 & \text{Uniaxial oblate ellipsoids type} \\ 1 & \text{Plane strain ellipsoid type deformation} \\ 0<K<1 & \text{Flattening ellipsoids type deformation} \\ 1<K<\infty & \text{Constriction ellipsoids type deformation} \end{cases}$$

The advantage of this method is that the X, Y, Z values on the principal axes of the strained object can be either measured on macroscale (i.e. field outcrop of lenses or boudinage) or on microscale (i.e. deformed quartz grain or subgrain size on oriented thin sections).

3.3.1.1 The Wulong area

Mylonite is very well developed in the Wulong area, and many microscale structures (such as sutured grain boundary, compressed grains, elongated grains) are readily observed, but structural lenses and boudinages are not common, so the finite strain measurement is based on microscale samples in this area.

Oriented thin sections of two directions (XZ and YZ) were prepared in the Yichang Institute of Geology of The Chinese Academy of Earth science. The XZ and YZ axes are parallel to mylonite fabrics and mineral lineations, respectively. Quartz

grain size was measured under microscope. All the measured data are processed using the equation proposed by Robin (1977).

$$\text{Log } R_j = (1/n)\ \Sigma\ \log(a_j/c_j), \qquad (j=1,2,3,\ldots n)$$

R_j : strain axial ratio of the strained mark on the j plane, a_j, c_j are the length of the long axis and short axis, respectively, n the number of measured strain marks.

The measurement results from five different sites of the Wulong area are listed in the table 3-2. The Flinn parameter (K) values of strained quartz grains range from 0.51 to 0.17, the average value of K is 0.37, $R_{x/z}$=6.04, $R_{y/z}$=3.27, the three axial ratio of X : Y : Z=1.85 : 1 : 0.31. On Wood diagram (Fig.3-14), the extension ratio along X axis is 125%, on Y axis is 16%, while on the Z axis, it was shorten 62%.

In summary, the shear strain in the Wulong area shows flattening ellipsoid type deformation (0<k=0.37<1). Azimuth of the plane of maximum flattening of the strain ellipsoid is 45 /130, this azimuth is in agreement with the pervasive fabrics in the shear zone, the azimuth of Z axis is 42/310, X axis is 42/132.

3.3.1.2 The Sidaogou area

According to Robin (1977), orientation of the tectonites were cut along the principle XZ, YZ strain planes as illustrated in figure 3-15.

The measured data are plotted on the Z vs.Y and X vs. Z coordinates (Fig. 3-16). The slope of the fitting line crossing the point of origin is the axial ratio of the strain ellipsoid on which the plane was measured.

The calculated average axial ratios of the measured sections are: $R_{x/z}$=2.90, $R_{y/z}$=1.80. Average Flinn parameter (K)=0.76. The three axial ratio is X : Y : Z=1.61 : 1 : 0.56. On Wood diagram, the X axis extends 65%, the Y axis extends 4%, while the Z axis shorten 40% (Fig.3-14).

Calculation results also indicate that the sericite quartz mylonites suffered flattening deformation (0<K=0.76<1). Since the K value is close to 1 and the extension along the Y axis is 4%, which is negligible, so the shear activity in the Sidaogou is similar to a simple shear of planar strain. Azimuth of the plane of maximum flattening on the diagram is 40 /125, this plane represents the S fabric, the azimuth of the X axis is 40 /145, and the Z axis is 46 /305.

3.3.1.3 The Jielishu area

Marble lenses were used to measure the finite strain in the Jielishu area as these lenses show excellent ductile deformation feature. Field measurements were carried out at an open pit (No.4) in the Jielishu mine. The XZ, YZ strain planes were determined based on the spatial relationships among the plane of the maximum flattening, mylonite fabric and the gliding lineation on the mylonite fabric. The measured data are listed in table (tab.3-3). The algorithm value ($R=(1/n)\sum R_i$) of all the measurements at one site was used to represent the preferred direction of the axial ratios of the strain ellipsoid. The final calculated results are $R_{x/z}$=3.14, $R_{y/z}$=1.76, the three axial ratio of the strain ellipsoid is: X : Y : Z=1.78 : 1 : 0.57, the Flinn parameter K=1.03. On Wood diagram, the plotted result indicates that the marble lenses were stretched 72% along X axis, no change on the Y axis and Z axis shortened by 40% (Fig.3-14).

The Flinn value (K≈1) suggests that marble lenses have been subjected to pure plane shear during deformation. The azimuth of the plane of maximum flattening is 55 /135, azimuth of X axis is 53 / 140, and 35 / 315 for the Z axis.

3.3.2 Shear strain measurements

The development of microstructure in mylonites with increasing shear strain has been the subject of many papers (i.e. Lister et al., 1977, Brown et al., 1980). According to White et al., (1980), with increasing shear strain (γ), a coarse-grained quartzite is converted into a protomylonite, then into a mylonite and finally into an ultramylonite, and the percentages of recrystallization increase during progressive deformation processes.

According to Ramsay (1980), the shear strain can be quantitatively described at various portion on a profile crossing shear zone based on the angle relation between the S and C fabrics in shear zone. The relation between shear strain and the angle of S and C can be expressed as:

$$\gamma = 2/\tan 2\theta'$$

θ': angle between S and C fabrics, γ: shear strain. Generally, from boundary to the center of shear zone, the angle gradually decreases because strain gradually increases toward the center of shear zone, and the orientation of fabrics will be sub-paralleled to the maximum extension axis of the ellipsoid.

Measurements of shear strain at various portions in the shear zone were undertaken by collecting oriented samples from several representative areas in the shear zone. The measured and calculated data are listed in the Table 3-4.

In addition, the modified R/Ø method by Jensen (1984) was also used to weigh the strain variation in the shear zone sections. Like the method discussed above, the R/Ø method, which was first introduced by Dunnet in 1969, is based on the assumption that the strain markers are randomly distributed and there is no viscous difference between matrix and markers. The relation between the axial ratio (R) and the orientation of the long axis in relation to the trace of the fabric (Ø) is strictly related to the intensity of the strain in the shear zone.

The measured samples were mainly from the Wulong and the Sidaogou areas. The grain shape is approximated by an ellipse, and for each grain the long axis (X) and short axis (Z) as well as the orientation of the long axis in relation to the trace of the fabric (Ø) were measured (if they were possible). Two mutually perpendicular planes (YZ and XY) were cut perpendicular to the fabric in each sample, so that one plane is parallel and the other is perpendicular to the lineation. Table 3-5 shows the measured data at the Sidaogou area and the data measured from the Wulong area are listed in Table 3-6. The following diagrams are the R/Ø plots of fabrics of deformed quartz grains at different sites in the Wulong shear zone (Fig.3-17, Fig. 3-18).

In summary, regardless of the lithology of the deformed rocks involved in the Wulong shear zone and the measurement methods, measured, calculated and plotted results suggest that the orientation of planes of the maximum flattening of various strain markers are in agreement with the principal axes of the strain ellipsoid. The plane of the maximum flattening of the strain markers is parallel to the foliation plane (S). Azimuth

of the long axis (X) of strain ellipsoid agrees with the dipping direction of the mylonitic lineations. The dipping direction of the short axis of the strain ellipsoid is perpendicular to that of the mylonite fabric and dipping to NW, the intermediate axis is generally stretching horizontally and striking NE – SW.

On Flinn diagram (Fig. 3-19), plots of the average K values from the Sidaogou and the Jielishu sites are on or close to the K=1 line, while plot of the Wulong area falls in the flattening area. These plots represent the strain features of rocks in different stress states. But in general, the Wulong shear zone was dominated by simple shear strain during its development.

The finite strain and the azimuth of the principal axes of the strain ellipsoid in different sections of the Wulong shear zone are summarized in Table 3-7.

3.4 Estimate of P-T conditions and strain rates in the Wulong shear zone

One of the difficulties in P-T estimation of the Wulong shear zone is that we must distinguish the metamorphic facies pertaining to the shear zone itself and the country rocks. The metamorphic facies of the country rocks vary from the amphibolite facies at the Wulong mine site to the greenschist facies in both the Sidaogou mine and the Jielishu mine. To recognize and identify the metamorphic grade pertaining the shear process, series of mylonite rock samples were observed under microscope to identify mineral associations in the shear zone. In addition, fluid inclusions were used to evaluate the thermal conditions during shear zone processes. Petrological and mineralogical studies revealed that, irrespective of the host rock types and their metamorphic facies in the Wulong mine camp, typical mineral associations within the

Wulong shear zone are Quartz + albite + sericite + epidote + calcite + chlorite. These mineral associations indicate that the shear zone was formed in greenschist facies environment, and the temperature range in which the greenschist facies was formed were between 300 – 400°C according to the metamorphic facies vs P-T diagram proposed by ConGillen (1985).

Previous work revealed that ultimate size of recrystallized grains in a monominerallic mylonite is dependent upon stress, strain rate and to a lesser extent of temperature (Mercier et al. 1977, Twiss 1977, White 1979). Many methods have been used to estimate paleopiezometers based on the microstructures formed in deformed quartz grains such as free dislocation, grain size of subgrain and dynamic recrystallization. The relations between subgrain size, recrystallized grain and stress has long been studied (Dunnet, 1969, Twiss 1977, Mercier et al., 1977, Robin, 1977, Fry, 1979, Jesen 1984, Lister 1984), and the function between grain size of recrystallized grain and the paleopiezometer can be expressed as :

$$\sigma = \kappa * D^{-\mu}$$

here, κ and μ are constants, σ is differential stress ($\sigma 1$-$\sigma 3$) (unit : MPa), D is grain size of recrystallized minerals (unit :μm).

Researchers gave different κ, μ values based on their different experimental materials and conditions, the representative κ, μ values obtained from dynamically crystallized quartz are listed in the table 3-8.

We use the κ, μ values recommended by Twiss since the two parameters are obtained from dry quartz experiments since we may assume that the shear processes in the deep crust were undertaken without the participation of fluids.

Strain rate during ductile deformation processes depends upon stress, temperature. In the condition of "dry" quartz deformation, the strain rate of quartz can be expressed as :

$$\varepsilon = A * \sigma^{n} exp(-10^{3} * Q/RT)$$

here, A : the thermal sensitive coefficient of material; R : the constant of gas (R=8.314 $Jk^{-1}mol$); σ: stress difference; T : temperature (^{o}K); assuming shear strain was undergone in "dry" quartz condition, A=6.7 x 10 $kbar^{-n}$ sec^{-1} , n=6.5, Q=267.52 kJ/mol (Mercier et al.,1977). Listed in table 3-9 are measured and calculated results of differential stress and the strain rates.

These calculated results indicate that, from ultramylonite to mylonite, and from the Wulong area to the Sidaogou and to the Sanguliu intrusion, the differential stress decreases. The ultramylonite in the Wulong area has the highest calculated differential stress of 146.6 MPa, while mylonite developed in the Sanguliu intrusion has the lowest value of differential stress of 61.1 MPa. The range of differential stress falls in the equivalent depth range of 2 - 6 km with the normal lithopressure gradient of 27.5MPa/km.

The calculated results indicate that ultramylonite developed in the Wulong mine area has the highest shear strain rates, while the lowest strain rate is in the shear zone developed in the Sanguliu intrusion.

3.5 Determination of shear sense of the Wulong shear zone

Shear processes not only cause the realignment of proto-structutre such as the original S and C fabrics or mineral lineations in host rocks, but also form new orientation of minerals or structures such as the macroscale boudinages and microscale mica-fish in the new formed mylonites. That is, these structures bear some imprints of shear processes. In fact, structural geologists found that preferred orientation of mineral lineations, gliding lineations, asymmetric rotating syntectonic structures both on microscales and macroscales are reliable shear criteria. Many structural geologists studied the possible genetic mechanism and their application in shear sense determination (Ramsay 1980, Simpson and Schmidt 1983, Lister and William 1979, Lister and Snoke 1984).

Based on field investigation, the following structural markers were reliable indicators of shear sense determination for the Wulong shear zone.

The S – C fabrics developed in gneissic mylonite and sericite-quartz mylonite (Fig. 3-8)

② Asymmetric lenses developed in the metasandstone and marble (Fig.3-10)

③ Microscale structural criteria such as "mica-fish", microfractures and oriented fabric minerals (Photo 3-3, Photo 3-6, Photo 3-9),

④ Orientation of quartz optical axis (Fig.3-20).

⑤ Various dykes and auriferous quartz lodes filling in the C• , R shears and T fractures in the shear zone are also excellent shear sense indicator. In the Wulong mine area,

auriferous lodes filling along the R shears demonstrate sinistral shear on plane (Fig.3-21).

In summary, the Wulong shear zone was formed in an environment of greenschist facies. Differential stress of the shear zone ranges between 61 – 146 MPa, which is equivalent of 2-6 km in depth. Though the strain stress and strain rates are quite variable from place to place in the shear zone, the shear mainly demonstrates simple shear, both the ductile and brittle structures are well developed in the shear zone. the Wulong shear zone shows sinistral with certain reverse movement.

3.6 Geochronological constraints of the Wulong shear zone

As its parental tectonic system - the Tancheng – Lujiang continental fault zone , the geochronology of the Wulong shear zone is quite disputed (Zhang 1992). Hu (1984) suggested that the shear zone existed as early as Precambrian because of the lithologic differences on both sides of the shear zone. While other workers (Xu et al., 1987) proposed that the shear zone was formed during Mesozoic. In this study, the geochronologic constraints of the Wulong shear zone is examined based on field investigation and isotope geochronological evidences.

3.6.1 Fossil chronological constraint of the Wulong shear zone

Before 1983, metamorphosed sandstone and schists were grouped into the Gaixian Formation of the Liaohe group in all literatures discussing geology of the

Sidaogou area, and all lithologic units involved in the Wulong shear zone were assumed to be Precambrian.

It was in 1983 that the first phylolite was found in shales in the Sidaogou area by a geologist named Ma (Wang 1996), since then, more phylolites and zoolites were found by Wang from 1992 to 1996. The fossil-containing strata were confined in the Wulong shear zone (Fig.3-22).

Identified fossils found in the area include:

Phylolite: Phoenicopsis, sp (T-K)

Podozamites (T3-K2);

Taenioptteris (C3 – K);

Pityophyllum sp (T3-K).

Zoolite: Mesoblastus (C1) and bivalve fossils.

These fossils were mostly well developed in the Mesozoic. These fossils involved in the Wulong shear zone indicated that the Wulong shear zone was active at least as late as Mesozoic. In NE China that period was the peak of the Yanshanian tectonism. From this point of view, it is clear that the Wulong shear zone was the result of the Yanshanian movement (whether or not the shear zone pre-existed the tectonism), at least, the shear zone was reactived at the Yanshanian event.

3.6.2 Isotope geochronological constraint of the Wulong shear zone

The Wulong shear zone not only controls the Wulong gold camp, but also controls various dykes. In fact, some dykes and the Wulong shear zone show conjugate

relationship, which indicates that the dykes were syntectonic results of the shear processes. Details of this relationship will be discussed in the following chapters. For these dykes, their geochronological ages can be used to constraint the formation ages of the shear zone.

21 samples including gneissic mylonite, sericite-quartz mylonite, Sanguliu granite, dioritic porphyry and granodioritic porphyry were analyzed using K-Ar age dating method. The analyzed data were plotted on the ^{40}Ar-^{40}K diagram (Fig.3--23). The plotted data indicate that isochrons of these geological bodies are mainly confined between 73 Ma and 156 Ma, and mainly concentrate on the isochron of 122Ma. It's clear that mylonites have three clusters of ages. The first cluster is located on the 156 Ma isochron, this line probably marks the first activity of the Wulong shear zone followed by a dense cluster of plots of the Sanguliu intrusive, granitic porphyry, dioritic porphyry, and sericite-quartz mylonites. The final group includes mylonites and dioritic porphyry. These Ar-K isotope data groups coincide with field evidences (refer to the next chapter about the relationships among the shear zone, mineralization and dykes).

3.7 Geochemical and mineralogical processes within the Wulong shear zone

Numerous works revealed that shear zone system not only involved strong structural events, but also resulted complex geochemical processes such as fluid flow, formation of new minerals, alteration and ore deposition (Cox et al., 1995, Ferry, 1989, Fisher 1987, Fisher and Byrne 1990). Many workers studied quantitative change of the geochemical processes during shear processes (Vrolijk, 1987). In this part, mineral

associations, REE contents of various mylonites and the gains and losses of materials within the shear zone domain will be discussed.

3.7.1 Mineralogical and geochemical features in mylonites

Samples from two sections across the Wulong shear zone were collected from the Wulong mine area and the Sidaogou area. Mineral association study and mineral content statistics were done under microscope. The statistic results of major mineral contents were plotted on the section corresponding to the position where the samples were collected (Fig.3-24, Fig.3-25).

Contents of major elements were analyzed on representative samples at different locations of the shear zone. Analyzed data are listed in table 3-1. In addition, contents of rare earth elements were analyzed in several samples collected from two sections of the Wulong shear zone. The data are listed in table 3-10.

These data in the table 3-1 and table 3-10 as well as the mineral content curves across the sections indicate that, from the boundary to the center of the shear zone, contents of quartz and white mica usually increase while plagioclase demonstrates a reverse trend. REE distribution pattern curves don't demonstrate differences with the progressive shear strain in the Wulong gold camp. This result is in agreement with that in the Hetai gold deposit, which is also a typical shear zone-hosted gold deposit in south China (Cheng and Wang, 1993)

3.7.2 Mass balance analysis in the shear zone

From the point of geochemical processes, in general, shear zone is characterized by breakdown of feldspar, biotite and formation of sillimanite, quartz and various fluids. Silica, alkali, and alkali earth elements were mobile during shear processes. Mass-balance calculations, based on major- and trace-element geochemistry, indicate as much as 50% - 60% volume loss in mylonites (Grant, 1986). Fluid / rock ratios estimated from the calculated depletions of silica are as much as 200 - 400, which indicate that the initiation and activity of the shear zones were accompanied by large amounts of fluids that infiltrated shear zones (Gresens, 1967, Morton and Nebel, 1984). Actually, shear zone activity not only involves extensive structural processes, but also strong chemical processes.

3.7.2.1 Principals of mass-balance analysis in shear zone

Mass-balance method can be used to measure the gains and losses of materials that occurred in shear zone. Before anything can be done in the gains and losses evaluation of material, the first critical work is to determine what the original rocks are before mylonitization processes. This can be achieved through careful fieldwork and (or) through petrochemical methods to identify the protoliths in the study area (Akella, 1966, Appleyard 1980, Olsen 1985, Grant, 1986, Liu et al., 1993). As described in the second chapter, the protolith identification in this area was based on petrochemical data.

Once the "original" rock is determined, the comparison of material gains and losses between the original rocks and deformed rocks is usually done under some

assumptions. These assumptions include: ① constant mass before and after structural deformation; ② constant volume during shear processes; ③ relatively immobile element components such as alumina or titanium during shear processes, this assumption is where the isocon method stands on.

For an original rock with a mass of M^0, after shear and alteration processes, mass of the deformed rock is M^A. The mass difference is ΔM. For any component (i) of the rock, its mass change after the deformation accordingly becomes:

$$M_i{}^A = M_i{}^0 + \Delta M_i \quad \text{----------(1)}$$

Dividing the equation (1) by M^0 to get concentration units, then:

$$M_i{}^A/M^0 = M_i{}^0/M^0 + \Delta M_i/M^0 \quad \text{----------(2)}$$

In fact, the ratio of $(M_i{}^0/M^0)$ is the original concentration of component *i* in the rock (M) before mylonitization. To get the final concentration (after the mylonitization) of the component *i* in the rock (M), multiplying equation (2) by (M^0/M^A):

$$M_i{}^A/M^A = (M^0/M^A)*(M_i{}^A/M^0) = (M^0/M^A)*[(M_i{}^0/M^0) + (\Delta M_i/M^0)]$$

Defining the concentration unit: $C_i{}^A = M_i{}^A/M^A$, then:

$$C_i{}^A = (M^0/M^A)(C_i{}^0 + \Delta C_i) \quad \text{----------(3)}$$

So, for any component in the rock, there is an equation of this form, in which (M^0/M^A) is constant. If we can identify in particular those components (the immobile components) for which $\Delta C_i=0$, then the concentration form is changed into the form of:

$$C_i^A = (M^o/M^A)*C_i^0 \qquad \text{----------(4)}$$

Clearly, this is a straight line across the origin, the slope is (M^0/M^A). This line, as $\Delta C_i=0$, is called "isocon", which means " a line connecting points of equal geochemical concentration" (Gary et al., 1974).

If alumina is assumed to be constant during shear processes, then from equation (3) we have:

$$(M^0/M^A)=(C_{Al2O3}{}^A/C_{Al2O3}{}^0),$$

and then the isocon equation becomes:

$$C_i^A=(C_{Al2O3}{}^A/C_{Al2O3}{}^0)*C_0,$$

If mass is assumed to be constant, then $M^0/M^A=1$, so

$$C_i^A=C_i^0,$$

If volume is assumed to be constant, then

$$C_i^A=(\rho_0/\rho_A)*C_i^0,$$

Here, ρ represents density of rocks.

Then the relative gains and losses of (mobile) components are given by the displacements of data points for all other components from the reference isocon.

But probably the most useful measure of gains and losses is the concentration change of components relative to its original concentration (prior to shear process or hydrothermal alteration). This is reached by dividing both sides of equation (3) by C_i0,

$$C_i^A/C_i^0=M^0/M^A[(C_i^0/C_i^0)+(\Delta C_i/C_i^0)]$$

After arranging the equation, we obtain:

$$(\Delta C_i/C_i^0)=(M^A/M^0)(C_i^A/C_i^0)\ -1, \quad \text{-------(6)}$$

In general, the (M^A/M^0) is determined from the best-fit isocon, if constant alumina is assumed, then

$$(\Delta C_i/C_i^0)=(\ C_{Al2O3}{}^0/C_{Al2O3}{}^A)(C_i^A/C_i^0)-1,$$

if constant mass is assumed,

$$(\Delta C_i/C_i^0)=(C_i^A/C_i^0)-1,$$

if constant volume is assumed,

$$(\Delta C_i/C_i^0)=(\ \rho_A/\rho_0)(C_i^A/C_i^0)\ -1,$$

Once the protolith is identified, and the isocon type is chosen, the gains and losses of each (mobile) component relative to concentrations in the original rock can be either graphically determined or calculated using the equation given above. In this project, the calculation method is chosen to compute the concentration change of the mobile components (only the major elements were used during the calculation) during shear processes, and a constant titanium is assumed during calculation.

3.7.2.2 Calculated results and interpretations

The calculated results are plotted on concentration vs. component diagram. These diagrams can give direct visual effect on the gains and losses of the (mobile) components.

In the Wulong mine area, it is clear that during the progressive deformation from gneiss to final ultramylonite, elements gained include Si, Al, K, Na, Mn, C (CO2), lost elements include Mg, P. Some elements show different behaviors at different processes, for example, Ca was gained during the transition from gneiss to protomylonite; while this element was lost when protomylonite was transitioned to mylonite, and finally increased at the last transition stage from mylonite to ultramylonite. Fe^{3+} was always lost, and Fe^{2+} increased during these processes (Fig.3-26). These gains and losses of elements reflect complex variation of fluid processes in the shear zone. In the Sidaogou mine area, Si, Ca, Na, Mn and C (CO2) were lost, only Fe and H_2O were involved in net gain during tectonite type transition, (Fig.3-27). In the Jielishu area, Si, K, Na, Fe are

gained in the shear processes, the gain of Mg is probably related to the dolomitization developed in the shear zone (Fig.3-28).

Table 3 - 1 Contents of major elements in progressive deformed mylonites in the Wulong gold camp, Liaoning province.

Locality	Rock type	Sample	SiO_2	Al_2O_3	CaO	MgO	K_2O	Na_2O	TFe	TiO_2	P_2O_5	MnO	CO_2	H_2O
Wulong area	Proto-mylonite	Am-13	72.35	14.96	1.58	0.23	3.35	4.09	1.53	0.2	0.02	0.07	0.15	-
	Mylonite	Am-20	73.8	14.1	0.5	0.11	4.59	3.69	1.34	0.17	0.03	0.08	0.22	-
	Ultra-mylonite	Am-81	73.71	14.15	0.84	0.14	4.07	4.29	1.21	0.16	0.02	0.06	0.22	-
Sidaogou area	Metasand	S1-7-2	73.02	10.87	2.69	1.55	2.38	2.57	3.47	0.37	0.10	0.116	2.2	1.48
	Schist	S1-6-1	63.06	12.17	3.32	3.12	3.03	1.99	6.06	0.5	0.13	0.13	1.14	2.6
	Sericite-qtz-mylonite	S1-12	59.91	19.12	0.87	3.01	4.14	1.08	8.24	0.56	0.17	0.12	1.73	3.55
	Ultra-mylonite*	S5-1	57.09	17.63	0.45	2.73	4.69	1.3	9.62	0.69	0.14	0.036	0.51	5.44

* the ultramylonite developed in the shear zone of the Sidaogou portion was once mistakenly recognized as "graphite" due to its bright gray color on the surface (Liu et al., 1991).

Data are cited from Wang Y M. (1990).

Table 3-2 Measurements of the dynamically recrystallized quartz grains in the gneissic tectonites in the Wulong area.

Sample No.	Location	Rock types	$R_{X/Z}$	$R_{Y/Z}$	K
W2-12	Level 12, #2 site	Gneissic proto-mylonite	4.80	2.63	0.51
WD4	Haojinggou	Gneissic mylonite	5.25	2.85	0.45
WD24	#4 open-pit	Gneissic mylonite	6.34	3.24	0.43
WD5	Ore processing Mill of the Wulong mine	Fine-grained granite mylonite	6.58	3.41	0.39
W3-6	Level 6, #3 site	Gneissic ultra-mylonite	7.21	4.20	0.17
Average			6.04	3.27	0.37

Table 3-3 Measurements of X, Y, Z parameters of marble lenses in the Wulong shear zone in the Jielishu area

No.	X_{axis}(cm)	Z_{axis} (cm)	$R_{X/Z}$	Y_{axis} (cm)	Z_{axis} (cm)	$R_{Y/Z}$
1	7.60	2.40	3.17	1.70	1.10	1.55
2	4.00	1.50	2.67	8.50	4.80	1.77
3	6.50	2.10	3.09	13.50	7.60	1.78
4	9.40	3.50	2.69	12.40	7.00	1.77
5	12.80	4.10	3.12	5.30	3.10	1.71
6	8.50	3.10	2.74	2.70	1.50	1.80
7	14.0	4.50	3.01	6.00	4.10	1.46
8	2.80	0.80	3.50	9.40	5.30	1.77
9	8.00	2.60	3.08	4.00	3.10	1.29
10	4.50	1.70	2.64	8.20	4.30	1.91
11	5.80	1.90	3.05	18.60	10.50	1.77
12	16.00	5.20	3.08	9.00	5.10	1.76
13	13.50	4.40	3.07	13.00	7.30	1.78
14	18.50	6.10	3.03	4.50	2.60	1.73

(Table 3-3 continued)

15	11.70	3.80	3.08	16.00	9.70	1.65
16	5.20	2.40	2.17	4.80	2.40	2.00
17	10.20	3.20	3.19	15.20	7.90	1.92
18	13.00	4.20	3.10	7.20	4.10	1.76
19	4.70	1.20	3.91	14.00	6.90	2.03
20	15.00	4.80	3.13	2.40	1.40	1.71
21	7.20	2.00	3.60	16.50	9.40	1.75
22	7.30	2.60	2.81	3.70	2.10	1.76
23	25.00	8.00	3.13	17.10	9.70	1.76
24	8.80	3.10	2.84	5.00	2.80	1.79
25	23.00	7.40	3.11	12.80	7.20	1.78
26	13.50	4.10	3.38	6.80	3.90	1.74
27	20.10	6.50	3.09	8.80	5.00	1.76
28	16.40	5.40	3.04	10.50	6.00	1.75
29	17.00	5.50	3.09	7.30	4.00	1.83
30	12.70	2.90	4.38	7.80	4.40	1.77
31	15.40	5.00	3.08	11.30	6.40	1.76
32	16.80	6.00	2.80	2.00	1.90	2.22
33	12.00	2.80	4.28	10.00	5.70	1.75
34	4.00	1.30	3.08	4.50	2.20	2.01
35	13.00	4.10	3.25	5.80	3.30	1.76
36	8.00	2.70	2.96	5.60	2.80	2.00
37	15.00	4.80	3.14	6.00	4.80	1.25
38	14.00	3.80	3.68	9.50	6.80	1.40
39	22.00	7.30	3.01	6.50	3.70	1.76
40	21.30	7.00	3.04	10.20	5.70	1.79
Average			3.14			1.76

Table 3-4 Measurements of the azimuths of S, C on oriented hand samples and Calculated shear strains in the Wulong shear zone.

Area	Sample	Tectonite types	Azimuth (C)	Strikes (S)	θ	γ
Sidaogou area	SB1-1	protomylonite	40/150°	55°	15°	3.5
	SD21-1	mylonite	50/138°	40°	10°	5.5
	SB3	Ultramylonite	50/145°	35°	5°	11.3
Wulong area	WD8	protomylonite	58/105°	35°	17°	3.0
	WD4-2	mylonite	55/115°	38°	13°	4.0
	WD2-1	ultramylonite	56/155°	26°	6°	9.5

Table 3-6 Measured and calculated strain parameters of mylonites from representative samples in the Wulong area

Sample	Rock type	Strain domain	$R_{X/Y}$	$R_{Y/Z}$	K	R_f
Am-62	Protomylonite	low strain domain	1.23	1.89	0.258	2.40
Am-4	Mylonite	transition zone	1.45	2.46	0.308	3.60
Am-70	Ultramylonite	high strain domain	1.65	3.48	0.267	5.70

Table 3-5 Measurements of axial ratio and fai values on oriented hand samples in the Sidaogou area.

Sample No.	X	Y	φ	$R_{X/Y}$	Y	Z	φ	$R_{Y/Z}$	Sample No.	X	Y	φ	$R_{X/Y}$	Y	Z	φ	$R_{Y/Z}$
95S-14 (X : Y : Z=3:1 :0,4, K=1,2)	14	7	-20	2	5	2	-15	2,5	95S-15 (X : Y : Z=3:1 :0,3, K=1,0)	10	4	+30	2,50	8	3,00	+6	2.66
	13	6	+15	2,1	7	3	-16	2,3		11	5	-16	2,20	1,1	4,00	+10	2.75
	12	4	+2	4	6	3	+15	2		7	2	-15	3,50	12,0	4,00	+11	3.00
	13	4	+5	3,25	4	2	+17	2		10	4	-12	2,50	12,0	4,00	-4	3.00
	12	6	-10	2	8	3	-9	2,6		12	4	+17	3,00	10,0	5,30	-10	2.00
	14	7	-4	2	7	3	-10	2,3		15	5	-16	3,00	8,0	3.30	+11	2.66
	15	4	-6	3,75	6	2	+8	3		14	6	-6	2,30	7,0	3.50	-20	2.33
	20	6	+21	3,3	7	3	+10	2,3		12	5	-19	2,40	5,0	2.00	-14	2.50
	11	4	-19	2,7	8	4	+12	2		7	4	+22	1,75	4,0	2.00	+21	2.00
	12	3	-20	4	9	4	+13	2,26		9	3	+24	3,00	6,0	2.20	+8	3.00
	15	6	+8	2,5	10	4	-14	2,5		8	7	+25	2,66	7,0	3.00	+9	2.33
	12	5	+12	2,4	5	2	-9	2,5		6	3	-16	2,00	9,0	3.10	+10	3.00
	13	4	-13	3,25	8	3	-8	2,6		5	2	-15	2,50	8,0	3.10	-11	2.66
	16	7	-15	2,3	4	2	+8	2		4	2	-14	2,00	7,0	2.00	-3	3.50
	18	6	+17	3	7	3	+7	2,3		11	4	+7	2,75	6,0	2.00	-5	3.00
	19	7	-14	2,7	6	2	+16	3	95S-17 (X : Y : Z=3:1 :0,3, K=1,0)	12	4	-10	3.00	5	2	-16	2.50
	11	4	+6	2,75	8	3	+20	2,7		11	3	-21	3.66	4	2	-7	2.00
	12	5	-8	24	7	3	-21	1,8		13	4	-5	3.25	3	1	+5	3.00
	13	5	+16	2,6	9	5	-19	1,8		15	5	+6	3.00	5	2	+21	2.50
	14	6	-14	2,3	10	5	+18	2		14	4	+11	3.50	7	3	+30	2.33
	17	5	+17	3,4	7	4	-6	1,75		12	4	+25	3.00	9	4	+16	2.25
	15	7	+10	2,14	6	13	-7	2		9	3	-16	3.00	10	4	+17	2.50
	16	4	+12	4	7	2	+10	3,5		8	2	+17	4.00	8	4	+6	2.00
	10	4	-11	2,5	8	3	+11	2,6		6	2	-9	3.00	6	3	+6	2.00
	7	2	-13	3,5	91	4	+12	2,25		15	5	+6	3.00	4	2	+7	2.00
95S-15 (X : Y : Z=3:1 :0,3, K=1,0)	9	4	-31	2,25	7	3	-16	2,33		16	5	+17	3.20	4	2	-5	2.00
	8	3	4	2,66	8	3	-17	2,66		18	6	+18	3.00	3	1	+32	3.00
	6	3	6	2	9	4	-20	2,25		17	6	+20	3.00	5	2	-31	2.50
	7	4	-7	1,75	6	2	25	3		14	5	-5	2.80	7	3	-16	2.30
	10	4	-16	2,5	9	3	18	3		13	4	-7	2.80	8	3	-19	2.66
	11	5	-12	2,2	12	4	17	3		12	4	+11	3.00	4	2	-21	2.00
	12	5	-18	2,4	6	2	14	3		11	4	+12	2.75	6	2	-5	3.00
	14	6	9	2,3	9	3	-21	3		15	4	+16	3.75	7	3	+6	2.33
	7	3	16	2,3	7	3	-5	2,33		9	3	-3	3.00	6	2	+10	3.00
	9	4	21	2,25	6	6	-4	1,5		8	3	-6	2.66	10	3	+11	3.33

(Table 3-5 continued)

Sample No.	X	Y	φ	Rx/Y	Y	Z	φ	Ry/Z	Sample No.	X	Y	φ	Rx/Y	Y	Z	φ	Ry/Z
95S-15 (X : Y : Z=3:1 :0,3, K=1,0)	6	2	+11	3.00	10	3	+15	3.33	95S-22-1 (X : Y : Z=3:1 :0,4, K=1,0)	14	4	-21	3.50	8	4	+16	2.00
	7	3	+3	2.33	8	4	+16	2.00		12	3	-15	4.00	7	3	+7	2.33
	9	3	+4	3.00	6	3	-17	2.00		11	3	-6	3.66	5	2	+25	2.50
	10	3	+15	3.33	7	3	-18	2.30		16	4	+5	4.00	6	2	+30	3.00
	11	3	-16	3.66	6	3	-9	2.00		14	4	+7	3.50	4	2	+16	2.00
5S-21 (X : Y : Z=3:1 :0,3, K=1,2)	15	5	-6	3.00	6	3	-17	2.00		12	3	+19	4.00	7	3	-16	2.33
	16	5	-20	3.20	7	3	-6	2.33		11	3	+25	3.66	6	3	-15	2.00
	14	5	-17	2.80	6	2	-6	3.00		9	3	-8	3.00	8	3	-30	2.66
	17	6	+20	2.80	9	3	+7	3.00		10	3	-11	3.33	5	2	-31	2.50
	16	6	+16	2.66	8	3	+15	2.66		8	3	-12	2.66	4	2	-5	2.00
	14	4	+6	3.50	3	1	+6	3.00		7	2	-15	3.50	3	1	+4	3.00
	13	4	+7	3.25	4	2	+31	2.00		15	5	+16	3.00	3	1	+7	3.00
	12	3	+4	4.00	5	2	-10	2.50		14	5	+6	2.80	4	2	-9	2.00
	14	4	+25	3.50	4	2	-30	2.00		13	4	+15	3.25	5	2	-6	2.50
	14	3	-16	4.66	6	3	-15	2.00		15	8	+6	2.40	4	2	-4	2.00
	15	5	-14	3.00	7	3	+6	2.33		12	5	-4	2.40	3	2	+15	1.50
	17	5	-10	3.40	4	2	+8	2.00		11	5	+7	2.20	4	2	+16	2.00
	9	2	-15	4.50	5	2	+9	2.50		15	5	-15	3.00	6	3	-3	2.00
	11	3	-6	3.66	3	7	-12	3.00		9	4	-16	2.25	9	4	-6	2.25
	12	3	+7	4.00	4	2	-14	2.00		6	3	-35	2.00	8	4	+4	2.00
	13	3	+8	4.30	9	2	+15	4.50		9	3	+4	3.00	6	3	+5	2.00
	14	4	+10	3.50	8	3	+14	2.66		15	6	+30	2.50	4	2	-16	2.00
	16	4	+22	4.00	6	2	-6	3.00		16	6	+15	2.66	7	3	+14	2.33
	19	5	+25	3.80	5	2	+7	2.50		14	5	-16	2.80	6	3	+17	3.00
	20	5	-6	4.00	4	2	+2	2.00		11	4	-17	2.75	5	12	-13	2.50
	4	4	-10	3.50	4	2	+4	2.00									
	13	4	-12	3.25	5	2	+25	2.50									
	12	3	+6	4.00	6	3	-26	2.00									
	11	3	+7	3.66	7	9	-7	2.33									
	10	3	+8	3.33	6	3	+6	2.00									

Table 3-7 Summary of finite strain measured at different sections in the Wulong shear zone

Localities	K	Axial ratios (X :Y :Z)	Strain on principal axes	Azimuth of principal axes and planes
Wulong mine area	0.37	1.85 :1:0.31	X :+125% ; Y : +16% ; Z :-62%	S_{xy} : 45/130 ; Axis Z : 52/310 ; Axis X : 62/132 ;
Sidaogou mine area	0.76	1.61 :1:0.56	X :+65% ; Y :+4% ; Z :-40% ;	S_{xy} : 50/125 ; Axis Z : 45/305 ; Axis X : 50/145 ;
Jielishu	1.03	1.78 :1:0.57	X : +72% ; Y :0% ; Z :-40% ;	S_{xy} : 55 /135; Axis Z : 55 /315; Axis X : 53 /140;

Table 3-8 Different representative κ, μ values of dynamically recrystallized Quartz from different researchers.

Researchers	κ	μ
Twiss (1977)	603	0.86
Mercier et al., (1977)	381	0.71
White (1979)	794	0.70
Etheridge and Wilkie (1981)	668	0.68
Ord and Christie (1984)	4090	1.11

Table 3-9 Size of dynamically recrystallized quartz, differential stress and strain rates in the Wulong shear zone

Locality	Measured mineral	D (μm)	σ_1-σ_3 (MPa)	ε (sec^{-1})
Wulong mine area	Dynamically recrystallized quartz in mylonite	19 (58)*	81.5	9.428E-23
	Dynamically recrystallized Q in mylonite	8 (65)	146.6	4.284E-21
Sidaogou mine area	Dynamically recrystallized Q in sericite Q-mylonite	23 (70)	71.5	4.026E-23
Sanguliu intrusion	Diorotic mylonite	29(70)	61.1	1.449E-23

*number in bracket is the measurement times in each sample, D: average diameter of recrystallized quartz grain,

Table 3- 10 Contents of REE of diverse mylonites in the Wulong shear zone (ppm)

	Sample No.	Rock type	La	Ce	Nd	Sm	Eu	Gd	Dy	Yb	Y
Sidaogou section	S6-5	Metasandstone	28.00	63.00	23.00	3.60	0.95	2.60	2.50	1.70	15.00
	S5-6	Metasand proto-mylonite	40.00	84.00	30.00	3.60	1.40	3.00	2.90	0.43	2.50
	SD20-2	Ser-Q-mylonite	43.00	94.00	34.00	3.90	1.00	3.40	2.80	1.80	N*
	S5-12	Ultra-mylonite	35.00	76.00	28.00	3.20	1.30	2.70	2.40	1.50	12.00
Wulong section	WB3	Mica-gneiss	23.00	34.00	12.00	1.60	0.73	1.00	0.51	0.48	2.50
	WB3-9-3	Gneissic proto-mylonite	32.00	47.00	20.00	2.30	0.84	1.60	1.20	0.74	4.40
	W3-6-4-1	Gneissic ultra-mylonite	36.00	45.00	24.00	2.30	0.90	1.70	1.60	0.86	5.50

*n: not detected,

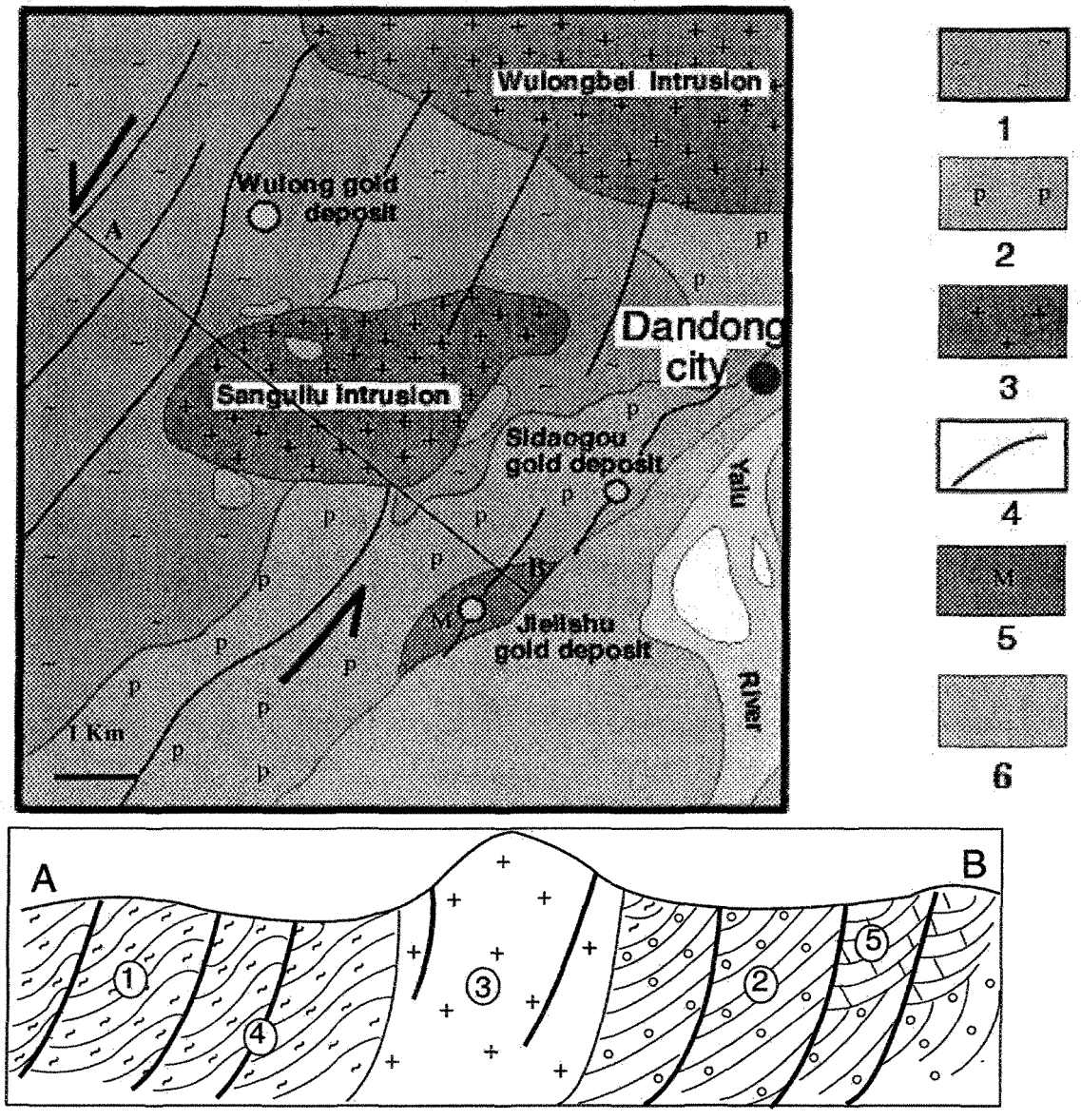

1, late Archean gneiss; 2, middle-late Proterozoic metasandstone;
3, Mesozoic intrusion; 4. The Wulong shear zone; 5, late Proterozoic marble;
6, Jurrasic volcanic breccia sedimentary rocks.

Figure 3-1 Simplified regional geological map of the Wulong shear zone

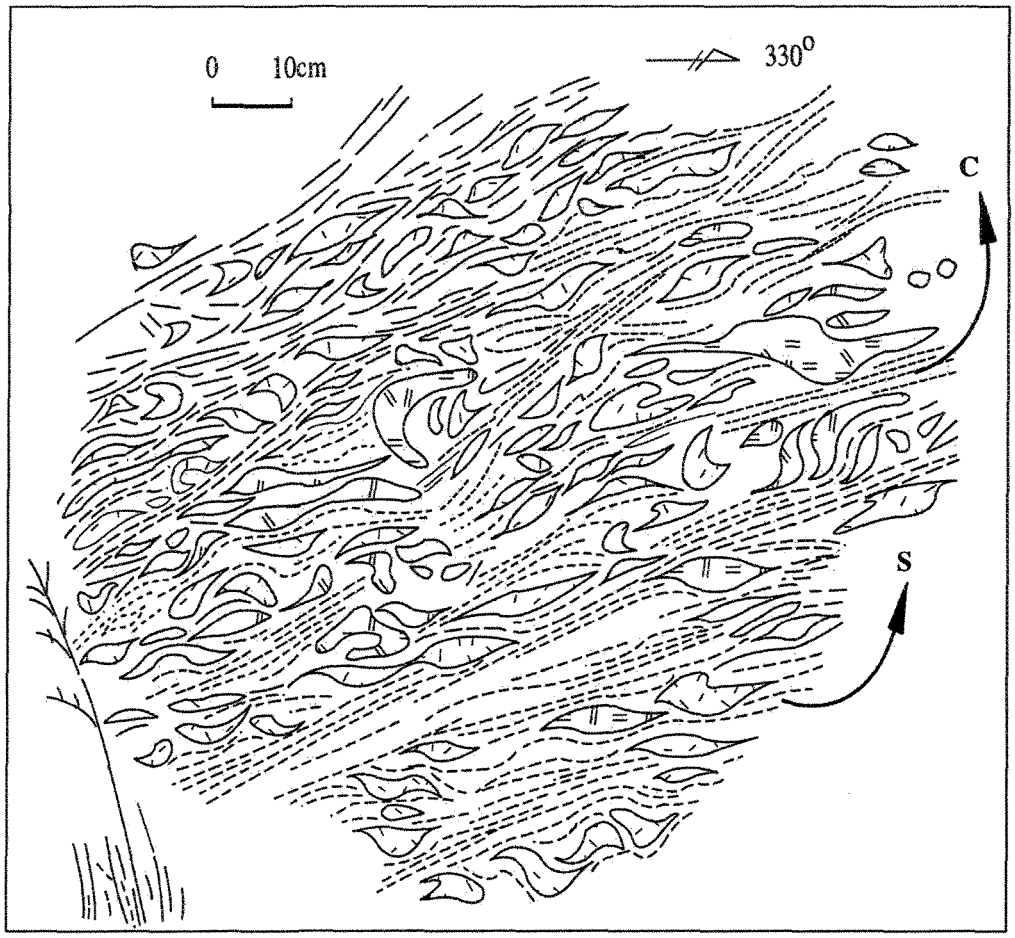

Figure 3-2 Sketch of the "quartz-bar" boudinages developed in the sandstone in the Wulong shear zone in the Sidaogou area(site Sdg-20)

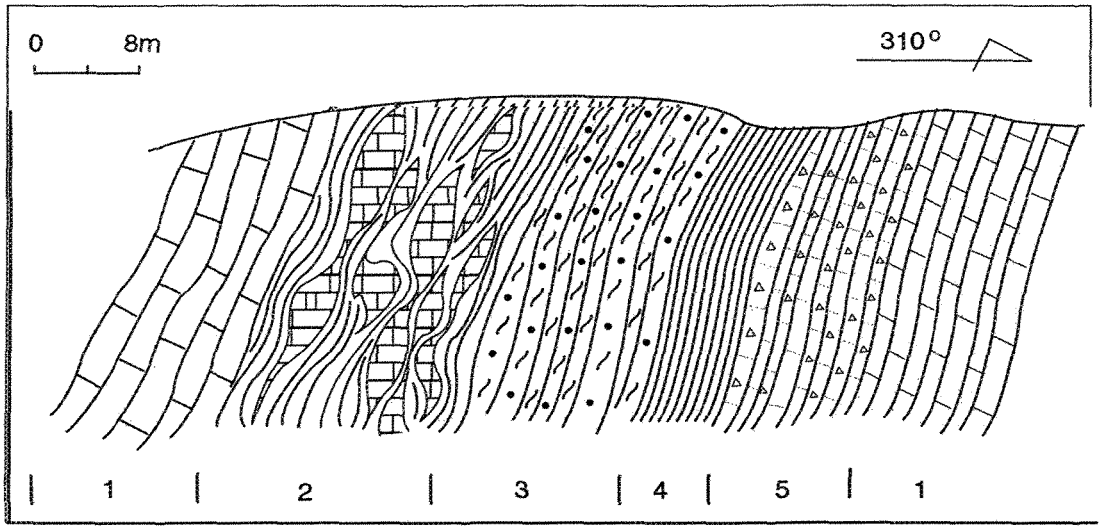

1. Silicified marble; 2. Marble protomylonite; 3. Marble mylonite;
4. Marble ultramylonite; 5. Mixing marble mylonite and brecciase;

Figure 3-3 Spatial variation of tectonite types in marble mylonite, Jielishu area

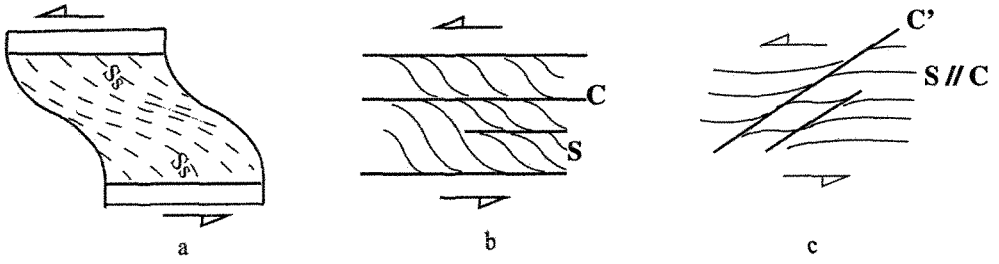

Figure 3-4 Formation mechanism of S-C structures during progressive development of shear

a. At early stage of deformation , only S fabric formed and its state and strain stength are variable with the variation of the azimuth of the strain ellipsoid.
b. With progressive shear, C fabric formed and it is usually parallel to the shear direction, the acute angle between the shear boundary and the S fabric usually points to the direction of the shear sense.
c. At the late stage of shear deformation, the C' fabric formed and the S and C fabrics are parallel to each other due to shear rotation.

(after Bursnall 1989)

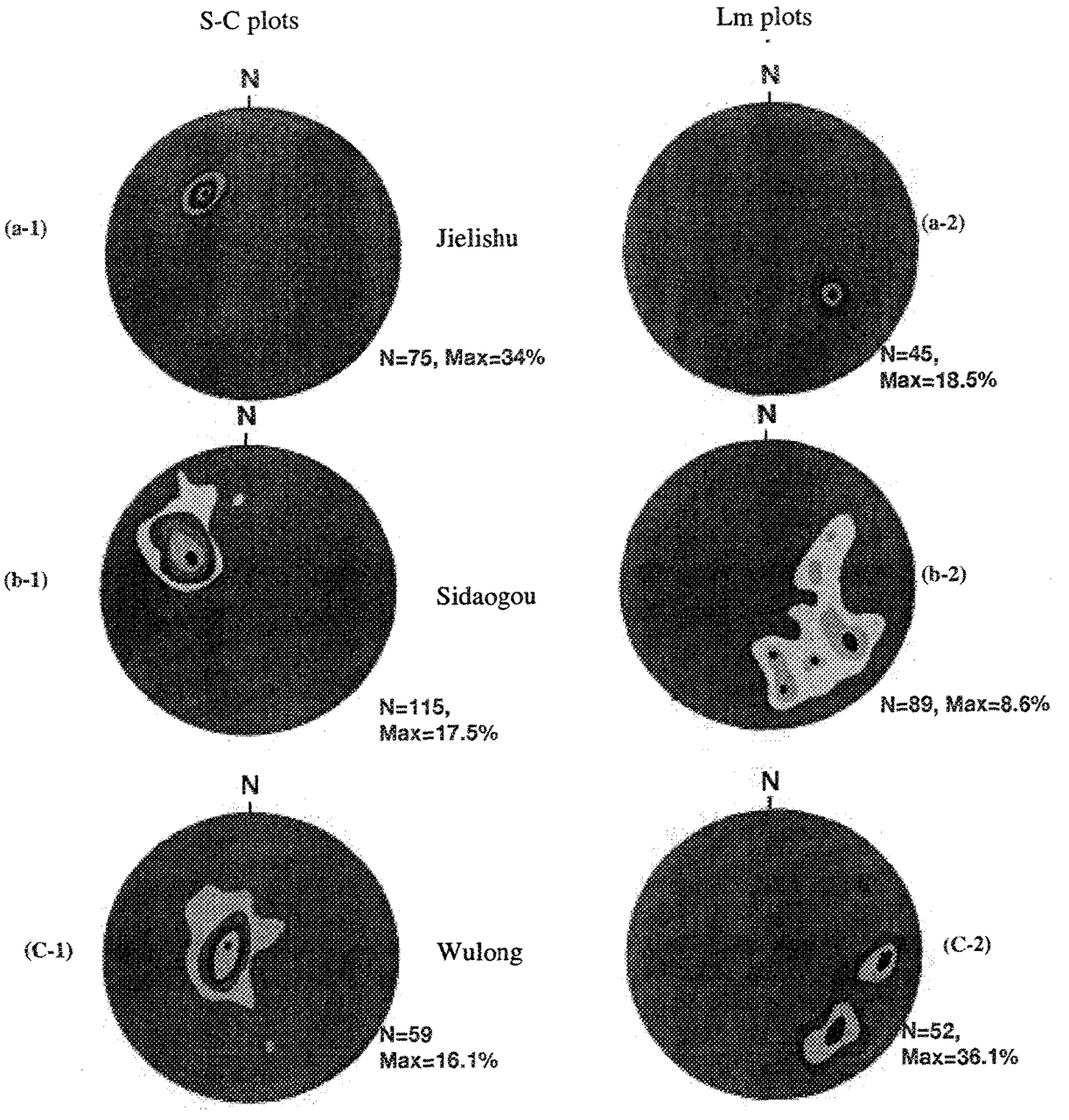

Figure 3-5 Plots of foliations and lineations at various locations within the Wulong shear zone

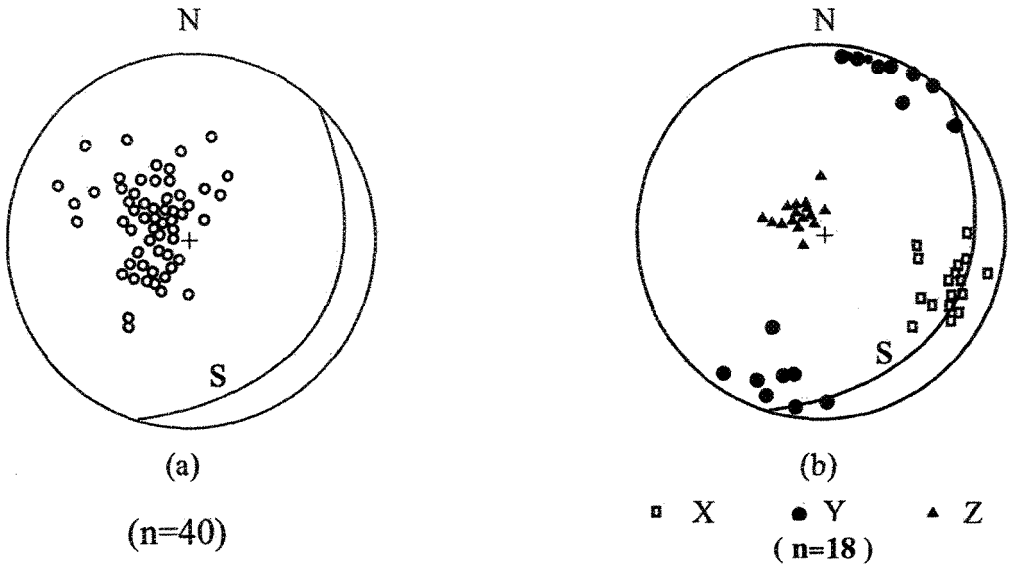

Figure 3-6 Pole projection of foliation (a) and triaxial projection of lineations (b) in gneiss, Wulong mine area

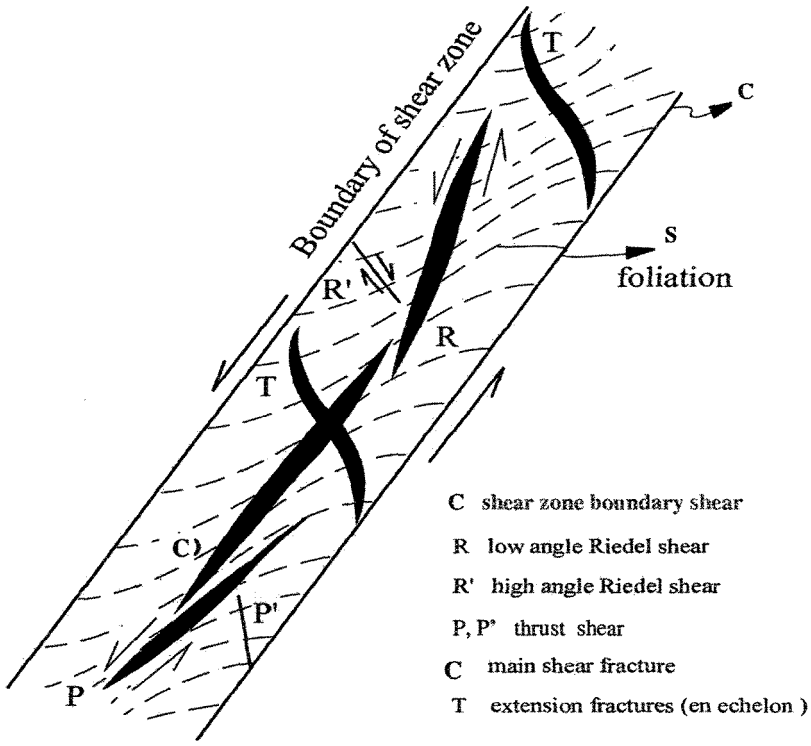

Figure 3-7 Identification of fractures and veins formed in shear zone

(modified from Ramsay and Huber, 1987, Roberts, 1987)

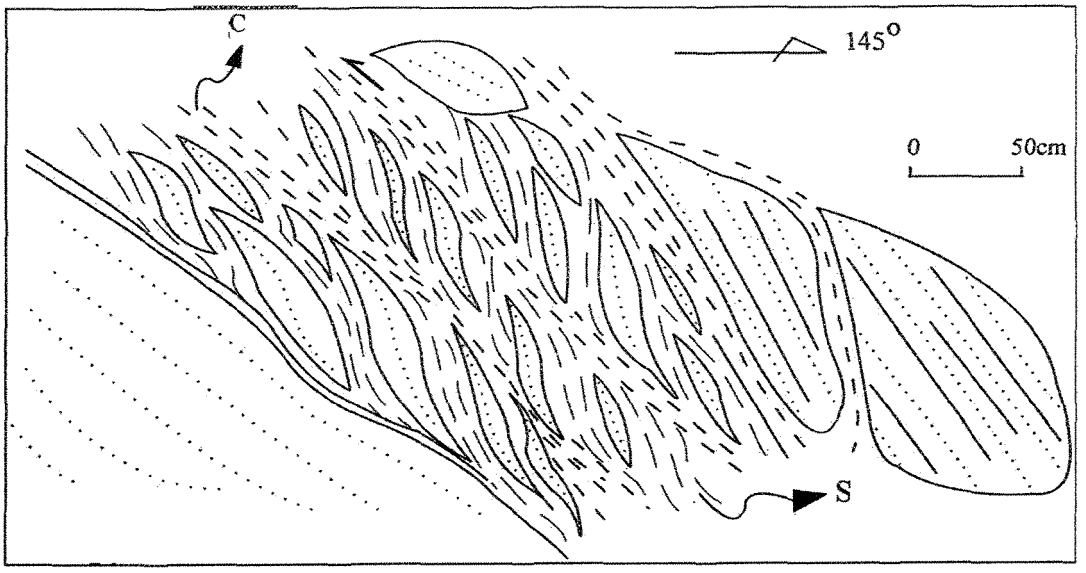

Figure 3-8 Sketch of the S-C structures in metasandstone mylonite

(level 6 in the Sidaogou gold mine)

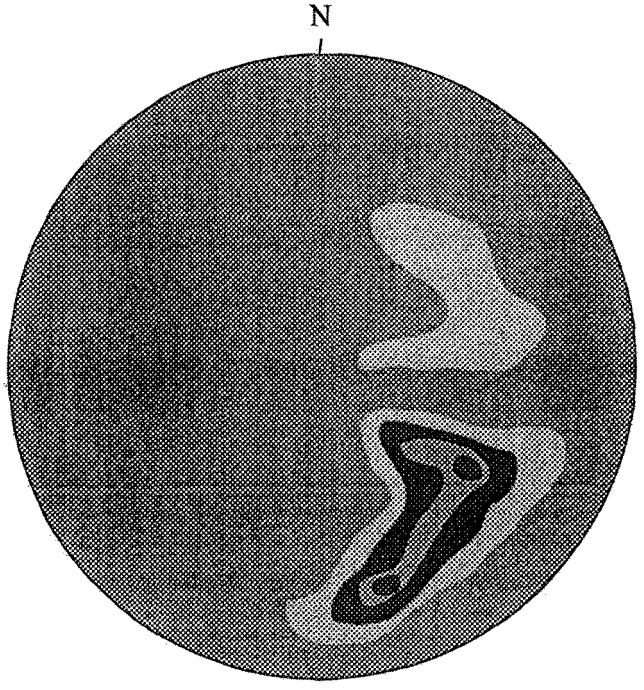

N=43, Max=15.2%

Figure 3- 9 Plots of maximum flatting planners of lenses developed in the Wulong shear zone in the Sidaogou area

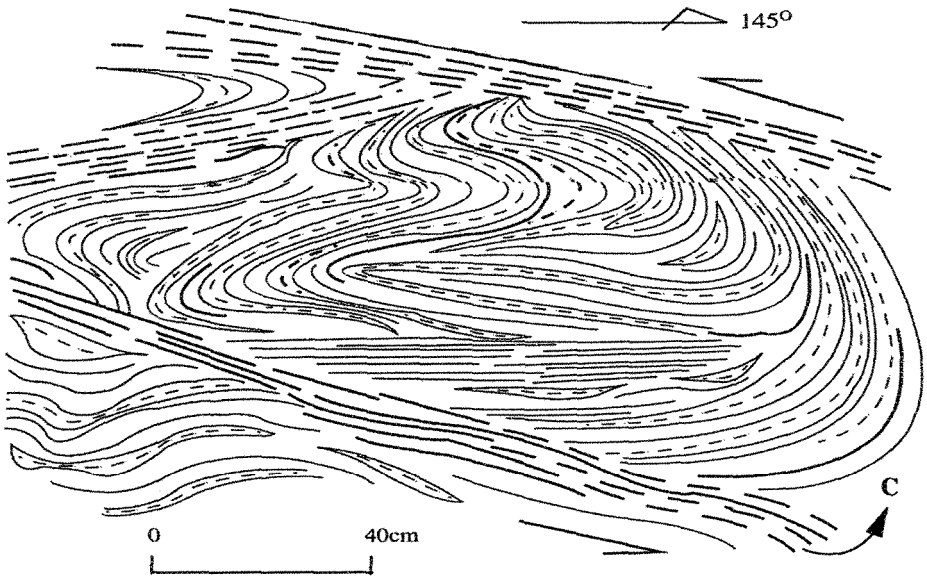

Figure 3-10 Intrafolial fold formed in the strong deformed section in the shear zone (level 6, Sidaogou deposit).

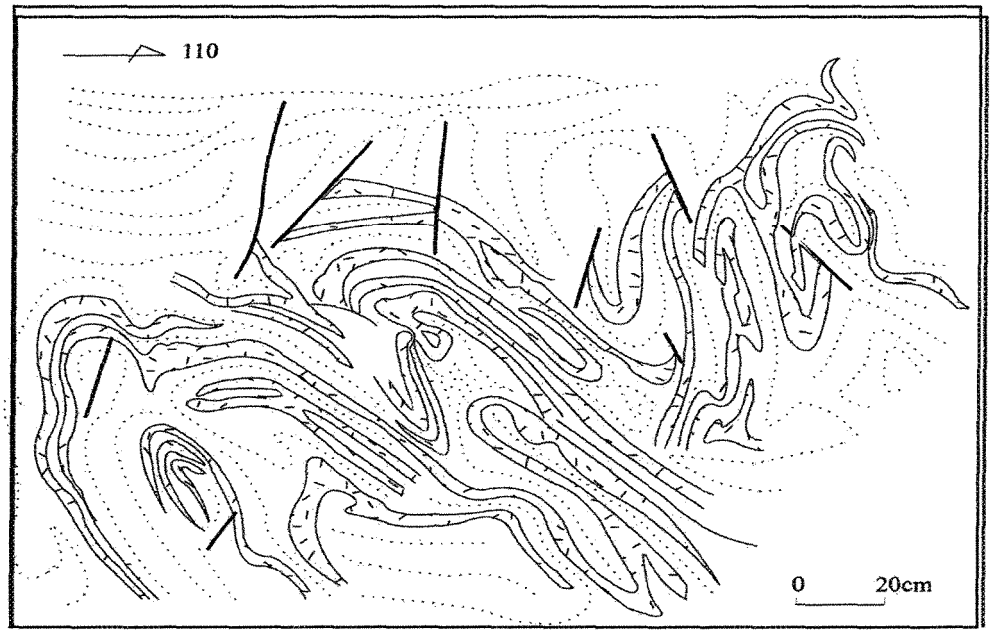

Figure 3-11 Ilustration of tight folds formed from original structures developed in quartzite close to the shear zone in the Sidaogou area

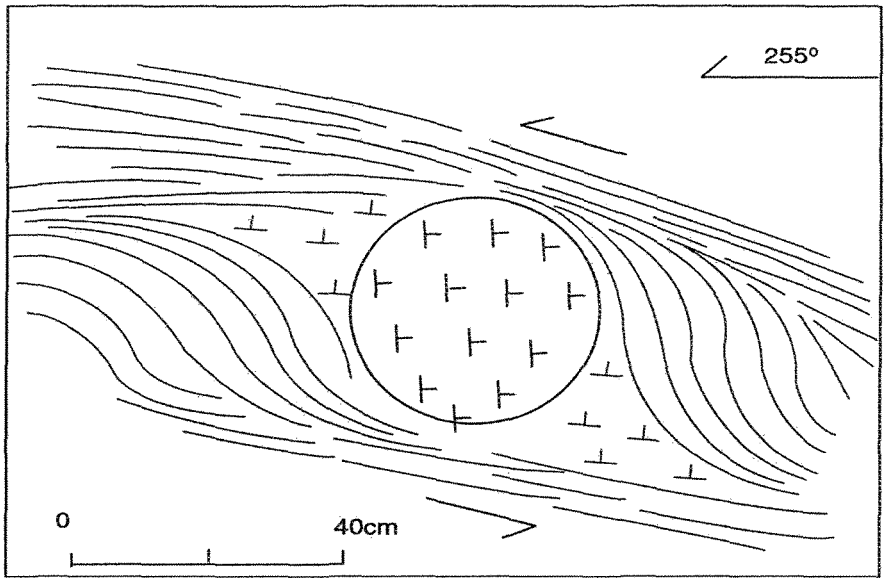

Figure 3-12 Strain pressure shadow formed in marble mylonite rocks in the Jielishu area

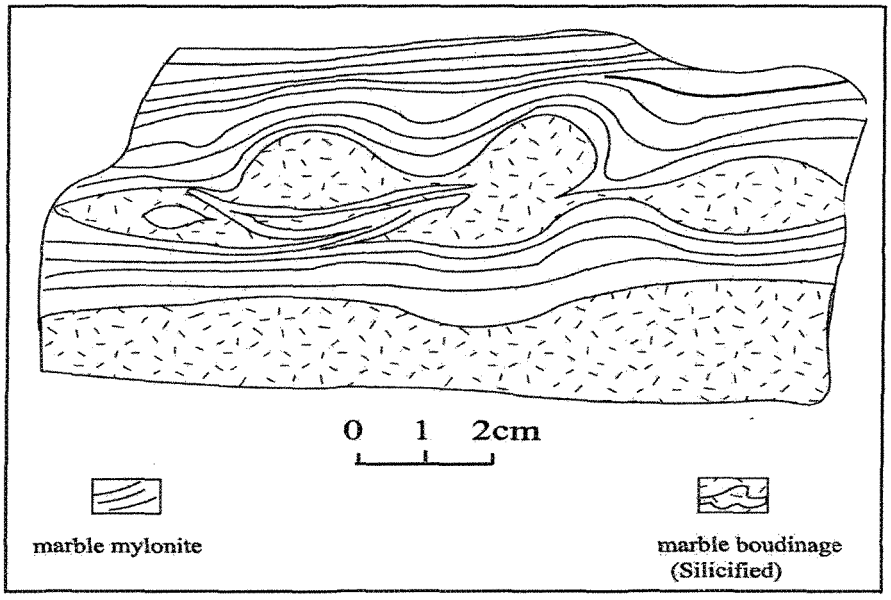

Figure 3-13 Illustration of hand specimen showing boudinages formed in marble, Wulong shear zone, Jielishu are

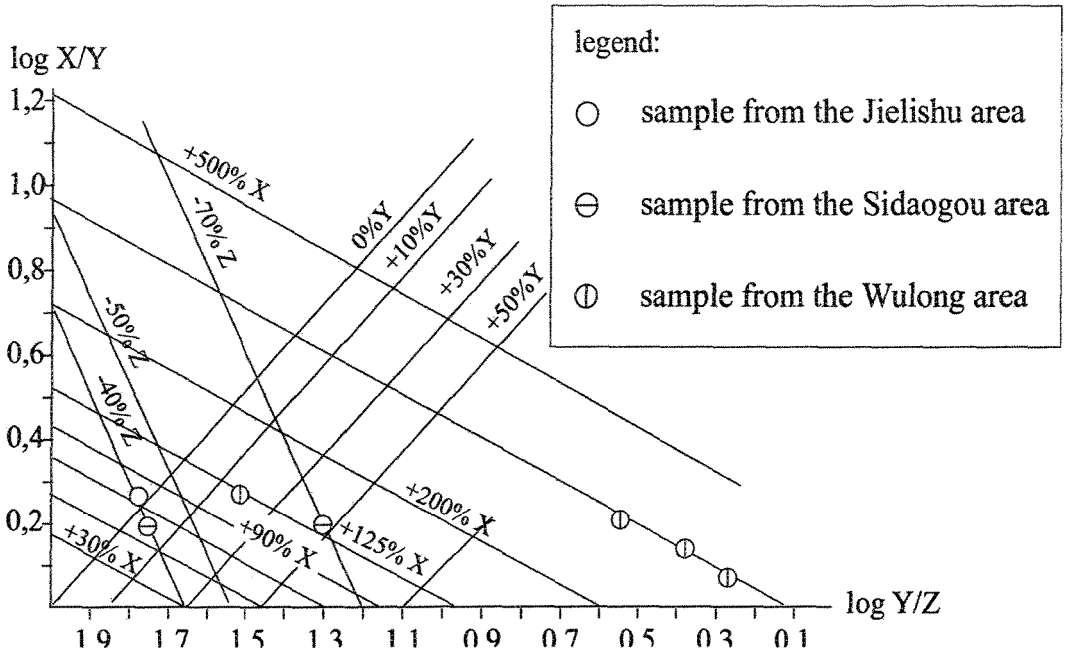

Figure 3-14 Log diagram of principal strain ratios of tectonies of typical locations in the Wulong shear zone

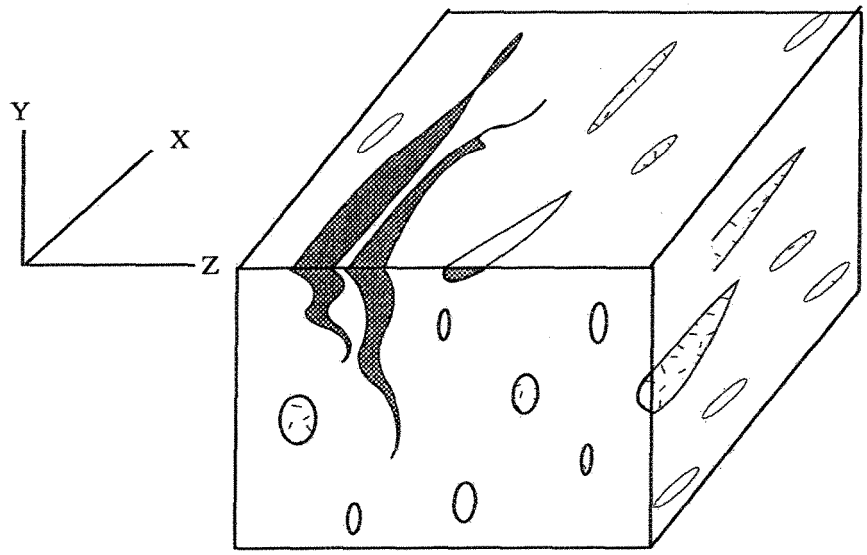

Figure 3-15 Illustration of spatial orientation of hand sample during thin section preparation

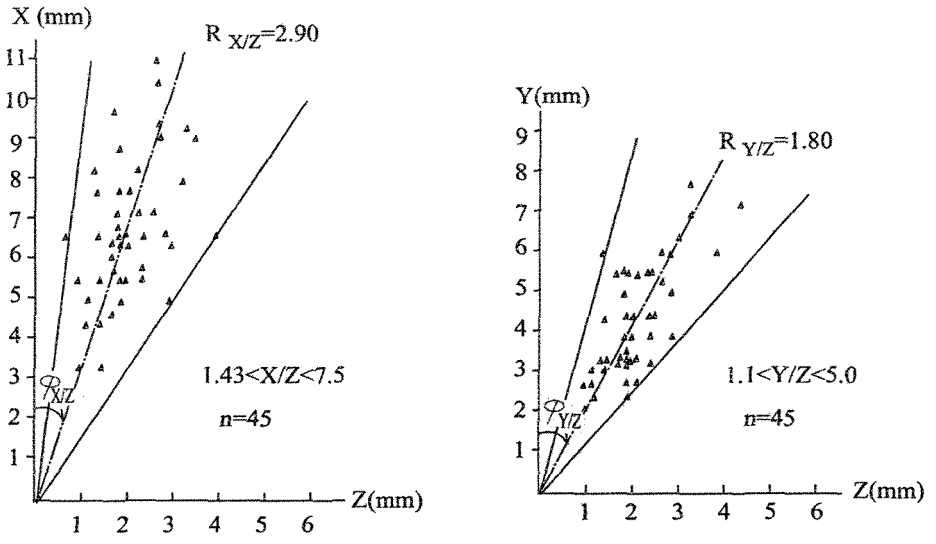

Figure 3-16 Plots of X vs. Z and Y vs. Z axial ratios of lenses developed in the shear zone, Sidaogou area

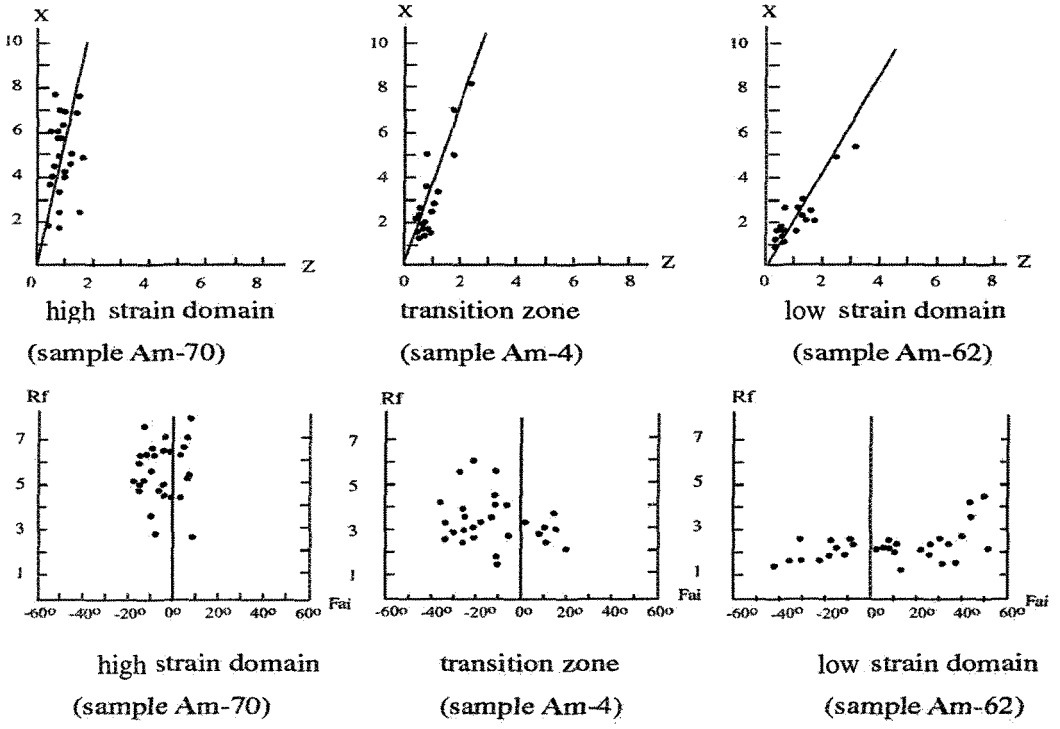

Figure 3-17 Rf-fai diagram and X vs. Z plots of representative mylonites in the Wulong shear zone

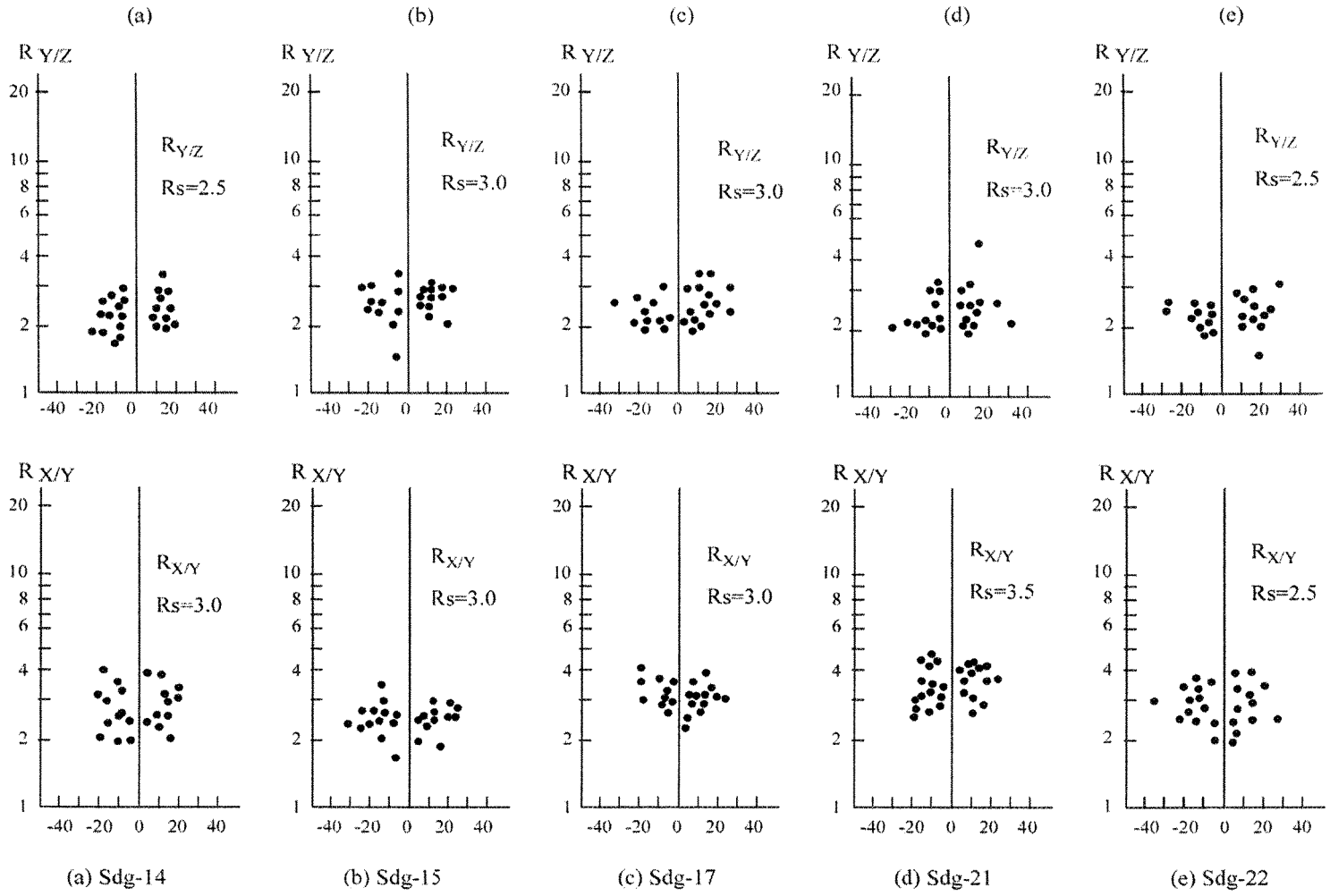

Figure 3-18 R_f - fai diagram of the mylonite in the Sidaogou area

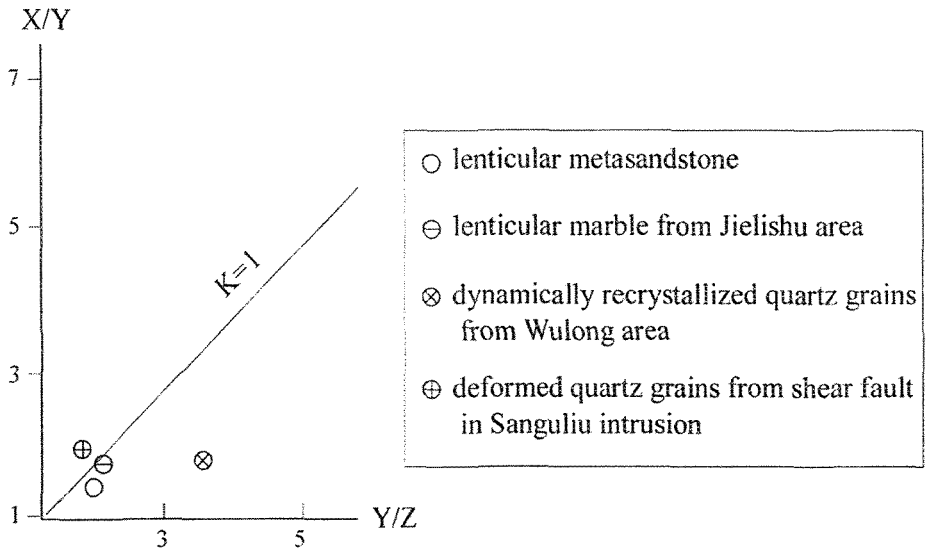

Figure 3-19 Plots of mean finite strains at various locations in the Wulong shear zone

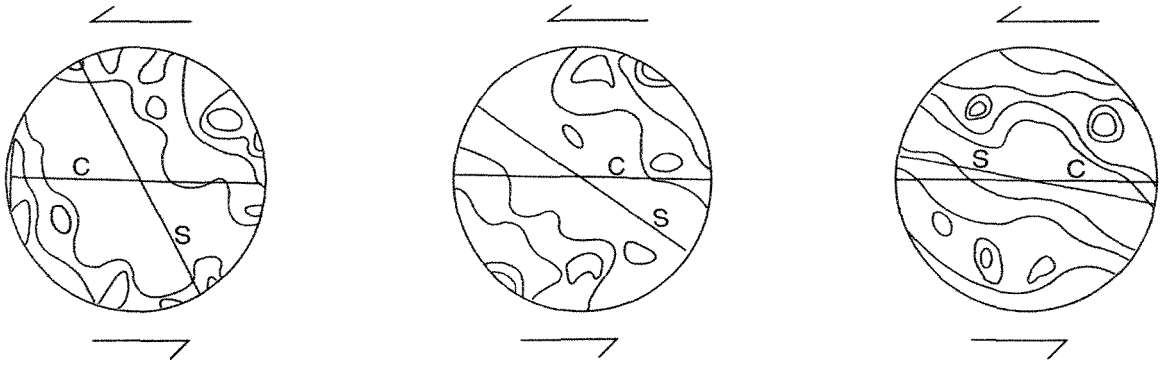

low strain domain
Am-15

transition zone
Am-31

high strain domain
Am-1

Contoured at : 1 – 2 – 4 – 6 – 8 points per 100/n% area.

Figure 3-20 Lower hemisphere equal-area plots of quartz c-axes of sample from the Wulong area.

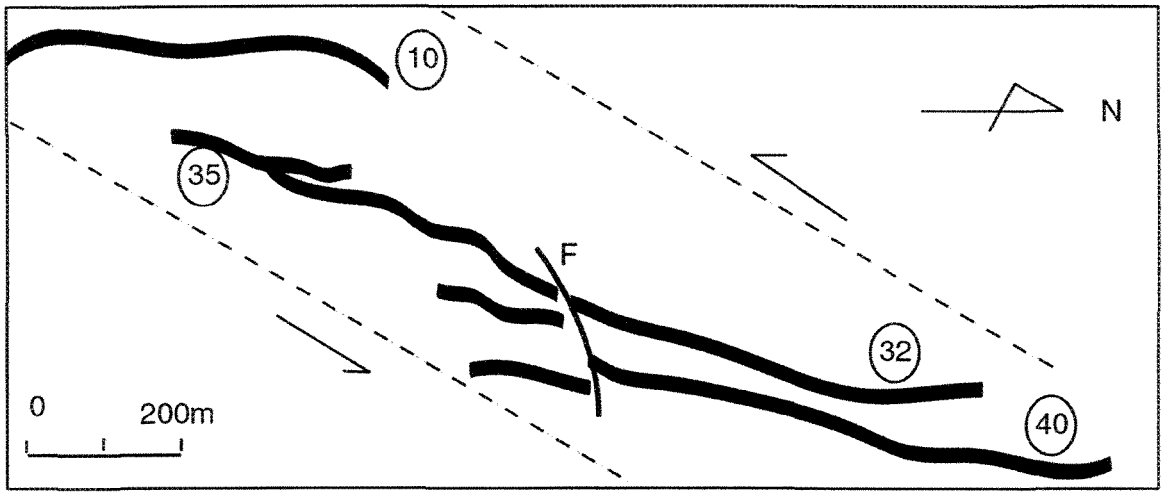

Figure 3-21 Gold lodes demonstrate sinistral display pattern in the Wulong gold mine. (numbers represent gold lode series numbers)

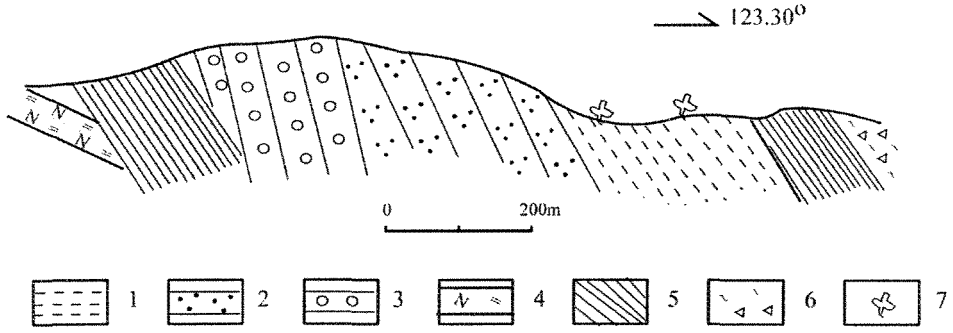

Figure 3-22 Geological section of the huishoumoshan site, Sidaogou area

1, shale with thin interval sandstone; 2, sandstone nd quartzite; 3, quartz conglomerate; 4, magmatite leuculeptite; 5, mylonite; 6, cataclasite; 7, site of fossile collection.

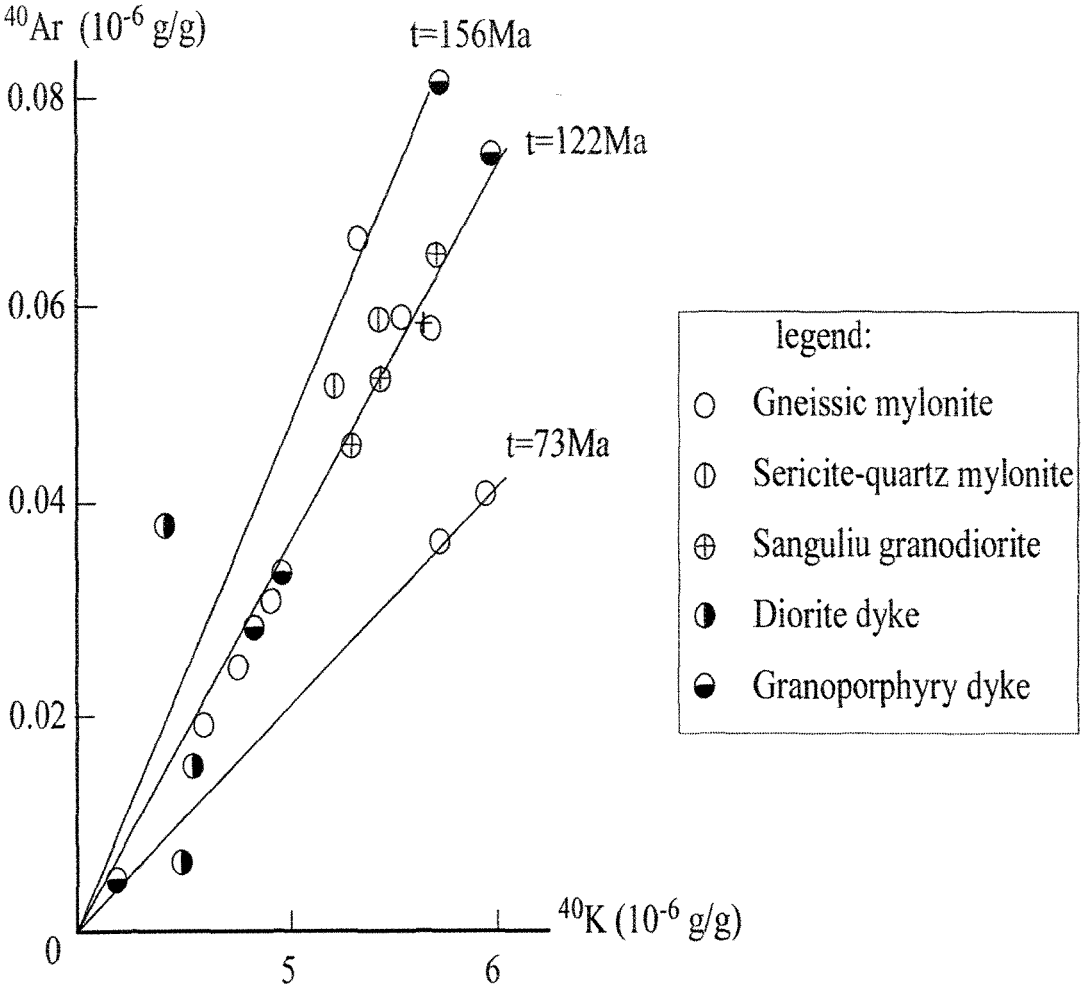

Figure 3-23 ^{40}Ar-^{40}K isochronological ages of mylonites and various dykes developed in the Wulong shear zone, Wulong gold camp

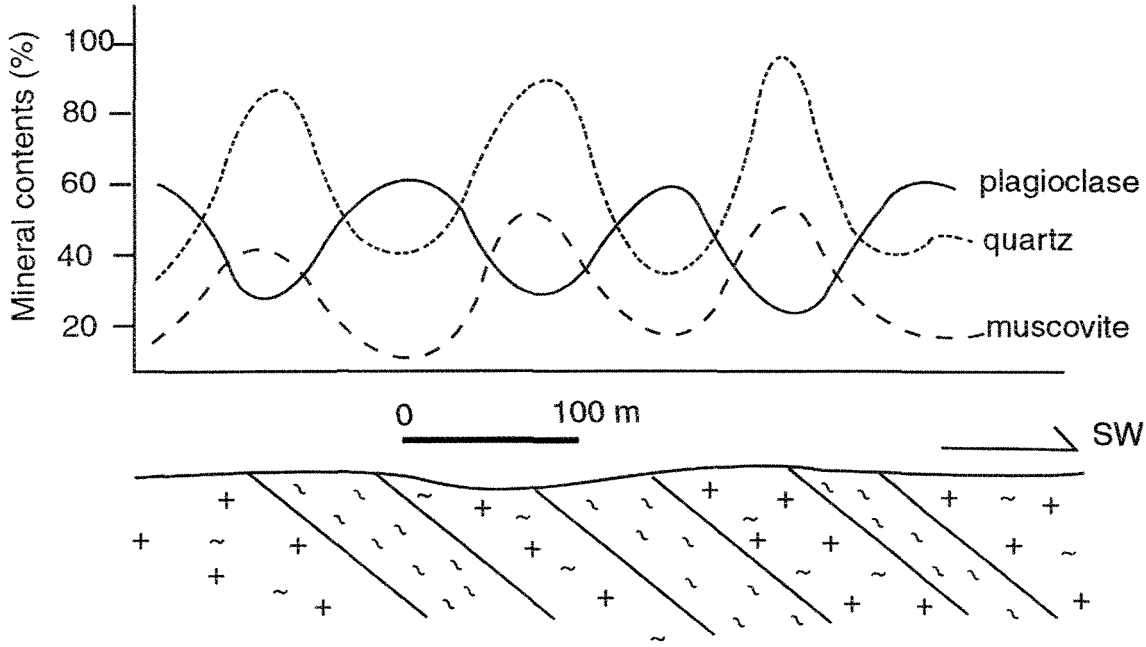

Figure 3-24 Variation of major minerals on a shear zone section in the Wulong mine area.

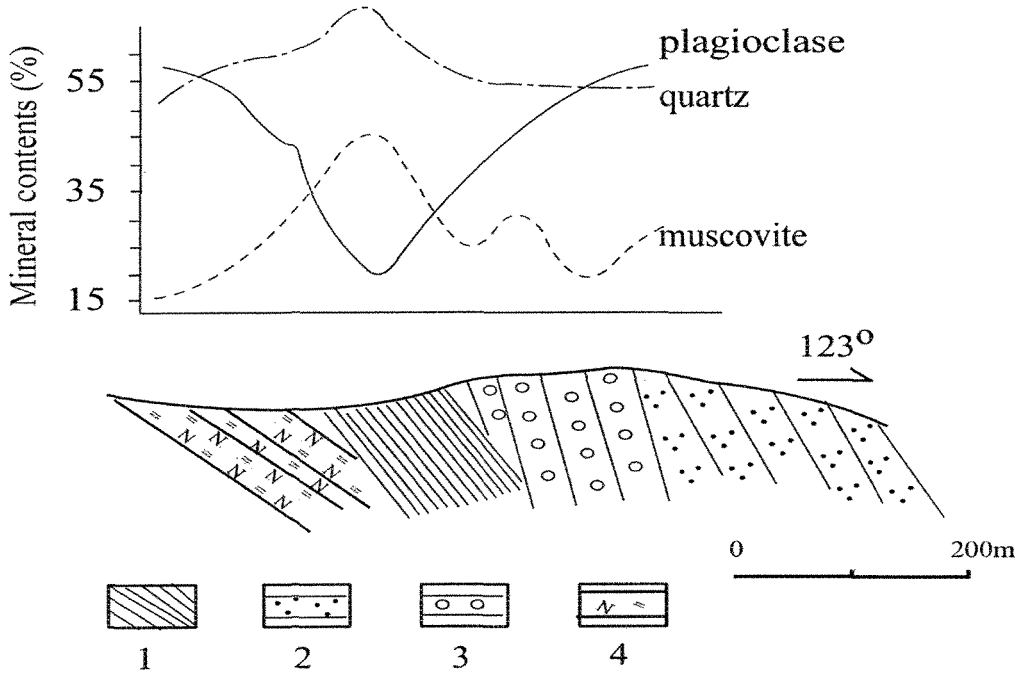

Figure 3-25 Variation of major minerals on shear zone section, Sidaogou area

1, mylonite; 2, sandstone nd quartzite; 3, quartz conglomerate; 4, magmatite leuculeptite;

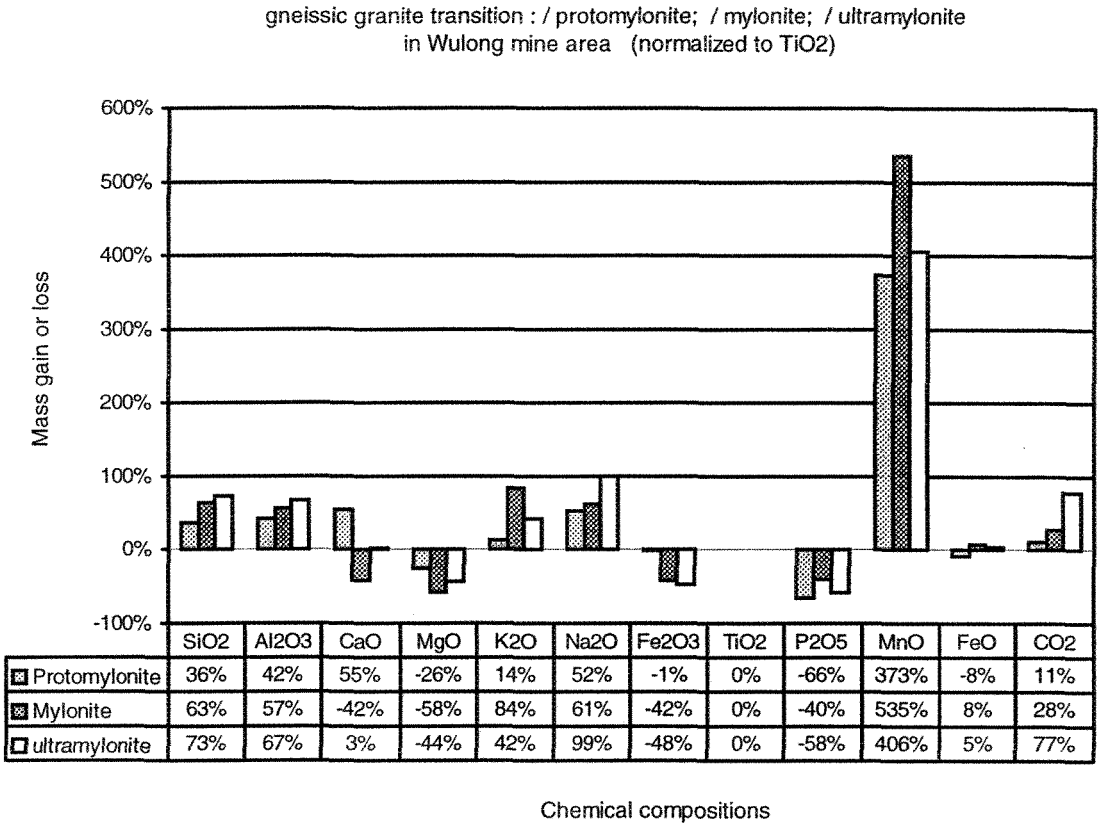

	SiO2	Al2O3	CaO	MgO	K2O	Na2O	Fe2O3	TiO2	P2O5	MnO	FeO	CO2
Protomylonite	36%	42%	55%	-26%	14%	52%	-1%	0%	-66%	373%	-8%	11%
Mylonite	63%	57%	-42%	-58%	84%	61%	-42%	0%	-40%	535%	8%	28%
ultramylonite	73%	67%	3%	-44%	42%	99%	-48%	0%	-58%	406%	5%	77%

Figure 3-26 Mass-balance calculation and TiO2-normalized histogram of the major elements in the shear zone in the Wulong area.

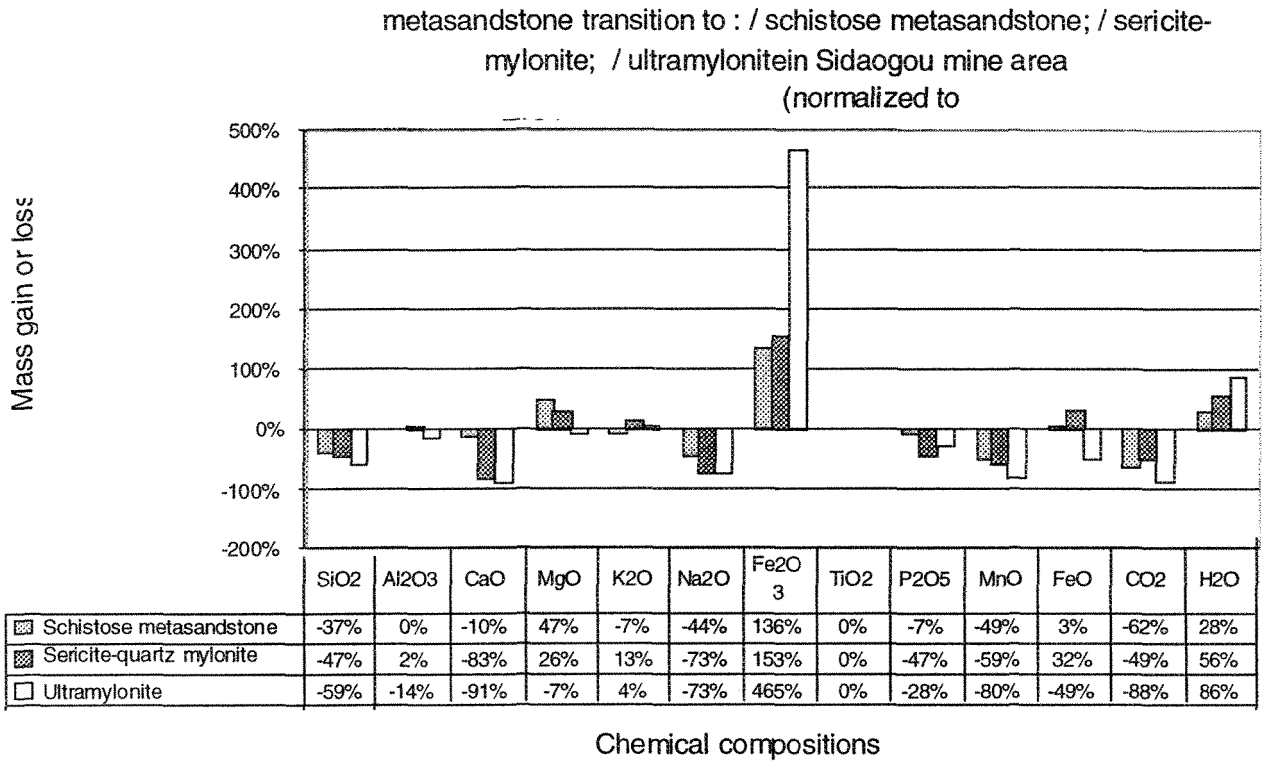

	SiO2	Al2O3	CaO	MgO	K2O	Na2O	Fe2O3	TiO2	P2O5	MnO	FeO	CO2	H2O
Schistose metasandstone	-37%	0%	-10%	47%	-7%	-44%	136%	0%	-7%	-49%	3%	-62%	28%
Sericite-quartz mylonite	-47%	2%	-83%	26%	13%	-73%	153%	0%	-47%	-59%	32%	-49%	56%
Ultramylonite	-59%	-14%	-91%	-7%	4%	-73%	465%	0%	-28%	-80%	-49%	-88%	86%

Figure 3-27 Mass-balance calculation and TiO2-normative diagram of mylonites developed in the Sidaogou area

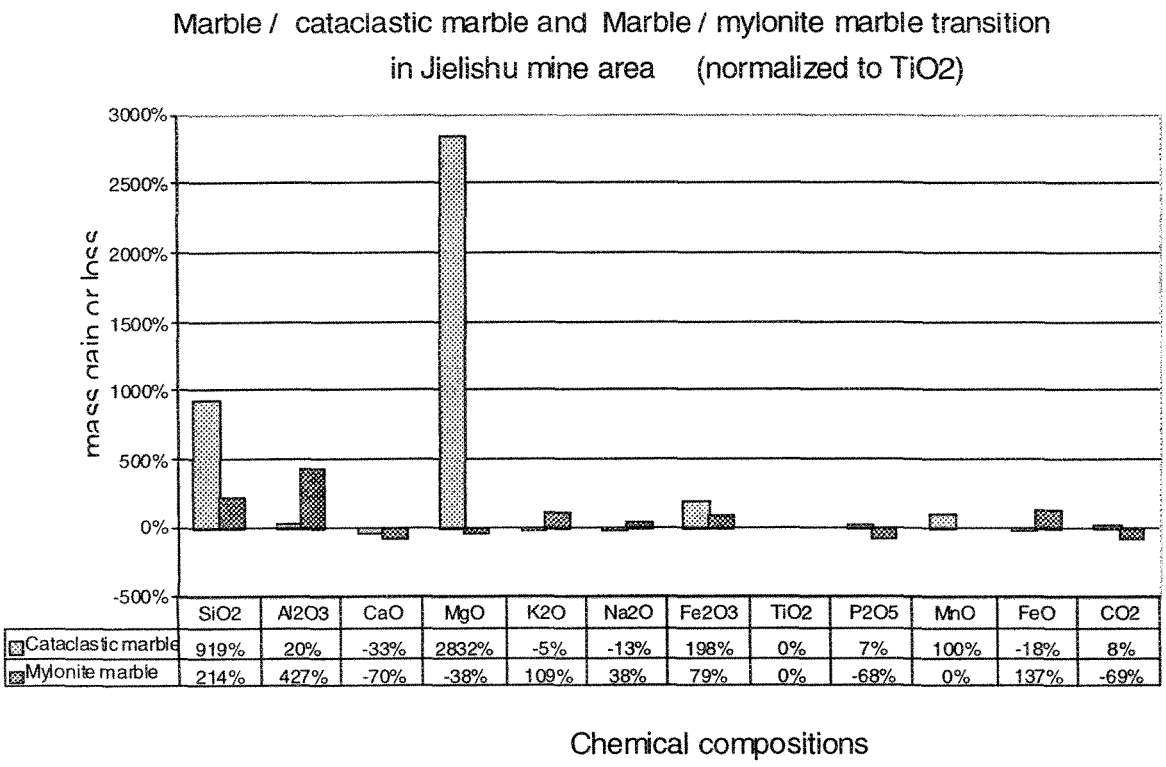

Figure 3-28 Mass-balance calculation and TiO2-normative diagram of major elements in mylonites developed in the Jielishu area.

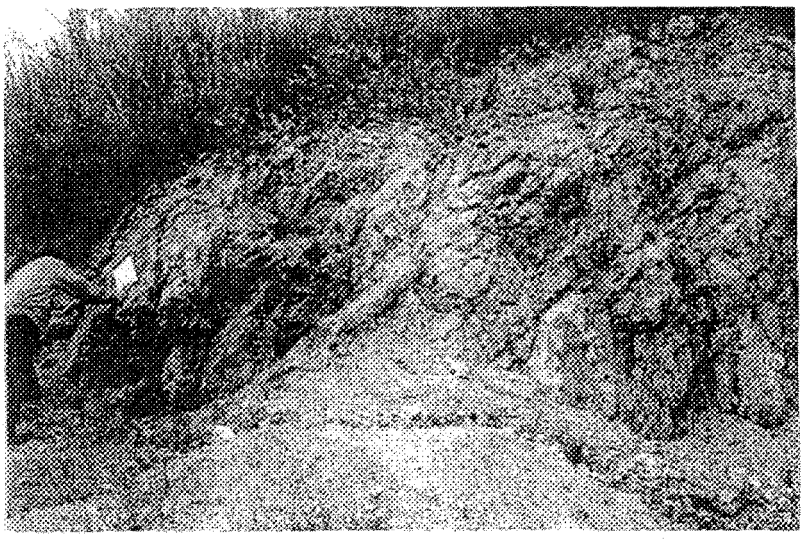

Photo 3-1 Outcrop of the Wulong shear zone at Jixingou, the Wulong gold mine.

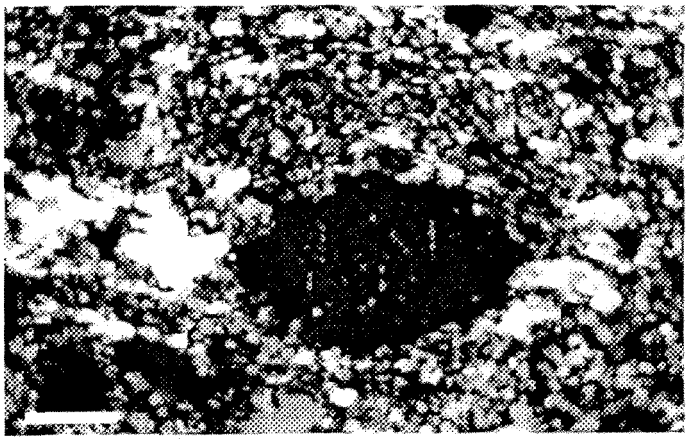

Photo 3-2 Eye-shaped plagioclase in gneissic mylonite. (scale bar 5mm)

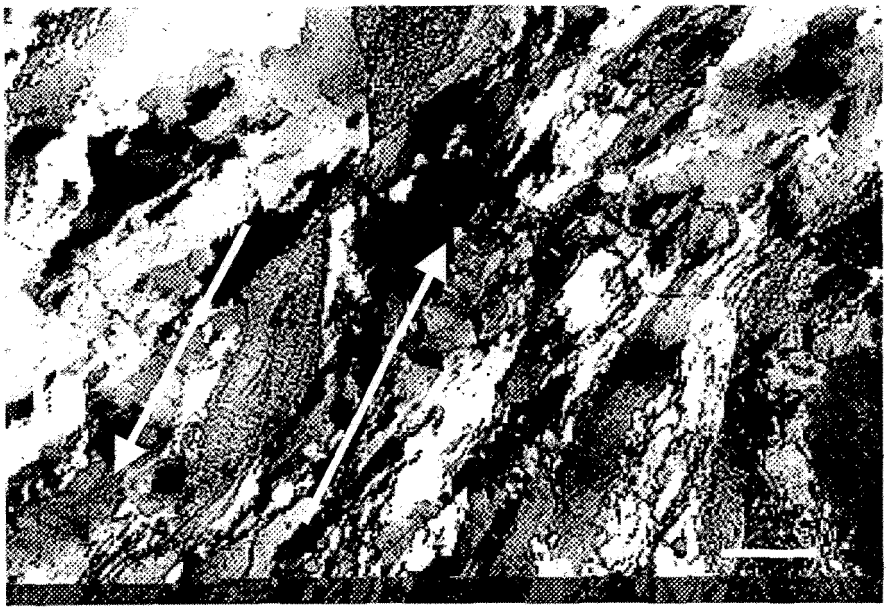

Photo 3-3 Mica-fish microstructure common in gneissic mylonite, Wulong area. (scale bar 5mm)

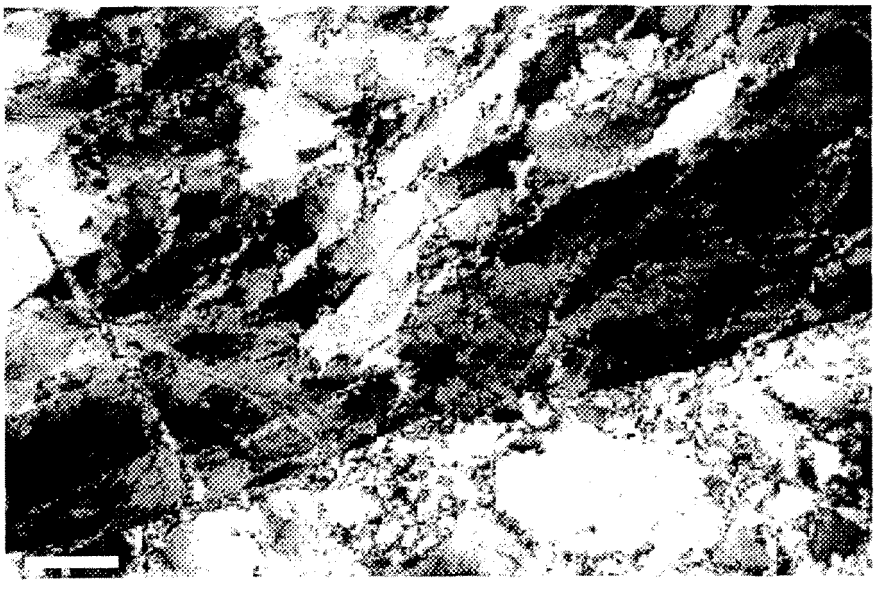

Photo 3-4 Subgrains formed around the parent quartz during recrystallization processes. (scale bar 5mm)

Photo 3-5 Strongly elongated quartz grains (length/width ratios reach 10 : 1) in ultarmylonites, (scale bar 5mm)

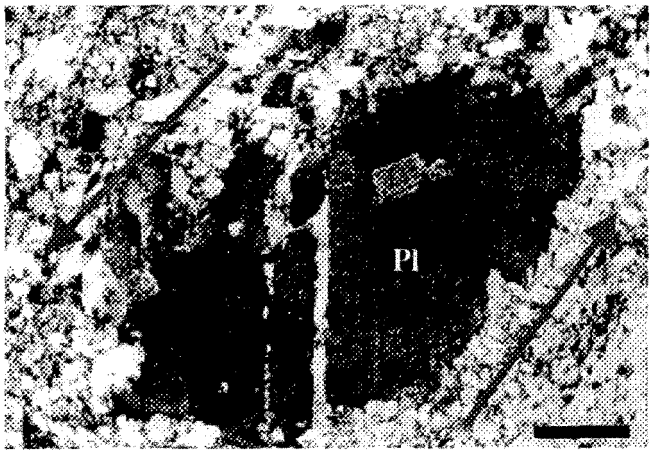

Photo 3-6 Microfractures developed in phenocrystal plagioclase filled with recrystallized quartz. (scale bar 5.5 mm)

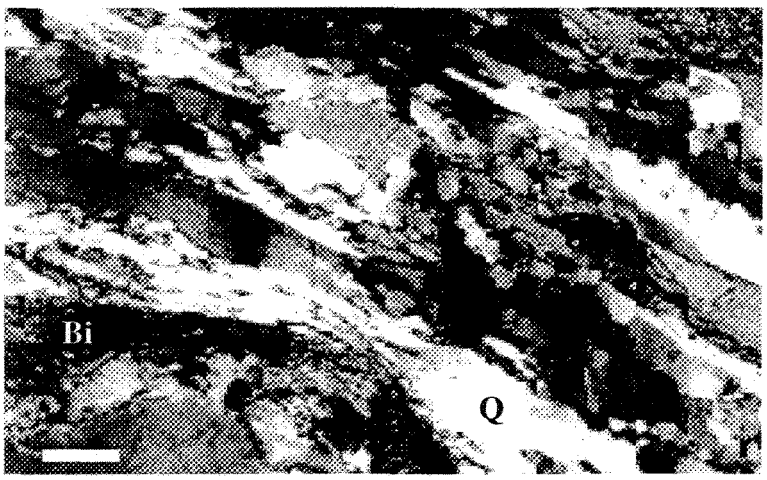

Photo 3-7 Extremely elongated quartz and mica grains in mylonite, Wulong area. (scale bar 3.5 mm)

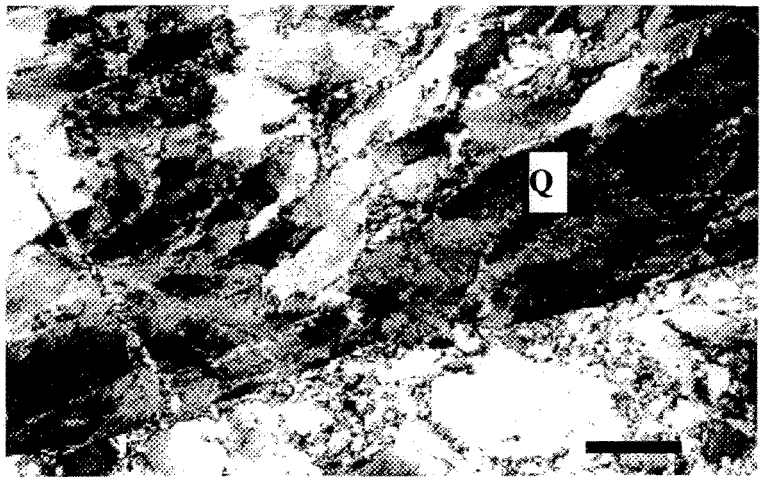

Photo 3-8 Wavy extinction of quartz aggregations is a common ductile deformation feature observed in the Wulong shear zone. (scale bar 5mm)

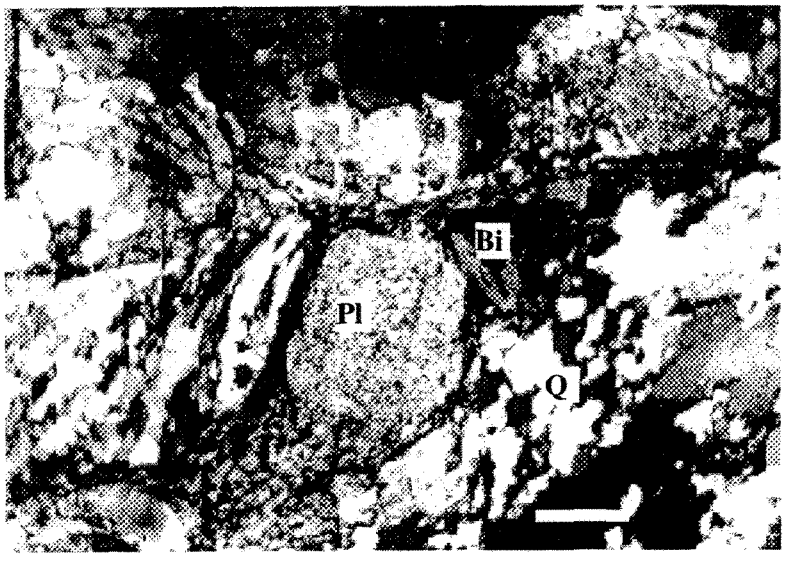

Photo 3-9 Pressure shadow formed in the Wulong shear zone. The core of the shadow is composed of plagioclase, the tail is formed by with mica, this pressure shadow shows a sinistral shear.
(sample site : Jixingou, Wulong mine) (scale bar 5.5 mm)

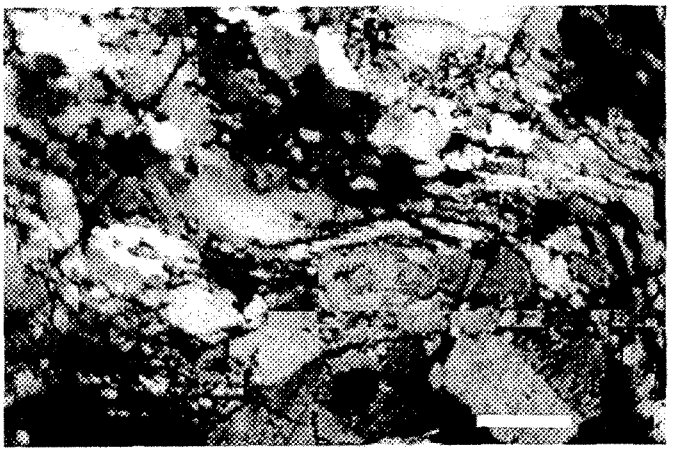

Photo 3-10 Rotated elongated quartz grains usually define the S fabrics, They are also relaible shear senes marker. (scale bar 5mm)

Chapter IV

Geology of the Wulong gold camp

Introduction

The Wulong gold camp is located 15km SW of Dandong city, Liaoning province. As the major gold producer in Liaoning province, it accounts for about 50% of the gold reserves of the province (Yao et al., 1988). The Wulong gold camp consists of three major gold deposits, namely the Wulong gold deposit, the Sidaogou gold deposit and the Jielishu gold deposit (Figure 4-1).

Mesozoic granitic complexes and the Wulong shear zone are generally considered as the predominant controlling factors for gold mineralization in the Wulong gold camp (Yao et al., 1988). The Wulong gold camp strikes NE and is structurally controlled by the Wulong shear zone. Among the three gold mines, the Wulong gold deposit is the largest in all. The Wulong gold deposit is hosted in gneiss, the Sidaogou deposit is hosted in metasandstone of the Liaohe Group, and the Jielishu deposit is situated in marble of the Liaohe Group. As the geological characteristics of individual deposit are quite different, geology of the three gold deposits will be discussed in separate sections.

4.1 Geological features of ore deposit

4.1.1 The Wulong gold deposit

Located 15km SW of the Dandong City, the Wulong gold deposit was first operated by the Japanese in 1939 during the world war two. There have been five mining sites in this mine (the No. 1, 2, 3, 4, 5, respectively). All the mining sites are still in operation, except the No. 1 site, which was shut down due to exhausted gold reserves. The No. 3 mining site is currently the major gold producer of the mine. Accumulated gold production to date is about 40 – 50 tons. Annual gold productions are currently about 890kg. Average gold grade is about 4.5 g/t. Ore process capacity is 500 tons per day.

Several hundreds of gold-bearing quartz vein were found in the Wulong gold deposit. Most of the ore veins are controlled by faults. Exposed dominant rock types include gneiss and dyke and they are the major ore hosting rocks (Fig. 4-2). Ore bodies generally occur as auriferous quartz lodes. About 70% of quartz lodes are large scale massive quartz veins with low Au grades. Auriferous quartz veins are mainly controlled by two sets of faults which are the Jixinling fault on the west, the Heigou fault on the east of the Wulong gold mine area(Fig. 4-2, Fig. 4-3). Auriferous lodes are mainly developed in the NNE striking faults confined by the two major faults and these gold lodes account for the major gold productions of the mine. Though some auriferous lodes developed at west of the boundary fault (the Jixinling fault), they are small in scale and economically less important. The NNE and NW striking ore controlling faults usually form rhombic-grid form on horizontal plane

with an area size of about 700x1000 m^2(Fig. 4-3). The NNE striking lodes are generally parallel to one another and steeply dip(or plunge) to SW. Generally, ENE striking individual gold lode dips to west or east with near vertical dipping angle. Length of individual gold lode is commonly 30m to 100m, and with a width variation of 0.7m to 17m. Controlled depth of gold lode reaches 600m below sea level. These NNE striking gold lodes form sinistral en echelon pattern on both horizontal plane and vertical plane as mentioned in chapter three.

A Group of NW striking gold lodes show extension features. These faults generally strike 320° and dip towards SW with an angle ranging from 40-75°. On the whole, NW striking gold lodes are relatively small. Individual lode is generally 0.1 ~ 6 meters in width and 10 ~ 200 meters in length. Similar to the NNE striking gold lodes, the NW striking auriferous quartz veins form sinistral en echelon pattern on both horizontal plane and on vertical plane.

One of the ubiquitous features observed in the Wulong gold deposit is that gold lodes spatially co-exist with various dykes. These dykes include fine diorite porphyry, granoporphyry, granodiorite porphyre, and lamprophyre. The diorite and granoporphyre are pre-ore dykes since they are always displaced by ore veins and hydrothermal alteration is common in the dyke along the contact zones with quartz veins. Diopsidite and lamprophyre are post-ore as they always displace the ore veins and are fresh. The gold-bearing quartz veins, together with the various dykes, are controlled by the NNE and NW striking faults and usually occur as swarms.

4.1.2 The Sidaogou gold deposit

The Sidaogou gold deposit is located about 8 km SW of Dandong city. This mine has been in operation since 1968. Ores from this mine are transported to the Wulong mine for processing. Gold resources of this mine is exhausted and gold reserves is only about 0.6 ~ 0.9 tons. Presently three mining levels are in operation.

Lithological units in this mine include the middle-late Proterozoic metamorphosed sandstone of the Gaiuxian Formation of the Liaohe Group and the Sanguliu intrusion, which is located 4.5 km west of the mine. The metasandstone is the predominant lithologic unit in the area. In addition, very minor Jurassic volcanic rocks developed in small sedimentary basins along the Wulong shear zone at its southeastern boundary (Fig. 4-4).
In addition to the Sanguliu intrusion, which located at the west of the mine, dykes of variable compositions are also well developed in the mine and have an intimate spatial and temporal relations with ore bodies. The major dyke types are diorite, lamprophyre, quartz-monzodiorite, plagioporphyre and granoporphyre. Lamprophyre dykes are dominant in amount and are syn-ore emplacement since they were altered by ore-forming fluids at one site and displaced the gold quartz veins at other sites in this mine.

Besides the regional Wulong shear zone and its splays, anticlinorium structures are also developed in the metamorphosed sandstone close to the shear zone. These anticlinoria are intrafolial folds formed during shear, and the "layers" of the folds represent the S or the C fabrics of the shear zone (Cui and Peng,1995) (Fig. 4-5). In the Sidaogou deposit, most of the host rocks are mylonites derived from the metasandstone of the Liaohe Group.

Gold mineralization is strictly confined to the Wulong shear zone with a width of about 200 meters in the Sidaogou mine area. Ore types are dominated by disseminated, stockwork and auriferous quartz veins. Six ore bodies are defined and numbered as #2, #8, #78, #77, #13, and #20. Ore bodies are generally 400-600 meters in length and 10-80 meters in width. The longest ore body defined in the Sidaogou deposit is 1300m with a width of 45m. In general, the ore body strikes NE and dips to SW with dip angle ranging from 45-80°. Most of the gold mineralizations are concentrated in the metasandstone where the Wulong shear zone is developed. Actually, the Wulong shear zone is composed of four NE striking faults in the Sidaogou mine area (namely the F1 to F4), and most of the ore bodies are confined between the F2 and F3 as illustrated in Figure 4-4.

Unlike in the Wulong deposit, ore bodies have very irregular forms in the Sidaogou deposit and common forms include vein, lens and pocket.

4.1.3 The Jielishu deposit

The Jielishu deposit is characterized by the both economically valuable copper and gold. The Jielishu copper-gold mine was first operated by the Japanese during the 1930's. It consists of two mine shafts. The old shaft was closed in 1980. The new one is now operated by a local investor. This deposit is located 10 km SW of the Sidaogou gold deposit.

Exposed host rocks are dominated by the marble of the Proterozoic Liaohe Group and minor Mesozoic dykes. Ore bodies commonly strike 20 ° –50° with an average dipping angle of 50° towards NW. Some ore bodies strike 320 ° - 350° (i.e. the #61 and #62 veins) with dip angle of 60° to NE (Fig. 4-6). Ore bodies are strictly controlled by faults. In fact, the structural trace of the shear zone and the quartz veins and dykes share quite similar spatial distribution features in the Jielishu area.

Ore bodies developed in mylonites usually have poor succession along strike and commonly take lens shapes. In general, ore bodies show sinistral splay pattern (Fig. 4-6). Diabase and dioritic porphyry are the two major dykes developed in the Jielishu deposit. These dykes have close spatial and temporal relations with ore veins.

4.2 Mineralogical features of the ore deposits

Although structurally controlled by the same shear zone in the Wulong gold camp, the Wulong gold deposit, the Sidaogou gold deposit and the Jielishu copper-gold deposits show many differences in many aspects. One of the differences is the mineralogy and mineral paragenesis in the three deposits.

Study of mineralogy and mineral paragenesis are based on microscope observation on polished thin sections and thin sections as well as field investigation in the three deposits. 56 standard thin sections and 25 polished thin sections were prepared in the Yichang Institute of the Chinese Academy of Geology and Mineral Resources. Microscope observation work was done in the laboratory of the Science de la Terre, UQAC.

4.2.1 The Wulong deposit

4.2.1.1 Mineral description

Species of minerals in ore are generally simple in the Wulong gold deposit. Contents of sulfides in ore are about 8%. Identified ore minerals are predominated by pyrite, pyrrhotite, chalcopyrite and minor galena, sphalerite, arsenopyrite, bismuthinite and free gold. Gangue minerals are dominated by quartz with minor calcite, sericite, chlorite and fluorite.

Quartz: quartz accounts for major part of ores. Contents of quartz are over 90% in ores. Three generations of quartz are recognized in this ore deposit.

The first generation of quartz (Q1): With milky color, the Q1 accounts for 90% in the total quartz contents of ore. Most of the quartz veins are composed of Q1. Wavy extinction is common in quartz grains. Ductile deformation of quartz is not rare. Fractures formed in quartz are usually filled by late stage sulfides. The second-generation of quartz (Q2): the Q2 usually shows granular form and co-exists with pyrite and pyrrhotite filling fractures in Q1. Though the Q2 also show wavy extinction, but not as intense as the Q1. The third generation of quartz (Q3): the Q3 commonly co-exists with calcite and fluorite. They form veinlets and are distributed in early quartz veins and in host rocks. Q3 is characterized by its euhedral form and clean surface. Amount of Q3 is less than 5% in total quartz contents.

Pyrite: Pyrite accounts for about 5% in content. It is the most common sulfide specie in ores in this mine. Like quartz, pyrite can also be classified into three generations. The

first generation of pyrite (Py1) occurs as coarse, euhedral crystal. Py1 is less than 1% in total sulfide contents. Py1 is sporadically distributed in the Q1 veins. Py1 is characterized by its breccia structure and cemented by late quartz and sulfide veins. The second generation of pyrite (Py2) occupies about 3% of the in total sulfide content. Py2 mostly show euhedral –semi-euhedral form. Py2 usually co-exists with pyrrhotite, chalcopyrite and galena or occasionally forms independently pyrite veinlets filling fractures in early quartz. The third generation of pyrite (Py3) accounts for about 1% of the total sulfide content, and it is sporadically distributed in quartz veins formed with Q3. Py1 and Py2 are the major gold carrier minerals in ores.

Pyrrhotite: pyrrhotite occupies 2% ~ 3% of the total sulfides. It occurs as euhedral or anhedral fine-grained aggregates filling fractures in early quartz veins. Pyrrhotite usually co-exists with Py2. Based on 12 polished thin section observations, contents of pyrrhotite in different levels are quite variable in this mine. Generally, contents of pyrrhotite are high on upper levels in ore body (i.e. in #6 and #7 level), low contents of pyrrhotite usually occur at lower levels (i.e. #10, #12 level).

Chalcopyrite: contents of chalcopyrite are generally less than 1%, and it mainly co-exists with Q2 and (or) Py2 in small quartz veinlet. Chalcopyrite may also occur as droplets in sphalerite.

Bismuthinite: this minor mineral is the most reliable indicator for gold mineralization in the Wulong gold deposit. Free gold was observed where bismuthinite occurs. Bismuthite and free gold are interlocked, and they mainly occur in Q2 veins (Photo 4-1). It is not uncommon that the interlocking bismuthinite and gold were often observed at ends of the

Q2 veinlet or far sides of the quartz vein (Photo 4-2). These phenomena suggest that Bi and Au are readily transported in ore-bearing hydrothermal fluids during fluid migration. Bismuthinite was only observed in the Wulong gold mine during this study, though it was reported by other researches in the Sidaogou deposit (Liu 1988).

Sphalerite and galena together account for less than 1% in total sulfide concentration. They mainly occur in Q3 veins. Occurrences of sphalerite and galena as well as chalcopyrite in small quartz veins are generally considered as the end of gold mineralization in this ore deposit.

4.2.1.2 Mineral paragenesis and paragenetic successions

Based on microscope observations and field investigations, mineral parageneses are classified into four Groups with a successive order of : Quartz + Pyrite → Pyrite + Pyrrhotite + Quartz + Arsenopyrite + Bismuthinite + Au → Quartz+ Pyrite+ Chalcopyrite + Galena + Sphalerite + Au (?)→Calcite + Dolomite.

Four mineralization stages are marked by these mineral paragenetic successions. The first mineralization stage is characterized by the formation of giant quartz veins and the growth of the euhedral coarse pyrite sporadically distributed in quartz. The second stage of mineralization was formed after a structural event of the Wulong shear zone. As the result of the structural event, two sets of shear fractures were formed in early quartz veins. These fractures provided spaces for the second stage mineral precipitation. Minerals deposited at this stage are mainly pyrite, pyrrhotite, quartz, calcopyrite, arsenopyrite, bismuthinite, and

free gold. The second stage of mineralization constitutes the major gold reserves of the Wulong mine. The third stage of mineralization is marked by the formation of polymetallic precipitation. Though species of sulfides formed in this stage are more than those formed at the second stage, the contents of these sulfides in the third stage are much lower than that in the second stage and no significant gold deposited at this stage. Formation of calcite veinlet in both the quartz and host rocks indicates the ending of ore–bearing hydrothermal fluid processes and the whole mineralization episode in the Wulong gold deposit. Mineral parageneses and mineralization stages are summarized in Table 4-1.

4.2.2 The Sidaogou gold deposit

In the Sidaogou gold mine, ore bodies mainly occur as massive sulfide lens, quartz-sulfide veins and veinlet-disseminated ores. Massive sulfides usually contain high gold contents.

4.2.2.1 Mineral description

Comparatively, mineral assemblages are relatively simple in the Sidaogou gold deposit. Pyrite accounts for 95% of the total sulfides in ores with minor chalcopyrite and sphalerite. No arsenopyrite and galena were observed in this study, but these two minerals were reported in previous papers (Peng, 1993). Gangue minerals are mainly quartz, calcite, sericite and chlorite.

Pyrite: as the dominant ore mineral, two generations of pyrite (Py1 and Py2) were recognized. Py1 shows euhedral-semi-euhedral form, and is usually brecciated and cemented by Q2 and chalcopyrite. Free gold was observed in both Py1 grains and fractures. Py2 occurs as veinlet cutting through chalcopyrite and Py1.

Pyrrhotite: with contents ranging from 2% to 3%, pyrrhotite usually co-exists with Py1 and occurs as veinlet in early-formed veins.

Chalcopyrite: accounting for 1% to 2% in contents of the total sulfides, it co-exists with pyrrhotite and fills fractures.

Quartz: three generations of quartz (Q1, Q2, Q3) were identified. The early generation of quartz (Q1) is characterized by its milky color and euhedral form. Q1 co-exists with Py1. Q2 forms veinlet filling along fractures in quartz-pyrite veins formed by the first generation of quartz. Q2 co-exists with pyrrhotite and chalcopyrite. Q3 is limited in amount and co-exists with Py2 and occurs as veinlet.

Calcite: calcite is relatively well developed in this mine. Usually occurring as veins and massive form, calcite was often observed in host rocks.

4.2.2.2 Mineral paragenesis and succession

Based on ore textures, structures and mineral species, four mineral parageneses and mineralization stages are identified:

Stage 1: major mineral assemblages formed at stage 1 are dominated by quartz (Q1) and pyrite (Py1). This stage is important because gold was precipitated at this stage. Pyrite is the major gold hosting mineral.

Stage 2: mineral assemblages are dominated by Q2, pyrrhotite, Py2, chalcopyrite and free gold. Major gold was precipitated at stage.

Stage 3: mineral precipitation was weak at this stage, mineral assemblages are Q3 and Py3. Gold deposition was not as significant as the previous stage.

Stage 4: this stage is characterized by the formation of calcite. Occurrence of calcite indicates the ending of hydrothermal fluid processes in this area.

Mineral parageneses and mineralization stages are summarized in Table 4-2.

4.2.3 The Jielishu deposit

Stockwork, brecciated structures are the major ore structural types observed in the Jielishu gold deposit.

4.2.3.1 Mineral description

Identified ore minerals developed in the Jielishu deposit include pyrite, chalcopyrite, chalcocite, malachite and minor sphalerite and galena as well as free gold. Gangue minerals are dominated by calcite and dolomite.

Pyrite: two generations of pyrite (Py1, Py2) were identified. Py1 is characterized by its euhedral and coarse grains brecciated by late structural deformation. The brecciated pyrites are cemented by late quartz and sulfides. Py1 always accompanies Q1. Py2 is characterized by its fine grain size and euhedral form. Py2 usually contains free gold, and it is the major gold carrying mineral in the Jielishu deposit. In addition, chalcopyrite and minor sphalerite also precipitated at this stage.

Quartz: also shows two generations (Q1, Q2), the Q1 is *characterized* by coarse crystal form and milky color, and shows wavy extinction and brecciated structure. Q1 formed the major part of the quartz veins in the Jielishu deposit. Though minor in amount, Q2 is characterized by the vug structure developed in massive quartz veins (Photo 4-3). Q2 co-exists with Py2 and chalcopyrite.

Chalcopyrite: contents of chalcopyrite account for 30-40% of the total sulfides, chalcopyrite often co-exists with Py2 and occurs as veinlet cutting the early quartz-pyrite veins. Chalcopyrite is one of the gold-bearing minerals, and free gold is observed in chalcopyrite.

Chalcocite: as the result of secondary oxidation of *chalcopyrite*, chalcocite always distributes around chalcopyrite.

Malachite: the amount of this mineralis not high. It is *characterized* by its vivid interference color. Occurrence of this mineral indicates that the Jielishu deposit was sublested to oxidation after the deposition of the deposit.

4.2.3.2 Mineral paragenesis and successions

Based on mineral form and ore structure observed on polished thin sections as *well* as field investigation, three mineralization stages are classified and mineral assemblages are different at each stage in the Jielishu deposit.

Stage 1: *precipitated* minerals are predominated by quartz + pyrite + free gold. This mineralization stage is a major gold precipitation period in the Jielishu deposit.

Stage 2: *mineralization* is characterized by formation of polymetallic mineral assemblages and extensional structure formed in ore veins. Most of the sulfides were precipitated from hydrothermal fluids at that stage.

Stage 3: *mineralization* at this stage is weak and mineral assemblages are dominated by calcite and dolomite, together with very minor chalcopyrite and pyrite. No free gold was observed in minerals of this stage.

Stage 4: this stage *is* a post-ore stage, and it is characterized by the formation of chalcocite and malachite. Formation of these minerals indicates that the Jielishu ore deposit was exposed in an oxidized environment. Mineral parageneses and mineralization stages are summarized in the Table 4-3.

4.3 Species and distribution of gold-bearing minerals and minor element contents

Gold-*bearing* minerals were identified under the ore microscope. Minor element concentrations of selected gold-bearing minerals were analyzed using electronic

microprobe in the laboratory of Tianjin Institute of Metallogeny Geology, China. Part of the ore mineral microscope work was done in the laboratory of sciences de la terre, UQAC. Traditionally, gold minerals are classified into three species based on the ratios of R (R=1000* Au/(Au+Ag)): free gold ($R \geq 850$); electrum ($500 < R < 850$); and goldargentid ($150 < R \leq 500$). Based on the spatial relationships of free gold and its host minerals, four kinds of gold distribution patterns were recognized: trapped gold (free gold occurs as solid inclusion in pyrite); fracture gold (gold occurs in fractures of such minerals as pyrite, chalcopyrite); lattice gold (gold located at the lattice position of minerals); and interlocking gold (gold interlocked with bismuthinite).

Frequency of occurrence of gold was analyzed on 12 polished sections. *Listed* in table 4-4 are the statistical results of distribution features of free gold from the Wulong gold deposit. The statistic results from the Sidaogou deposit are listed in Table 4-5. These results indicate that gold distribution states in the two gold deposits are different. In the Wulong gold deposit, gold distribution is complex compared with the Sidaogou deposit. These differences reflect different gold mineralization stages and mineralization processes occurred in the two deposits. The Wulong gold deposit experienced more complex mineralization processes than the Sidaogou deposit. Gold bearing minerals are predominantly pyrite and quartz in the Sidaogou deposit, but in the Wulong gold deposit, bismuthinite is major gold-bearing mineral besides pyrite and quartz. Generally, free gold occurred in host minerals is in simple form such as fine rounded grain or irregular grain, occasionally, sheet-like and tree branch forms are also observed. Observations indicate that

most of the gold grain size is less than 0.074 mm. Table 4-6 lists grain size results on 40 gold grains:

Gold trapped as solid inclusion is mainly located in quartz and pyrite. Fracture gold *occurs* in mineral fractures such as quartz and occasionally in pyrite, pyrrhotite and bismuthinite. Grain boundaries of quartz, pyrite, pyrrhotite grains are dominant locations where lattice gold grains developed according to Peng (1993). Bismuthinite is the favorite mineral with which interlocking gold is mostly well developed. Seven samples were analyzed using electronic microprobe for minor element compositions in identified gold grains. Analyzed data are listed in Table 4-7.

Zhao (1993) analyzed a number of purified quartz samples of different quartz generations to compare variations of gold concentrations at different mineralization stages. These analyzed data are listed in Table 4-8. It's clear from these data that gold was mainly precipitated at the second stage of mineral formation in the Wulong gold deposit, this conclusion is supported by both microscope observation and individual mineral analysis results. Only three polished ore thin sections from the Jielishu deposit were observed, and five gold grains were identified. 10 gold grains are enclosed in early pyrite and the rest are located at grain boundaries of chalcopyrite and pyrite. No composition analysis was conducted for gold minerals in the Jielishu deposit.

In general, free gold has higher fineness (R value) and Au/*Ag* ratios in the Wulong gold deposit. The Sidaogou deposit contains higher silver contents.

4.4 Hydrothermal alteration

Although *hydrothermal* alteration doesn't always indicate ore mineralization, hydrothermal alteration often follows ore mineralization regardless the scale of hydrothermal alteration. Various mineral assemblages formed in different mineralization stages indicate the variation of fluid compositions during hydrothermal fluid evolution. Since the scales of mineralization episodes are varied, accompanying alteration results are accordingly changed and alteration minerals are usually zoned around the mineralization center. Alteration is of importance because it contributes much information on ore mineralization. In addition, hydrothermal alteration has usually wider range than the ore body from which the hydrothermal fluids were sourced, alteration pattern has been used as one of the useful mineral exploration tools for economic geologists.

In the Wulong gold camp, development of alteration patterns is different as *mineralization* features are different in individual ore deposit. In this section, alteration features will be discussed based on observation on individual ore deposits.

4.4.1 The Wulong gold deposit

Proximal host rock alteration is very common in the Wulong gold deposit. Recognizable alteration types include silicification, sericitization, muscovitization, chloritization, pyritization and carbonatization.

Silicification: It is the most well developed alteration type in the mine, and has an intimate spatial relation with gold lodes. Silicification usually distributes along both sides

of quartz lodes. Silicification zone has usually an average width of 3 ~ 5m. The maximum measured width of the silicification zone is 10m at the 11^{th} level in the No. 3 shaft. The width of silicification zone is positively proportional to the size of quartz lodes.

Sericitization: Mainly occurs where hydrothermal alteration is well developed. Sericitization is restricked in deposit and altered protoliths are mostly gneiss or granitic mylonites. Sericitization has no spatial relation with gold mineralization in the Wulong gold mine.

Pyritization: three stages of pyritization are developed in the deposit. The early stage pyritization is developed along both sides of early quartz veins, while the late stage pyritization accompanies along sides of or within late stage quartz veins, which are mainly small veinlet developed in early quartz veins. The third stage of pyritization is weak and mainly associated with carbonatization.

Carbonatization: this alteration is formed at the end stage of hydrothermal fluid processes. Carbonatization occurred as calcite veinlet and these veinlets are distributed in early-formed alteration rocks.

Chloritization is only developed in altered pre-ore diorite dykes.

Alteration types are commonly overlapped and zonation of alteration is accordingly not clear, however, from proximal alteration to distal host rocks, alteration is gradually decreased.

4.4.2 The Sidaogou deposit

Alteration is commonly developed in the Sidaogou deposit. The most important alteration types are pyritization and silicification, in addition, sericitization, carbonatization and minor chloritization are also recognized in the Sidaogou gold deposit.

Pyritization: the most important hydrothermal alteration type developed in the Sidaogou deposit, pyritization can be classified into two generations: (1) the syn-ore pyritization characterized by the yellow – gray yellow color and anhedral form of pyrite. Pyrite occurs as fine disseminated, veinlet or massive ore. Pyrite formed at the syn-ore pyritization is the dominant gold-bearing mineral in the Sidaogou deposit. (2) The post-ore pyritization is characterized by its bright yellow color and euhedral cubic form, it usually occurs in veinlet or disseminated in silicified metasandstone. Pyrite formed at this generation is barren in gold.

Silicification: it is also an important alteration in this deposit. Three stages of silicification are recognized: the pre-ore silicification is represented by the quartz boudinage developed in shear zone, and such quartz boudinages demonstrate strong ductile deformation features. The pre-ore silicification was the result of metamorphism and shear deformation, not the results of hydrothermal fluid processes related to gold mineralization. The syn-ore silicification occurs as veins and (or) massive quartz blocks. Quartz formed during this stage often contains high-grade gold. Typical mineral parageneses of this alteration are quartz + pyrite + gold. The post-ore silicification is generally weak and commonly occurred as fine veinlet distributed in fractures displacing ore veins.

Sericitization: mainly developed in metasandstone, it was the result of decomposition of plagioclase and clay minerals of the sandstone during the hydrothermal fluid processes

(Cui and Peng et al., 1988). Sericitization is not genetically related to gold mineralization in the Sidaogou deposit.

Carbonatization: occurrence of calcite veinlet marked the presence of the carbonatization in the Sidaogou deposit. Besides the dominant calcite formed at this alteration process, quartz and minor dolomite were also the products of the process. Carbonatization marked the end of the hydrothermal fluid processes in the Sidaogou deposit.

Chloritization is the result of decomposition of biotite during hydrothermal fluid processes and it is not spatially related to gold lodes in this deposit.

Unlike the Wulong deposit, alteration in the Sidaogou gold deposit demonstrates spatial zonation on either horizontal direction or on the vertical direction. Apart from ore body, alteration pattern varies in an order of: massive pyritization zone → pyritization → silicification → carbonatization → protolith.

4.4.3 The Jielishu deposit

Host rock alteration is poorly developed in the Jielishu gold deposit. Identified host rock alteration types include silicification, pyritization and carbonatization.

Silicification is mainly developed along both sides of gold lodes with an average width of 3.5m. Pyritization is limited to the vicinity of quartz veins. Carbonatization occurred as veinlet distributed in both marble and gold bearing veins. No host rock alteration zonation was observed in the Jielishu gold deposit.

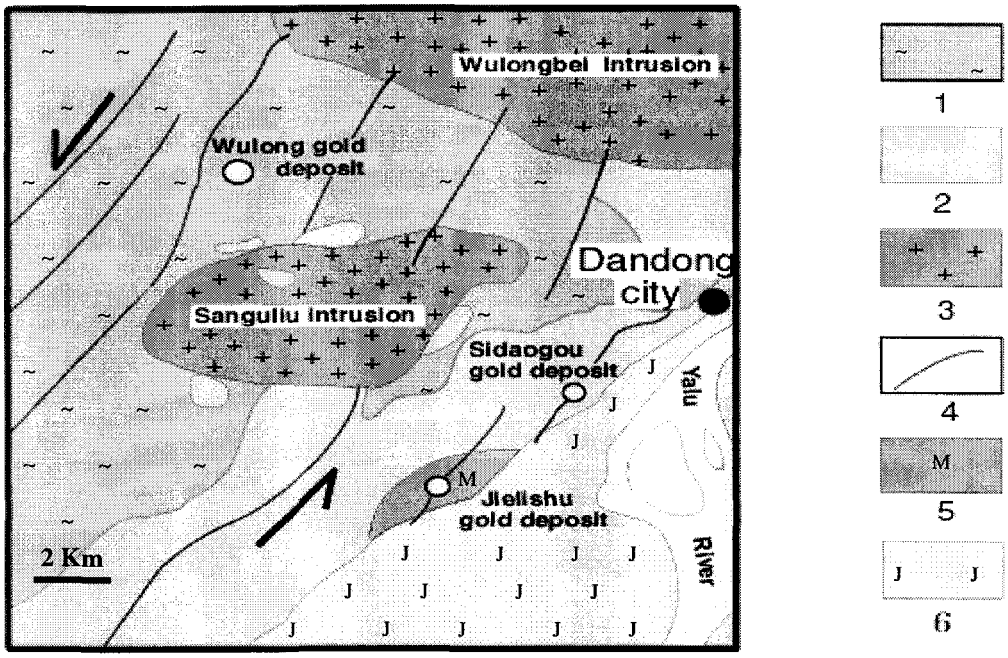

1, Late Archean gneiss; 2, late Proterozoic metasandstone;
3, magmatic intrusion; 4. The Wulong shear zone; 5, late Proterozoic marble;
6, Jurrasic volcanic breccia sedimentary rocks.

Figure 4-1 Simplified regional geological map of the Wulong gold camp (modified from Wang 1990)

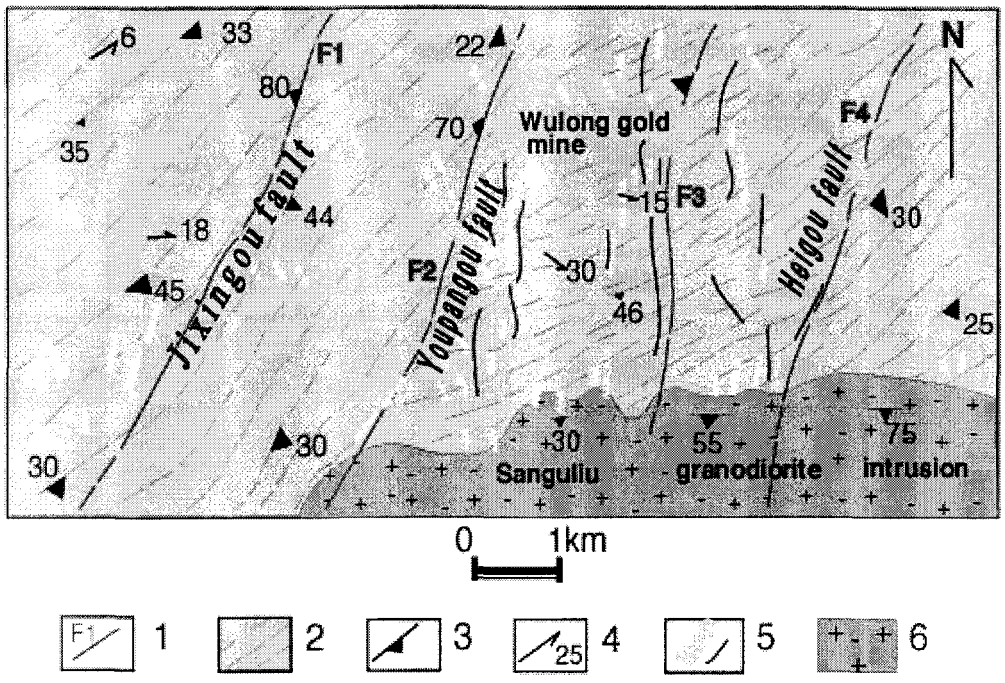

1, major shear zone; 2 gneiss; 3, dip direction of gneissosity;
4, extension direction of lineation; 5, gold lode and dyke; 6, granodiorite.

Figure 4-2 Simplified geological map of the Wulong gold mine, Wulong gold camp (modified from Wang 1990)

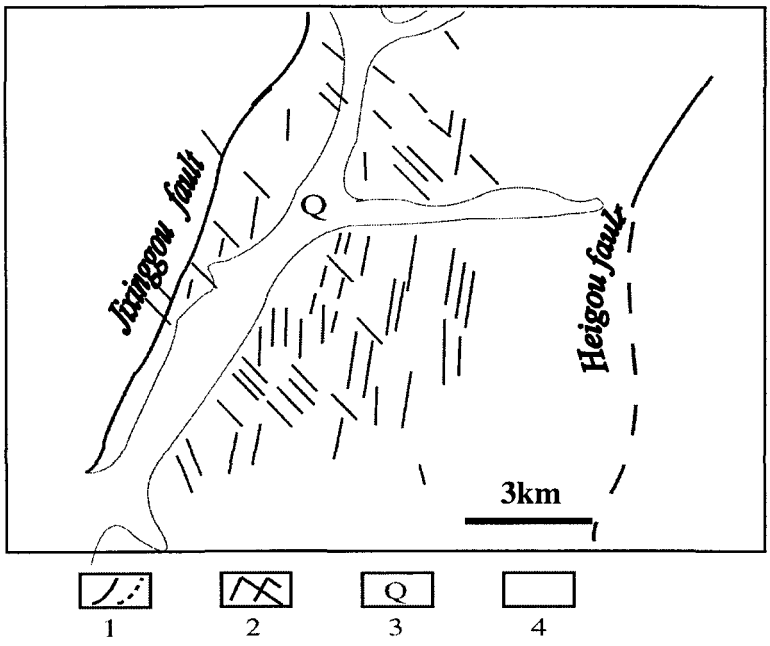

1, major shear fault; 2, ore-controlling fault; 3, quartanary;
4, gneiss

Figure 4 - 3 Rhombic structural system controlling the major gold lodes in the Wulong gold mine, Wulong gold camp.
(Cited from Zhao (1993))

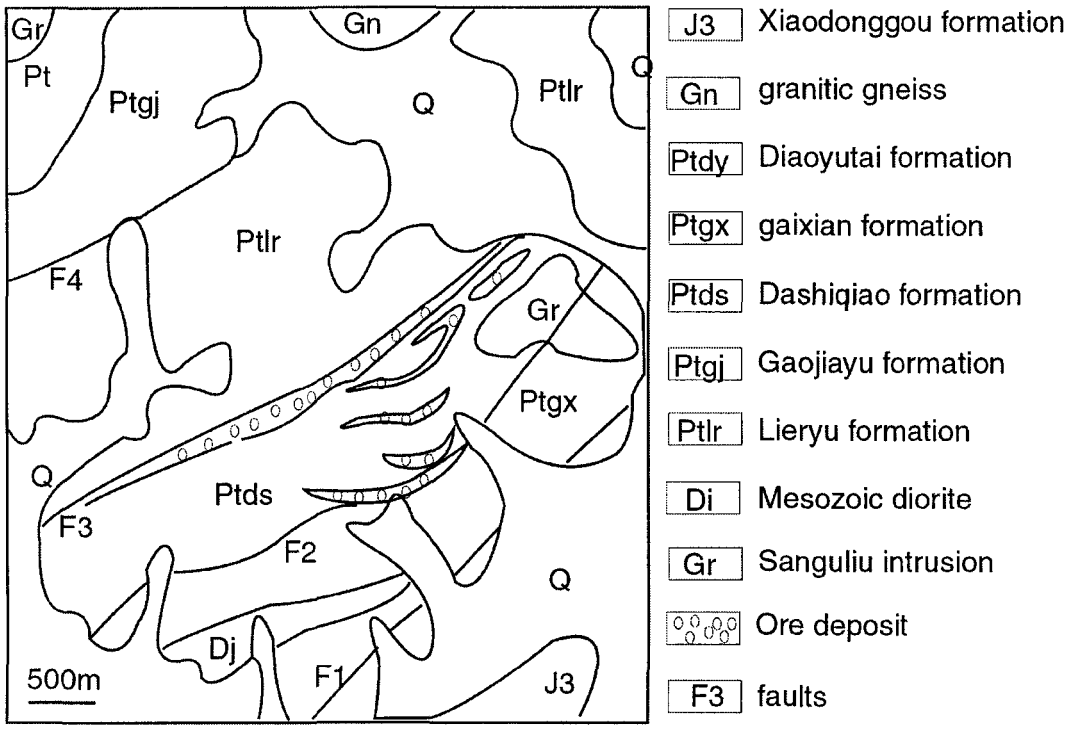

Figure 4-4 Simplified geological map of the Sidaogou gold mine
(abbreviation : Fm: formation; SZ: shear zone; Gr: granite)
(cited from Zhao et al., 1993)

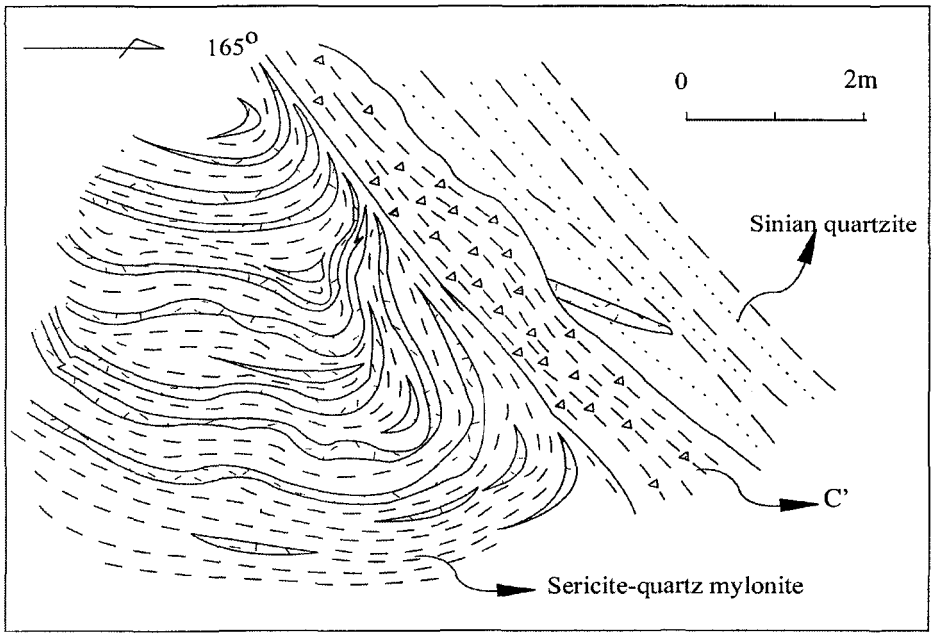

Figure 4-5 Intrafolial folds and C fabrics formed in sericite quartzite mylonites in the Sidaogou area

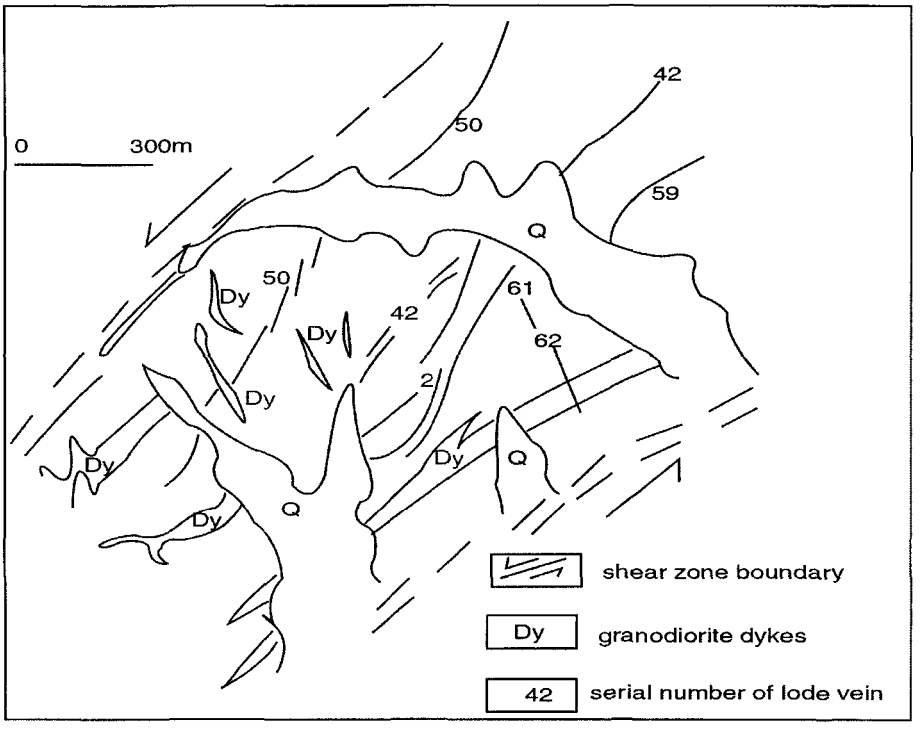

Figure 4-6 Simplified geological map of the Jielishu gold-copper mine of the Wulong gold camp (cited from Wang 1990)

Table 4-1 Mineral parageneses and mineralization stages of the Wulong gold deposit

	Stage one	Stage two	Stage three	Stage four
Quartz				
Pyrite				
Pyrrhotite				
Arsenopyrite				
Free gold				
Bismuthite				
Chalcopyrite				
Sphalerite				
Galena				
Calcite				
Chlorite				

Table 4-2 Mineral parageneses and mineralization stages of the Sidaogou gold deposit

Mineral	Stage 1	Stage 2	Stage 3	Stage 4
Quartz				
pyrite				
Pyrrhotite				
Chalcopyrite				
Free gold				
Calcite				
Chlorite				

Table 4-3 Mineral parageneses and mineralization stages of the Jielishu deposit

Precipitated Mineral	Sulfide precipitation episode			Post-ore episode
	Stage 1	Stage 2	Stage 3	Stage 4
Quartz	▬▬▬	▬▬▬	———	
Pyrite	▬▬▬	▬▬▬	.....	
Chalcopyrite	.....	▬▬▬	------	
Sphalerite		———	.....	
Galena		---------	---	
Gold	-·-·-·-	-·-·-·-·-		
Calcite + dolomite			----------	
Chalcocite				----------
Malachite				.....

Table 4-4 Distribution states of gold in major gold-bearing minerals in the Wulong gold deposit

Minerals	Trapped Au		Fracture Au		Lattice Au*		Interlocks Au		Total	%
	Grain	%	Grain	%	Grain	%	Grain	%		
Py	1	0.64	3	1.92	8	5.13	-	-	12	7.69
Po	-	-	2	1.28	7	4.49	-	-	9	5.77
Bi	-	-	2	1.28	-	-	44	28.2	46	29.48
Qz	15	9.62	54	34.62	20	12.82	-	-	89	57.06
Total	16	10.26	61	39.10	35	22.44	44	28.2	156	100

Py: pyrite; Po: pyrrhotite; Bi: bismuthite; Qz: quartz

* data of lattice gold are cited from Zhao(1993)

Table 4-5 Gold distribution features in gold-bearing minerals in the Sidaogou gold deposit

Distribution states	Occurrence frequency (%)			references
	Pyrite	Quartz	Total	
Fracture Au	51.79	19.64	71.43	1, 2
Trapped Au	23.31	5.36	28.57	2
Total (%)	75	25	100	

*1, Peng (1993); 2, this study

Table 4-6 Statistic results of free gold grains in the Wulong gold camp

Size ranges	0.074 ~ 0.037 (mm)	0.036 ~ 0.01 (mm)	<0.01 (mm)	total
Grain counts	28	78	6	112
percentage	25	69.6	5.4	100

Table 4-7 Minor element compositions of free gold in the Wulong gold camp

Sample No.		W8	W8-1	W3-8-9	W3-6-9	W3-8-1	S-1-10	S-1-6	S-1-6	S-1-10
minor element contents (%)	Pb	N	N	N	N	0.17	N	N	N	N
	S	N	N	N	N	N	N	N	N	N
	Te	0.02	N	N	N	N	N	N	N	N
	As	0.02	N	N	N	N	N	N	N	N
	Ni	N	0.2	N	N	N	N	N	N	N
	Fe	0.28	0.77	0.07	N	N	N	N	N	N
	Cu	N*	N	N	N	0.14	N	N	N	N
	Bi	N	0.56	0.50	N	N	N	N	N	N
	Ag	8.47	7.00	7.14	5.75	6.11	10.00	14.96	17.02	7.86
	Au	91.22	89.13	92.15	91.14	93.63	86.01	85.69	80.96	63.79
R values		915.0	927.2	923.8	942.6	938.7	895.82	814.53	826.36	890.36
Fracture Au		Free gold	Free gold	Free gold	Free gold	Free gold	Free gold	electrum	electrum	Free gold

*N, not detected

Table 4-8 Concentrations of Au and Ag in different quartz generations in the Wulong gold camp

Sample	quartz	Sample description	Au * (ppm)	Ag (%)
W2-2-1	Q1**	Massive, milky color, with greasy luster	0.05	3.0
W2-11-1	Q1	Massive, milky color, with greasy luster	0.05	2.0
W3-9-1	Q1	Massive, milky color, Co-existing with pyrite	0.12	4.0
W2-8-1	Q2	Light gray color, co-existing with pyrite and pyrrhotite	5.00	4.0
W4-8-7	Q2	Light gray color, co-existing with pyrite and pyrrhotite	5.50	3.0
W4-2-4	Q2	Gray color, co-existing with pyrite, bismuthite and free bismuth	27.50	8.0
W4-5-1	Q2	Gray color, co-existing with pyrite and pyrrhotite	11.00	3.0
W3-8-9	Q2	Dark gray color, co-existing with pyrite, bismuthite and free bismuthite	54.00	5.0
W3-8-20	Q3	White color	5.50	10.0
S1-0-2	Q2	Dark gray color, co-existing with pyrite and pyrrhotite	96.00	6.0
S1-0-8	Q2	Gray color, fine grain and co-existing with pyrite	80.00	0.00

*data are cited from Zhao, (1993), **numbers after Q correspond to generations of quartz

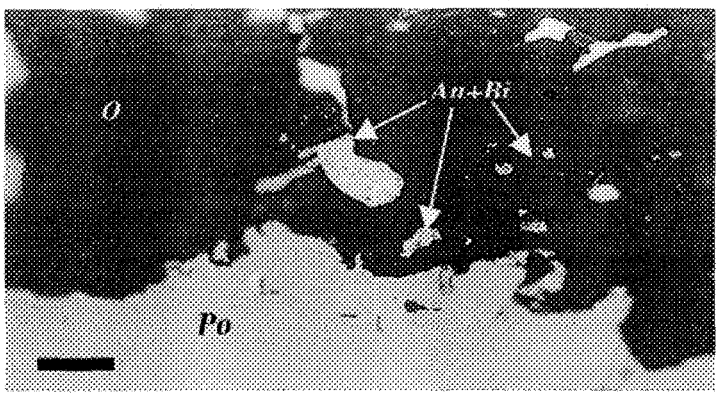

Photo 4-1 Coexisting free gold and bismuthite in second stage quartz veins (site : 10 level, Wulong mine, reflected light. (scale bar: 5um)

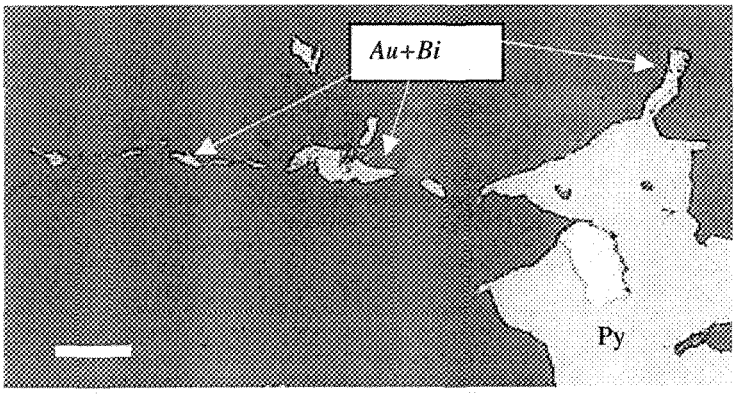

Photo 4-2 Coexisting Au +Bi minerals usually distributed at ending of sulfide venlets. (site : level 10 Wulong mine, reflected light, x 40) (scale bar: 5μm)

Photo 4-3 Vug structure and euhedral quartz crystals are common in the Jielishu mine, this structure indicates an extension environment during ore precipitation (site : Jielishu mine, open pit)

Chapter V

Geochemical features of the Wulong gold camp

5.1 Geochemical characteristics of the host rocks

Host rocks spatially relating to gold mineralization are dominated by granitic rocks and metamorphosed rocks. The late Archean gneiss, Proterozoic metamorphosed sandstone and marble are geochronologically too older than that of gold mineralization (Mesozoic) to be genetically considered with gold mineralization in the Wulong gold camp according to Yao et al. (1988). For this reason, discussions of geochemical characteristics of the Proterozoic metamorphosed sandstone and marble are not included in this chapter. However, the late Archean gneiss is included in geochemical feature discussion in this part because many researchers suggested that the Archean gneiss was genetically related to late intrusive granites and dykes (Yao et al., 1988, Cui et al., 1988). So geochemical characteristics of host rocks are mainly focused on the Archean gneiss and the Mesozoic granites represented by the Sanguliu intrusion and the Wulongbei intrusion as well as the various dykes developed in this gold camp. Geochemical comparisons of these magmatic rocks were emphasized during the discussion.

5.1.1 Major elements

As discussed in chapter 2, petrological geochemistry of the gneiss is characterized by the stable petrochemical compositions. Petrochemical analyses indicate that the late Archean gneissic rocks contain high silica (average SiO_2 contents are 72.85%) and are Al-saturated with average contents of Al_2O_3 of 14.44%, contents of Mg and Fe are low, total Fe contents are lower than 1.6%, MgO is less than 0.47%; enriched in potassium and alkali with a sum of K_2O+Na_2O ranging from 7.17% to 9.06%. On the contrary, the Mesozoic Sanguliu and the Wulongbei intrusions are characterized by their variable petrochemical compositions and complex petrological features (Yao et al., 1988), for example, contents of SiO_2 of the Sanguliu and the Wulongbei intrusions vary from 50% to 75%. A number of petrochemical composition data of representative intrusions are listed in Table 5-1, and the calculated CIPW minerals are listed in Table 5-2.

According to Rittmann (1973), normative values of Ab are allocated to Or and An to form Af and Pl. On the Q-A-P diagram of igneous rocks, the plots of these data mainly fall in the boundary of admellite and granodiorite and the quartz monzodiorite domain (Fig. 5-1). Most of the samples have DI values over 80, and two samples from the Wulongbei intrusion contain fairly high normative corundum (>1), while samples from the Sanguliu intrusion are mostly absent of corundum, only one sample contains corundum. The Harker diagram of major elements is illustrated in Figure 5-2. From this diagram, it is shown that the granite complexes have wide variations in petrochemical composition. Contents of SiO_2 change from 58% to 75%. With the increase of SiO_2, contents of Al_2O_3, FeO, MgO, MnO, CaO, P_2O_5 and TiO_2 gradually decrease. Content

of K_2O is proportional to SiO_2. These petrochemical features of the intrusions in the Wulong gold camp represent typical calc-alkaline series.

5.1.2 Trace elements

In general, contents of iron-group elements gradually decrease with the change of petrological types from diorite → granodiorite → granite. These variations are also demonstrated in trace element contents of the magmatic intrusive rocks in the Wulong gold camp (Fig.5-3). Compared to the Sanguliu intrusion, the Wulongbei intrusion has a wider variation range of iron-group elements. But these two intrusions have higher Sr and lower Ba contents than the average contents of the same type igneous rocks in the world (Yao et al. 1988). Contents of Rb vary between 50 –170 ppm, and Rb/Sr ratios vary in a range of 0.06 – 0.5; ratios of K/Rb range from 328 – 480. In addition, contents of volatile elements such as F and Cl of the Wulongbei intrusion are high and with an average value of 770 ppm and 260 ppm for the two elements, respectively.

5.1.3 Rare earth elements

REE study on magmatic rocks of the Wulong gold camp was carried out, but not complete and in detail. According to Peng (1993), the average contents of total REE of the Sanguliu intrusion is 197 ppm based on the analyzed results of six samples. The average ratio of LREE/HREE is 8.24 and $\delta Eu=0.70$. All the rocks show similar REE distribution patterns and enriched in light REE. The representative REE patterns of various magma rocks are show in Figure 5-4.

5.1.4 Geochronogical ages of intrusions

Constraint of geochronologic ages has long been quite a problem due to conflicting geochronological data obtained through different approaches in the Wulong gold camp. However, there is a concession on the relative age of the gneissic rocks that it is much older than the metasandstone since the gneissic rocks is considered as the production formed at Archean ages. Some workers suggested that the gneissic rocks resulted from migmatitization during the Proterozoic ages (Wang et al., 1988). These geochronological assumptions have a large time gap with isotope ages of 221.25 Ma dated on mica using the K-Ar method (Yao et al., 1988). Because of these conflicting geochronological ages, Yao et al., (1988) used both K-Ar and U-Pb methods to date the gneiss and the magma intrusions in the Wulong gold camp. The K-Ar method was used to date the mica group minerals separated from the magmatic rocks and the U-Pb method was employed to date the accessory minerals (zircon and monazite) collected from the same kind of rocks. Pb isotope compositions of ores were used to trace ore material sources and their formation ages. The analyzed Pb isotope data of ores are listed in Table 5-3, and the U-Pb data from granitic rocks are listed in Table 5-4. On the $^{207}Pb/^{204}Pb$ vs. $^{206}Pb/^{204}Pb$ and $^{208}Pb/^{204}Pb$ vs. $^{206}Pb/^{204}Pb$ diagrams (Fig. 5-5), most of the plots are close to the single stage growth curve as illustrated on Figure 5-5. But it is also clear that ore Pb isotope compositions in the Wulong mine and the Sidaogou mine are different, these isotope composition variations may indicate the modification of ore fluids during their migration processes.

The calculated single stage model ages of the ores from the Wulong mine and the Sidaogou mine are listed in the Table 5-3, the U-Pb isotope ages of the gneiss are listed in Table 5-4. The calculated single-stage model ages are roughly grouped into two sets: one set ranges between 719 ~ 779Ma, the other set ranges from 814 to 874 Ma, the single stage model ages of the Sidaogou deposit are 558Ma. Obviously, these calculated ore isotope ages are much older than they are thought to be (gold mineralization are soppoed to had been formed during the Mesozoic ages), while the ages of the gneiss are much younger than the ages they are thought to be(the generally assumed Archean for the gneiss, and the Late Proterozoic for the Liaohe Group). This is where caused the arguable statements about the relative geochronological ages about the gneiss and the gold mineralization in this region (or the whole NE China metallogenic province). As proposed by Li (1987), the much large single stage model ages suggest that ore materials were mainly sourced from Precambrian terrain. These ages don't represent the mineralization age of the ore, rather they represent their material sources from which they formed. And the U-Pb ages of the gneiss suggest that the gneiss was subjected to strong thermal disturbence during Mesozoic, and the much younger isotope ages don't represent the formation ages of the gneiss. These data also suggest that U-Pb isotope signatures are not reliable for old geologic units (older than the Mesozoic ages) in geological age determination in the Wulong region.

The age variations of granitic dykes and the Sanguliu intrusion from the U-Pb dating method range from 148.9 to 198 Ma. The K-Ar dating results of four samples from the different metamorphic rocks and pegmatite form two age groups (Table. 2-5). K-Ar ages of mica from gneiss range from 116 ~ 160 Ma, while the metamorphosed rocks from the Liaohe group have ages ranging from 1100Ma to 1500 Ma. Once again,

K-Ar ages for gneiss are much younger than they are should be. The isotope ages of the Liaohe Group are in agreement with other geological evidences. From this point the isotope-dating results for the Mesozoic intrusions and the Liaohe Group are reliable and acceptable.

Regardless of the isotope dating methods used in this region, isotope data suggest that all the granitic rocks are of Mesozoic, and the metamorphosed rocks of the Liaohe group are of middle-late Proterozoic, while no reasonable geological ages for the gneiss rocks were obtained in this project. And the reason why the U-Pb and K-Ar dating methods are not useful for the Archean gneiss developed in the Wulong region is beyond this project. The isotope ages of the magmatic rocks are in agreement with isotope ages dated in other area for the same type of magma in China and the time period of the plate collision between the Pacific Ocean plate and the Sina-Korea Plate (Wang et al., 1998). The youngest granite was formed at 98 Ma. The large age values calculated from 207Pb/206Pb ratios probably resulted from the mixing of radiogenic Pb sourced from the old Precambrian rocks.

5.2 Geochemical characteristics of ore deposit

As noted above, though the three gold deposits are pronouncedly controlled by the Wulong shear zone and share many geological features, they also demonstrate many differences in terms of mineralogy and geochemistry. It is these similarities and differences that promote various interpretations for the hydrothermal fluid sources, and ore genesis of the gold camp. Geochemical characteristics of the individual gold deposit will be discussed and compared in this section.

5.2.1 Rare earth elements

Rare earth element contents of six ore samples were collected and are listed in Table 5-5. Chondrite normalized REE patterns of ores are plotted in Figure 5-6. REE contents of the ores from the two ore deposits indicate that ores are generally enriched in light REE. Ores from the Wulong gold deposit have similar total REE contents, while the total REE contents in ores of the Sidaogou deposit are quite variable. δEu values in the Wulong gold deposit are roughly close to 1 and have slight depletion of Eu, while ores in the Sidaogou deposit show both strong Eu depletion and enrichment. These differences may indicate their different mineralization processes.

5.2.2 Pb isotope

Listed in Table 5-3 are eight Pb isotope data, these analyzed minerals are closely related to gold mineralization in the Wulong gold camp. Most of the data are relatively consistent. $^{206}Pb/^{204}Pb$ ranges from 17.487 to 17.793, $^{207}Pb/^{204}Pb$ ranges from 15.514 to 15.860, and $^{208}Pb/^{204}Pb$ ranges from 38.269 to 39.521. • values are generally large and similar in the Wulong gold camp. The • values indicate that Pb was mainly sourced from the upper crust. The characteristic parameter ω has wide variation range (40.01 ~ 48.22).

5.2.3 Sulfur isotope

Sulfides (especially the pyrite) are the predominant gold-bearing minerals in the Wulong gold camp. Sulfur isotope study may disclose some information for the source of ore materials of the camp. 47 sulfur isotope data of the Wulong deposit and 35 sulfur isotope data from the Sidaogou deposit were collected from literatures. Analyzed minerals for the sulfur isotope include pyrite, pyrrhotite and sphalerite as well as arsenopyrite. Compiled δ34S data are listed in Table 5-6. On histograms of $\delta^{34}S$ (Fig. 5-7), concentration of the $\delta^{34}S$ values in the two different mines are quite clear. $\delta^{34}S$ values of sulfides from the Wulong gold deposit are uniform and stable. Irrespective of the sulfide species, average $\delta^{34}S$ values are around +1.55 ~ +2.5 ‰. Sulfur isotope of pyrite from the Sidaogou deposit still have very gentle variation, but average $\delta^{34}S$ value shifts to much higher value than that of the Wulong deposit.

$\delta^{34}S$ values of most magmatic rocks have been believed for years to be within a range of 0‰ ± 5‰ (Ohmoto and Rye, 1979). However, new data from worldwide indicate that $\delta^{34}S$ values of 0‰ for magmatic rocks do not necessarily indicate that sulfur in the magma was from immediate mantle or homogenized crustal origin. In fact, $\delta^{34}S$ values of magmatic rocks drifting from the 0‰±5% domain are quite common, this is because considerable sulfur proportions were obtained by magma from the host rocks through bulk-rock and selective assimilation during the intrusion processes of magma (Ohmoto and Goldhaber, 1997). Sulfur isotope values from the Wulong gold camp indicate that, though sulfur isotope values have different variation domains in the two studied deposits, the Wulong gold deposit has steady sulfur isotope sources, and these sulfur isotope data reveal strong magma source feature. High $\delta^{34}S$ values in the

Sidaogou deposit suggest that ore-bearing fluids experienced strong water-rock reactions with host rocks during hydrothermal fluid processes.

5.2.4 H , O and C isotope

Bulk analyses of fluid inclusions sampled from ore quartz veins were operated in the Yichang Institute of Geology to determine δD and $\delta^{18}O$ values. $\delta^{18}O_{H2O}$ values were calculated using the equation proposed by Shiro and Sakai (1972):

$$1000\ln\alpha_{Q\text{-}H2O}=3.55*10^{6}*T^{-2} - 2.57 \quad (T: 195 - 573^{o}C)$$

for calcite sample, $\delta^{18}O_{H2O}$ values are calculated using the equation given by O'Neil et al., (1969):

$$1000\ln\alpha_{Calcite\text{-}H2O}=2.780*10^{6}*T^{-2} - 2.89 \quad (T: 0 - 500^{o}C)$$

Analyzed δD and δO_{quartz} as well as the calculated δO_{H2O} values of the Wulong deposit are listed in Table 5-7. Four calcite samples collected from the Sidaogou and the Jielishu deposits were analyzed for $\delta^{13}C$ and $\delta^{18}O$ values are reported in both $\delta^{18}O_{\text{-}CPDB}$ and $\delta^{18}O_{\text{-}SMOW}$. The analyzed $\delta^{13}C$ and$\delta^{18}O_{\text{-}CPDB}$ and $\delta^{18}O_{\text{-}SMOW}$ are listed in Table 5-8. The $\delta^{18}O$ data alone could not be used to constraint the fluid source of calcite. The $\delta^{13}C$ values vary from –5.51‰ to –1.21‰, average value is –3.46‰, which is located in the range of igneous carbonate (Spooner et al., 1987). The $\delta^{13}C$ data and the $\delta^{18}O$ data signatures together suggest that the material source of the calcite developed in the Wulong gold camp are probably of magmatic hydrothermal source.

On δD vs. δO diagram (Fig. 5-8), plots of quartz samples are located outside of the origin-known-sources. Apparently, δD and $\delta^{18}O$ data of quartz samples are unlikely to determine source of ore-bearing fluids, but if $\delta^{13}C$ data are considered together with the δD and $\delta^{18}O$ data, we may suggest that ore-bearing fluids were of magmatic derivative, but these fluids were modified during their migration processes.

5.2.5 Trace elements

Nine purified sulfide samples were analyzed for trace element contents in different sulfide species. Analyzed sulfides include pyrite, pyrrhotite, sphalertie, and chalcopyrite. The analyzed results are listed in Table 5-9. Sulfides have generally high gold contents, this is concordant with the fact that free gold is frequently observed in sulfides. Pyrrhotite and the second generation of pyrite have high contents of Bi and Te. Contents of Te are positively proportional to that of Bi. At early stage of gold mineralization, Ag/Au ratios are relatively low with an average value of 0.69, while at late stage, this ratio increases to an average value of 1.12. Co/Ni ratio is particularly interesting in that it shows a regular change at different stages. In the first generation of pyrite, this ratio has an average value of 18.57; in the second stage of pyrite, this ratio has a range from 3.02 to 7.08; while at the last stage of pyrite, this ratio is very low, only 0.41.

5.3 Fluid inclusion study

To study the geochemical features of ore-bearing fluids trapped in ores and the spatial evolution of such hydrothermal system on the Wulong shear zone profile, a number of selected fluid inclusion samples collected from the Wulong gold camp were studied. 27 double polished thin sections were prepared in the laboratory of the Institute of Geology and Mineral resources, Yichang. Thin section processes followed the procedures proposed by Shepherd et al. (1985) and Lu et al. (1990).

In general, fluid inclusions are well developed in various stages of quartz veins, though fluid inclusions in calcite are occasionally observed, calcite is not the major fluid inclusion study target due to small size of fluid inclusions in calcite. Only one exception of microthermometer measurement on fluid inclusion on calcite sample was performed in a sample from the Jielishu deposit since no useable fluid inclusion was observed in quartz in that mine. During fluid inclusion selection, two types of fluid inclusions were selected. The first group fluid inclusions are those with obvious primary inclusion features; the second group of inclusions are secondary fluid inclusions, though they are secondary in genetic relation to their host minerals, they have clear temporal relations to ore precipitation. Origin identification of fluid inclusion follows the criteria defined by Roedder (1984).

5.3.1 Petrographic description

Optical observations of all the double polished thin plates were undertaken in the petrographic laboratory of UQAC. Total of 150 fluid inclusions were found in 15 of the 27 double polished thin sections. Most of the useable fluid inclusions have an average dimension size of 4x6 μm^2, occasionally, some fluid inclusions reach dimension size

10*15 μm^2. All of the examined fluid inclusions were either located in quartz grains or along healed fractures within quartz vein. Highest populations of fluid inclusions are usually developed in the later form. These fractures cut across grain boundaries and usually coeval with sulfides. Both the primary and the ore-genetically related secondary fluid inclusions are equally important in this gold camp. Classification of fluid inclusions is illustrated and described in Figure 5-9.

At room temperature, the aqueous inclusions contain an aqueous liquid phase and a vapour phase with a consistent liquid/vapour ratio of about 5:1 (Photo 5-1). CO_2-rich inclusions contain a CO_2 vapour phase with minor amounts of liquid phase(10%) rimming the CO_2 vapour (Photo 5-2). Occasionally, the CO_2-rich inclusions contain three phases at room temperature : an aqueous phase, a CO_2 liquid and a CO_2 vapour phase (Photo 5-3), but the L_{CO2} phase disappears once the temperature slightly rises a little bit. No daughter mineral was observed in all fluid inclusions, but black particles were observed in several inclusions (Photo 5-4), and these particles were not dissolved in heating cycle even when temperatures reached 500°C. These particles are probably sulfides based on their incumbent sulfide distribution features, and these sulfide particles were entrapped into the inclusion through mechanical processses during the formation of fluid inclusions.

Occurrence of these three types of inclusions within one individual quartz vein is not uncommon. The presence of various proportions of CO_2 within coeval inclusions suggests that phase immiscibility (CO_2 effervescence) occurred during entrapment or healing of the fracture. Homogenization temperature features of those CO_2-HO_2 inclusions also indicate the existence of phase immiscibility during fluid inclusion

entrapment. This phenomenon is frequently observed in samples from the Wulong gold mine.

As proposed by Robert and Kelly (1987), the abundance of type 3 (CO_2+H_2O), type1 (H_2O) and type2 (CO_2-rich) fluid inclusions is present in decreasing order in the Wulong gold mine and in the Sidaogou gold mine. But in the Jielishu mine all fluid inclusions observed are type1 (H_2O), no type2 (CO_2-rich) and type3 (H_2O+ CO_2) fluid inclusions were found, and those visible fluid inclusions are too small to measure microthermometers on freezing-heating stage. At the Jielishu deposit, only one fluid inclusion is big enough to make homogenization temperature measurement in a calcite grain. Fluid inclusions study was mainly concentrated on the Wulong gold ores and the Sidaogou gold deposits.

5.3.2 Methods of microthermometric measurements

Microthermometric data were obtained using a United States Geological Survey (U.S.G.S) gas-flow heating -freezing stage at UQAC. The accuracy of the trendicator thermocouple was determined to be within 0.5°C using synthetic fluid inclusions provided by the geological department of University of Polytech. VA. USA. on the freezing/heating stage over a fairly wide rage (-95 °C -- +390 °C). Procedures of cutting and mounting the fluid inclusions containing sample chips on the freezing/heating stage followed the methods defined by Roedder (1984), Shepherd (1985) and Lu et al.(1990). Freezing experiments were carried out before heating to avoid stretching and damaging the target inclusions.

5.3.2.1 Freezing experiment results

aqueous inclusions:

Generally, the aqueous fluid inclusions have first melting temperatures (the Eutectic point) around -20.4 °C ~ -27.1°C. The final melting temperature of ice is mainly around -4.5--0.6 °C. Aqueous fluid inclusions usually have homogeneous temperatures at +150 °C ~ +220 °C, and they have consistent high DF (Degree of Fill $=V_{H2O}/(V_{H2O}+V_{vapour})$) of about 90-95%.

CO_2-rich inclusions:

Though population of this type of fluid inclusions is not as high as the H_2O-CO_2 fluid inclusions, CO_2-rich fluid inclusions are characterized by their large size and low DF values. CO_2-rich fluid inclusions usually have size range in 6 x 10 μm2, and DF values are usually as low as 5-10%; occasionally pure liquid CO_2 inclusions were observed at room temperature. The first melting temperatures are tightly clustered around -56.0 °C ~ -62.0°C. This first melting temperature ranges indicate that the CO_2 phase contains very minor amount of CH_4, H_2S or N_2 according to Holland et al(1988). Due to the low DF values of such kind of fluid inclusions, ice melting temperature of CO_2-rich fluid inclusions could not be measured.

CO_2-HO_2 inclusions:

This group of fluid inclusions demonstrates simple melting from frozen CO_2 to liquid and vapour CO_2 phase upon heating. The first melting temperatures of CO_2 are very tightly clustered around -56.7°C, with only a minor depression to -58.3°C, which is very similar to the phenomenon reported by Robert and Kelly (1987) in the Sigma gold deposit, Abitibi, Quebec.

CO_2 hydrates are observed in this type of inclusions. The techniques and criteria involved in CO_2 hydrate detecting and measuring of the decomposition temperatures of CO_2 hydrate follow the procedures given by Collins (1979) (p1439-1440). The temperatures of decomposition of CO_2 hydrate in CO_2-H_2O inclusions developed in the Wulong gold camp are clustered between +7.8 ~ +8.5 °C.

5.3.2.2 Heating experiment results

Based on the basic hypotheses proposed by Roedder (1984), fluid inclusions were assumed to be formed in a uniform monophase environment when they were entrapped into the host minerals. Reheating fluid inclusions on the heating stage is a process to retrieve the geological processes during which the fluids cool. When temperature raised to certain degree, the fluid inclusion will be homogenized into a uniform monophase of liquid or gaseous phase. This temperature at which the fluid inclusion is homogenized is called homogenization temperature (Roedder, 1984).

H_2O inclusions:

Fluid inclusions with H_2O phase dominant have generally lower homogenization temperatures in heating cycle, which ranges from 205°C to 295°C in the Wulong mine, in Sidaogou, this range varies from 105 °C to 245°C, and the vapour phase always vanished into liquid phase during heating runs.

CO_2-H_2O inclusions:

This group of fluid inclusions usually has intermediate vapour/liquid ratio value varying from 40% to 50%. During heating cycle, the gaseous bubble shrinks with

progressing temperature. The temperatures of homogenization range from 270°C to 358°C.

CO_2-rich inclusions:

CO_2-rich fluid inclusions generally have high vapour/liquid phase ratios of 75-90%. this group of inclusions are unique in that, upon heating, phase boundaries between gaseous phase and liquid phase don't change and the phase boundary abruptly disappears when homogenization temperatures are reached. These fluid inclusions were trapped at critical state based on the homogenization phenomenon defined by Roedder (1984) and Ypma (1963).

CO_2-rich inclusions have homogenization temperature range of 340°C ~ 390°C, this homogenization temperature range is generally higher than that of the CO_2-H_2O fluid inclusions and the aqueous inclusions. Though the similar fluid inclusion type in both the Wulong gold mine and the Sidaogou gold mine, the homogenization temperature ranges are quite different as illustrated in Figure 5-10. The homogenization temperature range of the Wulong gold ores are dominated by the 310-390°C range, while the predominated homogenization temperature of the Sidaogou gold ores is located in the range of 150-220°C. Though a 340-390°C range does occur, it's not the major temperature domain in which the ore precipitation processes took place.

Due to the small size of fluid inclusions, estimate of salinity of fluids in fluid inclusions was only taken on very limited ones based on different approaches. For the H_2O inclusions, salinity was estimated using the classic binary H_2O-NaCl system through the measurement of the final melting temperatures of ice following the methods described by Roedder (1984) and Lu et al., (1990). For the CO_2-bearing fluid inclusions, though the final melting temperatures of ice can't be used to estimate the salinity of the

aqueous solutions because of the formation of CO_2 hydrates in the CO_2-bearing inclusions during freezing cycle, Collins (1979) suggested that the depression of the decomposition temperature of CO_2 hydrate can be used to measure the salinity of the co-existing aqueous solution using the two salt-depressed curves. Regardless of the estimate methods of the salinity of fluid inclusions, the estimated results are quite similar. in general, the salinity of fluid inclusions in both the Wulong gold deposit and the Sidaogou deposit are low. the salinity of fluids estimated through fluid inclusions of the Wulong gold deposit ranges from 2.4 wt%NaCl equiv. to 6.1wt%NaCl equiv. with an average value of 4.2 wt%NaCl equiv.; the variation ranges of salinity of fluids from the Sidaogou is between 2.8 wt%NaCl equiv. to 4.0wt%NaCl equiv. with an average value of 3.2wt%NaCl equiv. It seems that fluid salinity of the Sidaogou gold deposit is lower a little bit than the Wulong gold deposit. Though the salinity value of the Jielishu deposit could not be estimated through freezing approach due to the small size of fluid inclusions due to the small size of fluid inclusions. But the several fluid inclusions observed are characterized by very low V/L ratios, homogenization temperature of 108°C and no daughter mineral was observed. These features maybe suggest that salinity of fluid inclusion is generally low in the Jielishu deposit. In short, salinities of fluid inclusions are generally low in the Wulong gold camp, this is similar to the same type of gold mineralization worldwide.

Estimate of entrapment pressures of fluid inclusions was realized through P-T diagram of pure CO_2 inclusions proposed by Roedder(1984). The estimated entrapment pressures (without pressure calibration to the lithostatic and hydrostatic pressure) ranges from 61MPa ~ 62MPa in the Wulong gold deposit, and 49MPa ~ 53MPa in the Sidaogou deposit.

Bulk compositions of fluid inclusions of a number of manually sifted syn-ore quartz samples from the Wulong mine and the Sidaogou mine were analyzed in the Laboratory of Yichang Institute of Geology. Releasing and extracting of contents from the fluid inclusions samples were realized using the procedures and methods introduced by Roedder (1984) and Lu et al.(1990). Gaseous compositions were analyzed using Gas Chromography and the liquid phase was detected using ICP-MS equipment. Analyzed results are listed in Table 5-10-a and Table 5-10-b. Bulk compositions of the analyzed samples demonstrate that ore-bearing fluids in the Wulong gold ores are characterized by the high volatile gaseous components such as CO_2, CH_4, CO, N_2, H_2. Species of cations are dominated by Na^+, K^+, anions are dominated by F^-, Cl^-, SO_4^{2-}, and NO^{3-}, contents of Ca^{2+} and Mg^{2+} are low. But in the Sidaogou deposit, beside the dominant K^+, Na^+, Cl^-, SO_4^{2-}, contents of Ca^{2+} are also very high, this probably resulted from the alteration of ore-bearing fluids from the hosting rocks during the fluid migration processes.

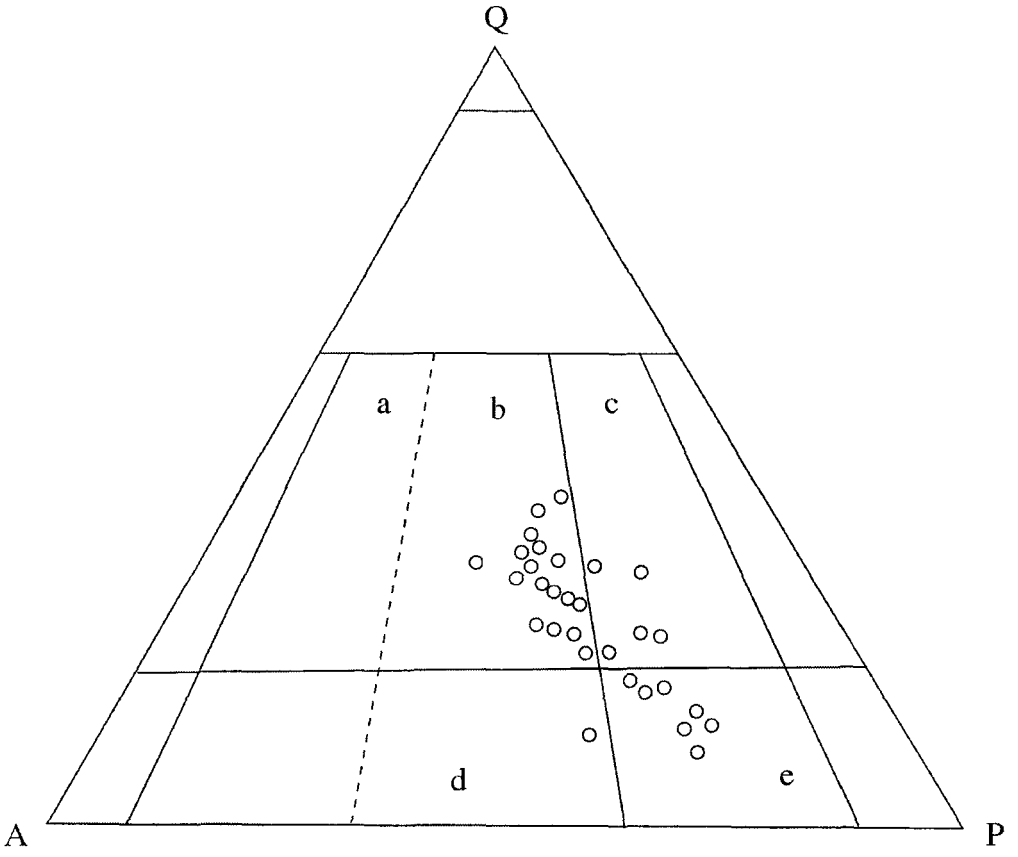

Figure 5-1 : normative QAP diagram of granites in the Wulong gold camp, Liaoning province classififcation is based on the IUGS (1972) method. Af and Pl are calculated from the CIPW Ab, Or and An data according to the procedures proposed by Rittmann (1973), Qz is CIPW normative values. a-granite; b-admellite; c-granodiorite; d-quartz monzonite; e-quartz monzo-diorite.

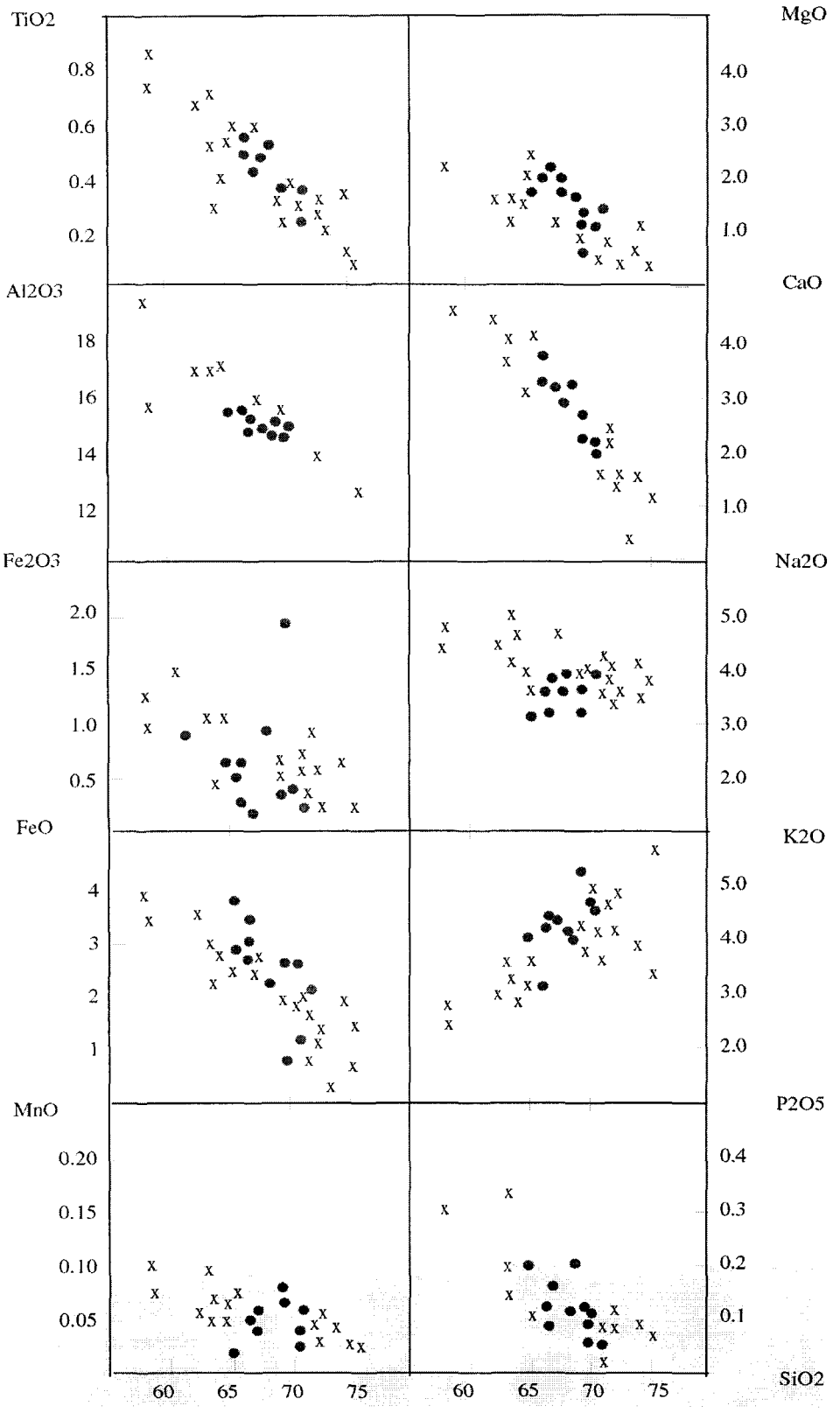

Figure 5-2 Harker diagram of granites in the Wulong gold camp

X :Wulongbei intrusion; ●: Sanguliu intrusion

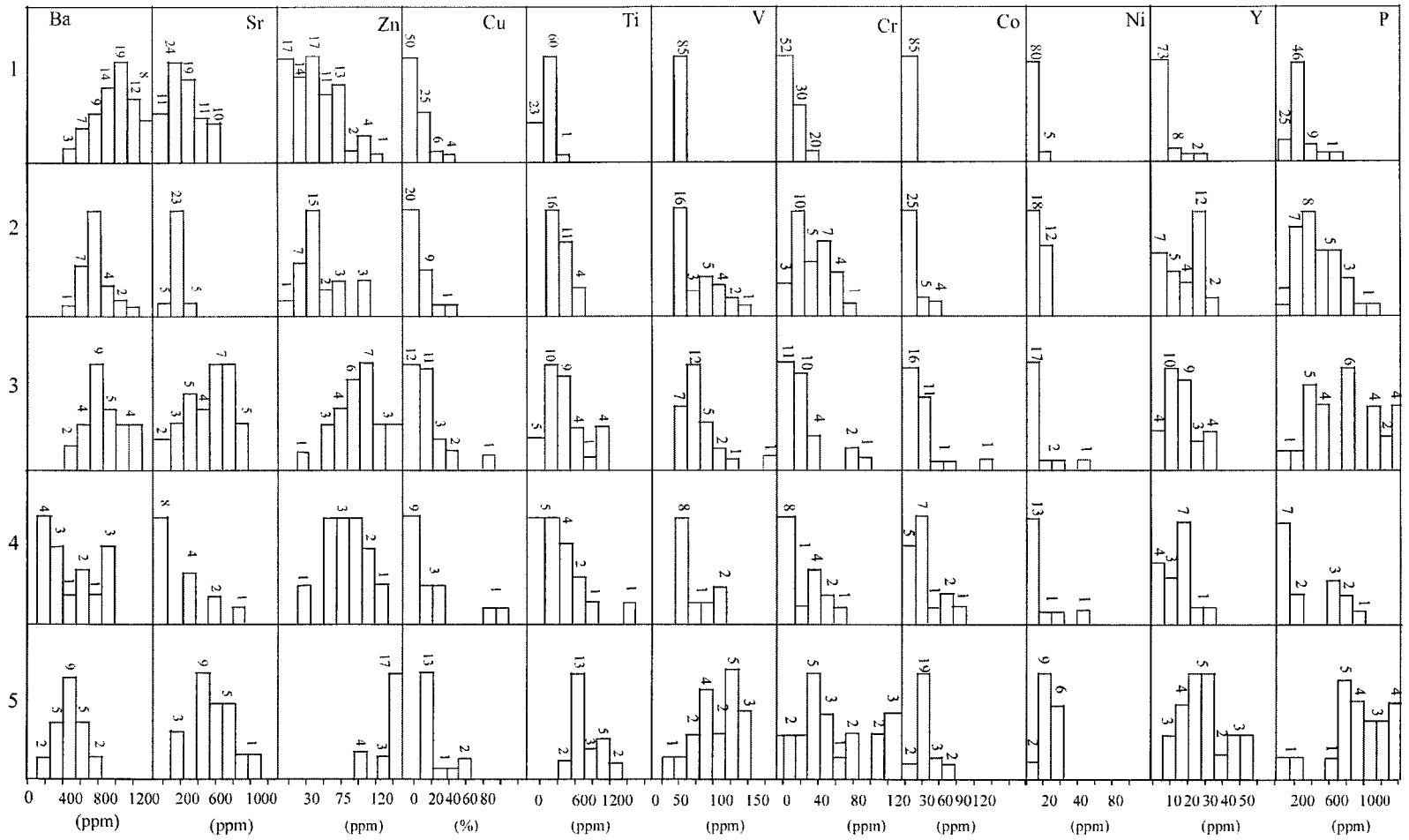

figure 5-3 Frequency distribution of trace elements in magmatic rocks in the Wulong region

1- granitic gneiss; 2-Sanguliu intrusion; 3-Wulongbei intrusion; 4- perthite granite; diorite dyke

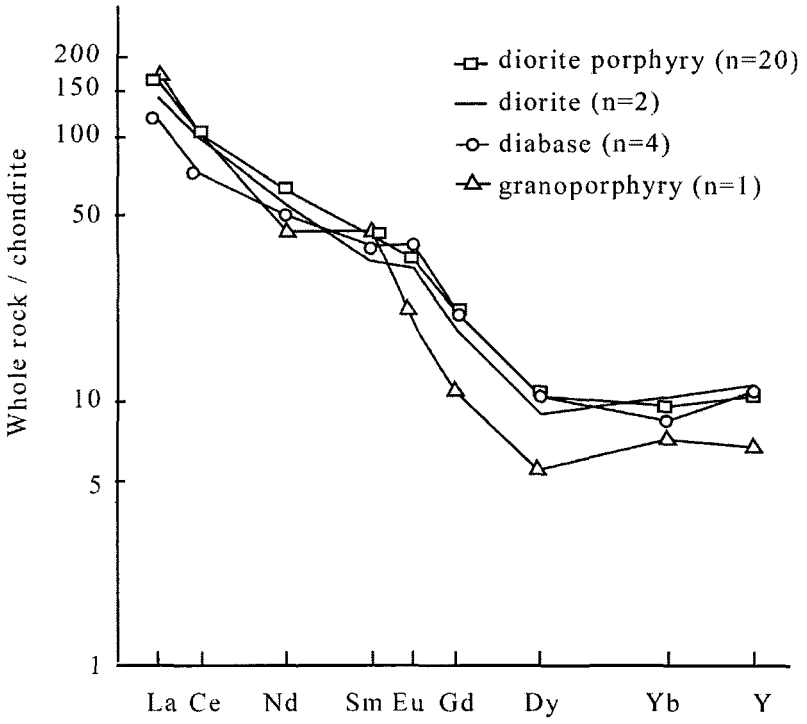

Figure 5-4 Normalized REE patterns of representative Magmatic rocks in the Wulong gold camp.

(refers to Peng et al. 1988)

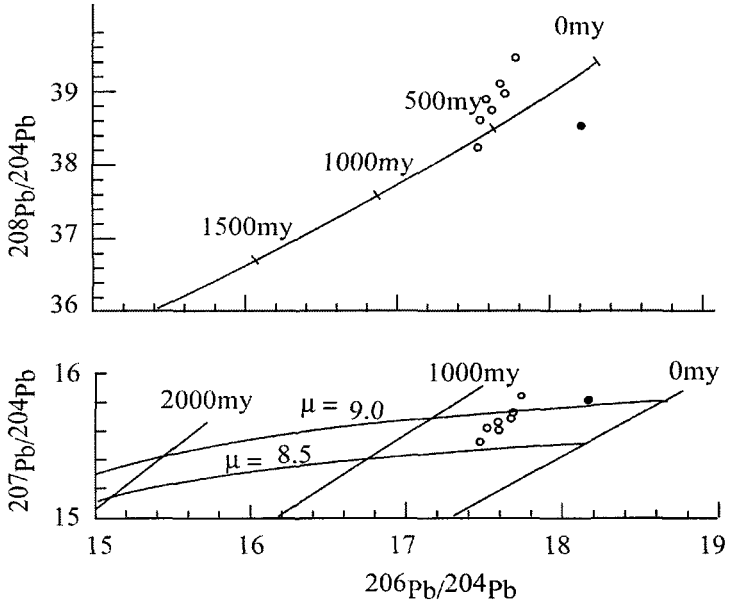

Figure 5-5 Lead isotope plots of ores from the Wulong gold mine (the circle) and the Sidaogou mine (the dot). Curvedline on the plots of 207Pb/204Pb versus 206Pb/204Pb are the single stage growth curves of 238U/204Pb for values of 9.0 and 8.5, and the steep sloping lines are the isochrons for the labled ages. the normal growth curve involving 208Pb/204Pb and 206Pb/204Pb is given in that plot with positions of model leads indicated for various ages. (after Doe, 1970)

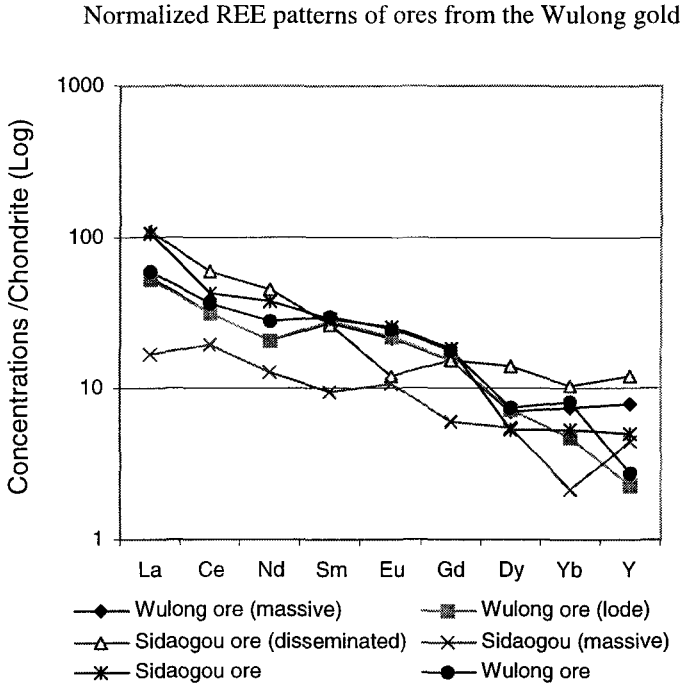

Figure 5-6 Normalized REE patterns of ores from the Wulong gold camp

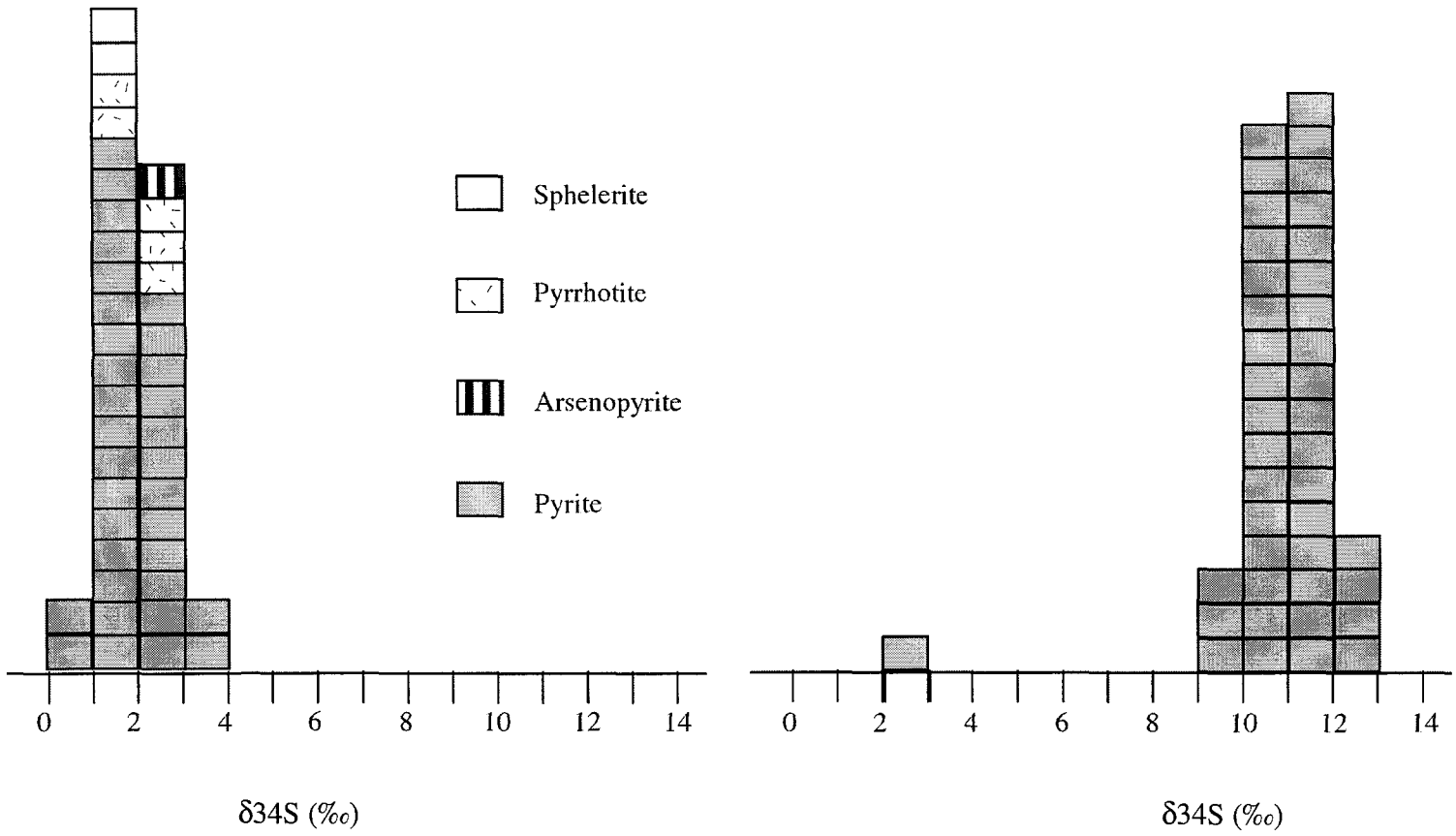

Figure 5-7 Histograms of δ34S values from the Wulong gold mine (left) and the Sidaogou gold mine (right), of the Wulong gold Camp, Laioning province. (data from table 5-6)

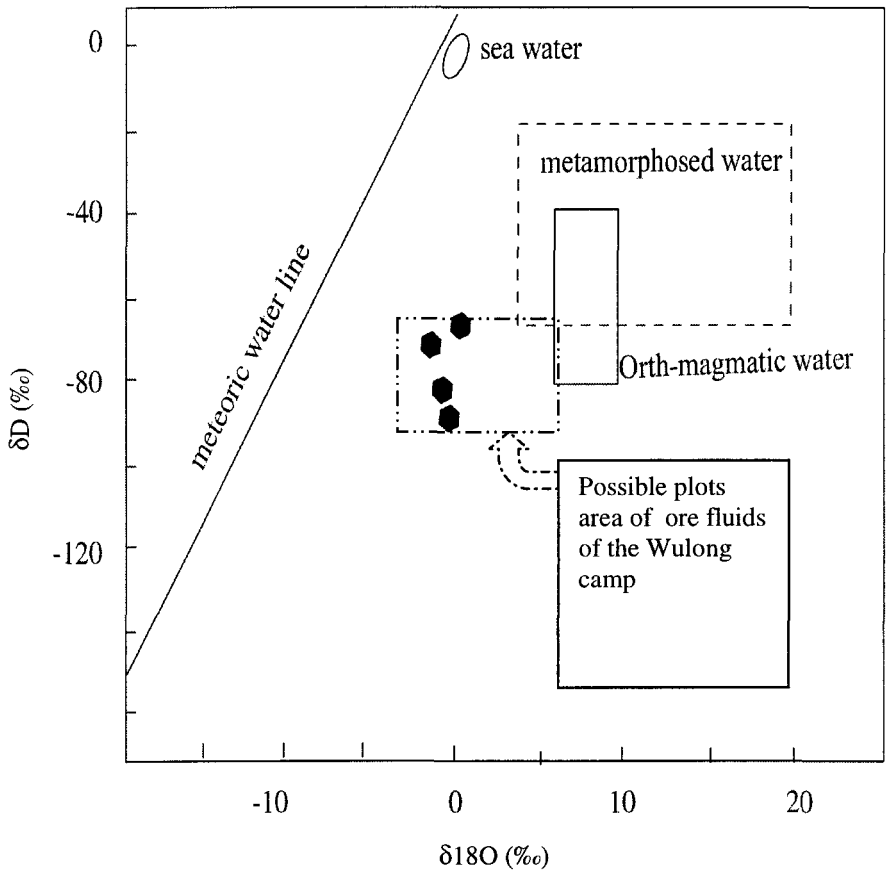

Figure 5-8 diagram of δD vs. δ18O of gold-bearing quartz samples in the Wulong gold camp, Liaoning province

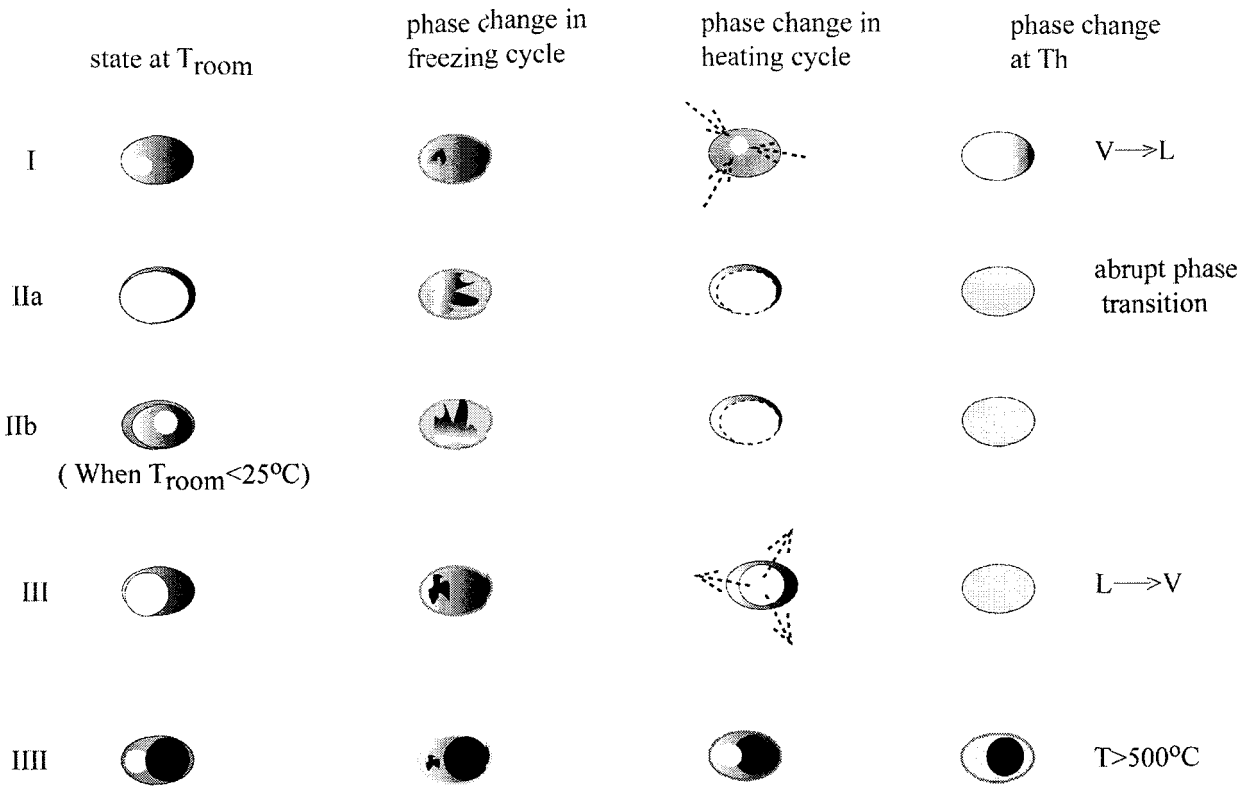

Figure 5-9 Classification of fluid inclusions identified in the Wulong gold Camp, SE Liaoning Province

I- aqueous inclusion, vapour bubble shrink during heating and finally homogenized into fluid phase; IIa- CO2-rich inclusion with high V/L ratios (>85% ~ 90%), the vapour phase keeps in no change of size (and accordingly the boundary) during heating, at homogenizati on temperature,the phase boundary abruptly disappears; IIb- this type is very rare, only when room temerature is below 25oC, the rest behaviours during freezing and heating are the same as the type IIa; III- in most of the cases, the vapour pahse enlarges during heating cycle, but in some case, the vapour phase behaviours as the type I; IIII- this case is, though, rare, but is very significant, because the black particle is quite probably sulfide. since the IIb and type IIII are very rare, the type I, type IIa and type III are the major fluid inclusion types studied during this study.

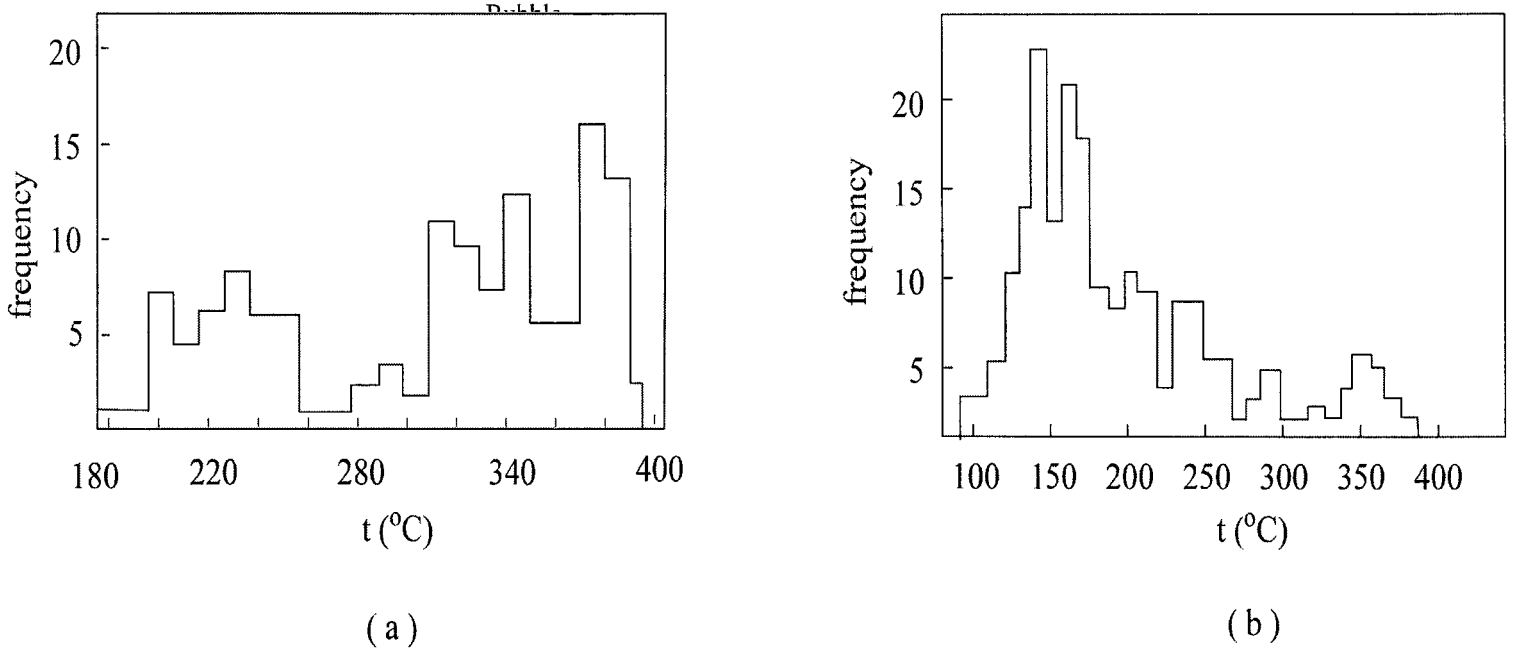

Figure 5-10 Histogram of the homogenization temperatures of fluid inclusions measured in ores of the Wulong gold deposit (a) and the Sidaogou gold deposit (b).

Table 5-1 Contents of major elements of representative intrusions in the Wulong gold camp (wt%)

Intrusion	Sgl-1	Sgl-16	Sgl-30	Sgl-25	Sgl-4	Sgl-12	Wl-2	Wl-9
SiO2	71.6	68.90	64.70	68.40	68.15	65.98	73.74	70.89
Al2O3	14.5	14.71	15.40	14.80	15.12	15.22	13.74	14.62
Fe2O3	0.68	0.62	0.73	0.68	0.66	0.75	0.61	0.84
FeO	1.50	2.01	3.50	2.33	2.74	2.99	0.67	1.76
MgO	1.00	1.00	2.43	1.50	1.09	1.82	0.38	0.76
CaO	1..9	2.86	4.00	2.9	2.99	3.07	0.92	1.44
MnO	0..04	0.05	0.064	0.057	0.05	0.11	0.04	0.03
Na2O	3.6	3.61	3.42	3.56	3.39	3.44	4.03	3.89
K2O	4.3	4.19	3.86	4.14	4.15	3.96	3.67	4.13
P2O5	0.3	0.39	0.13	0.29	-	0.10	0.04	0.13
H2O	0.20	0.36	-	0.28	-	-	-	-
CO2	0.3	0.50	0.80	0.53	-	-	-	-
TiO	-	-	0.00	0.48	0.53	-	0.14	0.28
Total	99.92	99.18	99.034	99.25	96.87	97.45	97.98	98.77

Table 5-2 Calculated CIPW minerals of the representative intrusions in the Wulong gold camp.

Intrusion	Sgl-1	Sgl-16	Sgl-30	Sgl-25	Sgl-4	Sgl-12	Wl-2	Wl-9
Ap	0.85	0.90	0.30	0.67	-	0.23	0.093	0.30
Il		-	-	-	1.0	-	0.27	0.53
Mt	0.98	0.90	1.05	0.98	0.96	1.09	0.88	1.22
Or	25.83	24.76	22.81	24.47	24.53	23.40	21.69	24.41
Di	-	0.001	3.08	0.20	0.88	0.15	1.56	1.44
Cm	1.02	-	-	-	-	-	1.56	1.44
An	7.36	11.64	15.27	12.48	13.78	14.39	4.30	6.29
Ab	30.80	30.55	28.94	30.12	28.69	29.11	34.10	32.92
Hy	4.78	5.76	10.46	7.46	5.98	9.53	1.52	4.02
Q	27.99	23.86	16.31	22.44	23.06	19.53	33.57	27.64
DI	92.00	90.80	83.30	89.5	90.1	86.4	93.7	91.3

Q : quartz; Ab : albite; Or: orthoclase; An : anorthite; Di : diopside; Hy : hypersthene; Mt : magnetite; Il : ilmenite; Cm: Corundum; Ap : apatite; DI : differentiation index . (The calculating procedure is taken from the web site: http://www.union.edu/PUBLIC/GEODEPT/COURSES/petrology/norms.htm)

Table 5 - 3 Pb isotope compositions of ores and calculated single-stage ages as well as characteristic parameters

Sample No.	Mineral	Location	Pb isotope composition			Single-stage model ages		Calculated character parameters *					
			206/204	207/204	208/204	f value	Ages (Ma)		n	w	K1	K2	K3
W23	Sphelerite	#33	17.639	15.660	38.836	0.64346	776	9.27	0.067	43.82	4.73	654.03	4.58
W26	Pyrite	#33	17.560	15.610	38.688	0.64358	772	9.19	0.067	43.13	4.69	643.73	4.54
W6	Pyrrhotite	#32	17.487	15.514	38.269	0.63760	719	9.11	0.066	40.65	4.46	615.91	4.32
W9	Pyrite	#32	17.625	15.659	38.831	0.64287	766	9.25	0.067	43.74	4.73	652.84	4.58
W21	pyrite	#32	17.694	15.736	39.121	0.64832	814	9.41	0.068	45.62	4.85	670.89	4.69
W29	Pyrite	#32	17.793	15.860	39.521	0.65536	874	9.64	0.070	48.22	5.00	688.86	4.84
W46	Pyrite	#32	17.689	15.704	38.985	0.64484	779	9.34	0.068	44.60	4.78	655.88	4.63
S-3	Pyrite	Sdg #48	18.203	15.818	38.457	0.62047	558	9.51	0.069	40.01	4.21	579.86	4.80

* $^{238}U/^{204}Pb$; $n=^{235}U/^{204}Pb$; $w=^{232}Th/^{204}Pb$; $k1=^{232}Th/^{238}U$; $k2=^{232}Th/^{235}U$; k3=Th/U. (Data are cited from Li et al., 1988)

Table 5- 4 U- Pb isotope dating of magmatic rocks in the Wulong gold camp

Sample No.	Mineral	U(%)	Th(%)	Pb(%)	Pb compositions (%)				Ages (Ma)				Accepted ages (Ma)
					204Pb	206Pb	207Pb	208Pb	206 Pb /238U	207 Pb /235 U	207Pb /206Pb	208Pb /232U	
Pao-2 (gneiss)	Zircon	0.1892	0.02778	0.01285	0.749	53.346	14.579	31.326	198	266	916.4	286.8	198
Pao-2-1 (gneiss)	Monazite	0.2060	3.4000	0.0268	0.072	11.790	1.640	86.498	100	101	109.5	148.9	148.9
Dj4 (granite)	Whole rock	0.0817	0.109	0.0029	0.68	49.67	12.51	37.11	98	103	48	66	98
Wl-1 (Grano-porpyry)	Whole rock	0.08572	0.07560	0.04043	1.34	26.69	19.82	52.14	121	-	-	418	121
Dj8 (perthite granite)	Zircon	0.1120	0.08227	0.03265	0.337	60.505	7.970	31.185	116.9	116.7	114.9	116.9	116.9
Laogugou (granite)	Zircon	0.1042	0.2137	0.01043	0.96	35.08	16.92	47.04	130	255	115	130	130

Data are cited from Li et al, 1988.

Table 5-5 Contents of REE of ores from the Wulong gold camp, Liaoning province, China

Sample	La	Ce	Pr	Nd	Sm	Eu	Gd	Tb	Dy	Ho	Er	Tm	Yb	Lu	Y
Wulong ore (6)	17.30	29.90	5.40	12.40	5.50	1.50	4.70	0.45	2.18	0.30	1.69	0.13	1.41	0.14	15.50
Wulong ore-1	17.12	29.92	5.46	12.32	5.57	1.55	4.79	0.45	2.25	0.39	1.90	0.18	0.90	0.10	4.40
Sidaogou dissm.	34.99	55.76	7.29	27.02	5.35	0.83	4.75	0.74	4.34	0.78	2.12	0.31	1.96	0.31	23.41
Massive ore Sidaogou	5.39	18.40	1.73	7.58	1.90	0.75	1.88	0.29	1.68	0.26	0.62	0.08	0.41	0.05	8.53
Sdg-ore	34,02	39,84	n**	22,98	5,84	1,80	5,70	n	1,63	n	n	n	1,01	n	9,90
Wulong Ore-2	19,22	34,15	n	16,72	5,95	1,76	5,44	n	2,31	n	n	n	1,56	n	5,29
Mean Chondrite values *	0.32	0.94	3.12	0.60	0.20	0.07	0.31	0.05	0.31	0.07	0.21	0.03	0.19	0.03	1.96

Sample	La/Sm	Gd/Yb	Sm/Nd	å REE	å L/å H	dEu
Wulong ore (6)	3.15	3.33	0.44	98.50	2.72	0.96
Wulong ore-1	3.10	-	0.45	96.56	4.86	0.96
Sdg dissm.	6.54	2.42	0.19	169.96	3.39	0.49
Massive ore Sidaogou	2.83	4.58	0.25	49.55	2.59	1.20
Sdg-ore	-	-	-	-	-	-
Wulong Ore-2	-	-	-	-	-	-

* the standard values of REE in chodrite are cited from Taylor and Gorton, 1977, Taylor and Gorton, 1977, Cosmochim Acta, 41, 1375-13;
** n: not detected, - : not calculated values

Table 5-6 Sulfur isotope data of sulfides in the Wulong gold camp

Location	Analyzed mineral	Samples number	δ34S variation (‰)	mean δ34S (‰)
Wulong deposit	Py*	38	+1.5, +1.5, +1.0, +1.6, +1.9, +3.5, +2.4, +1.5, +1.5, +1.6, +1.7, +2.5, +2.4, +2.6, +2.3, +2.5, +1.4, +1.2, +1.3, +1.7, +1.8, +1.4, +1.2, +3.2, +2.6, +3.0, +2.3, +1.4, +1.3, +1.5, +2.5, +0.9, +2.1, +2.9.	+2
Wulong deposit	Po.	5	+1.2, +1.8, +2.3, +2.8, +2.6.	+2.2
Wulong deposit	Apy.	1	+2.5	+2.5
Wulong deposit	Sph.	2	+1.3 ~ +1.8	+1.55
Sidaogou deposit	Py.	41	+11.4, +11.3, +11.6, +12.0, +11.9, +11.6, +11.6, +10.1, +11.4. +12.0, +12.0, +12.4, +12.6, +12.2, +10.7, +11.1, +10.9, +10.8, +11.3, +10.8, +10.4, +11.2, +11.8, +12.1, +11.6, +10.4, +10.8, +11.0, +11.0, +10.9, +10.6, +10.8, +10.9, +10.7, +11.9, +10.9, +9.59, +11.3, +9.2, +9.8, +2.3.	+11.33

*Py: pyrite, Po.: Pyrhhotite; Apy: Arsenopyrite; Sph.: Sphalerite;

(data are sourced from Chen J.Y. etal., 1995.)

Table 5-7 $\delta^{18}O$ and δD values and calculated δO_{H2O} of quartz samples in the Wulong gold camp

Sample No.	Mineral parageness	δD (‰)	$\delta 18O_q$	$\delta 18O_{H2O}$
Wl-#2	Q	-80.8+1.5	-	-
Wl-#520	Q	-77.8+1.5	-	-
Wl-wb66	Q	-	+12.66	+4.16
Wl-wb78	Q	-	+15.95	+7.45
Wl-wb83	Q	-	+13.05	+4.55
Wl-wb89	Q	-	+14.29	+5.69
Wl-wb109	Q	-	+10.87	+2.37
Wl-wb115	Q	-	+13.77	+5.27
S019	Q-py	-82.10	+11.79	-2.2
S026	Q-py	-77.0	+12.88	-4.1
S031	Q-py	-74.5	+12.37	-1.76
S071	Q-py	-83.0	+12.55	-3.34

Table 5-8 Carbon isotope and oxygen isotope values of calcite samples in the Sidaogou deposit:

Samples	Mineral	$\delta^{13}C$	$\delta^{18}O$-CPDB	$\delta^{18}O$-SMOW
8-15-1 (level7)	Calcite	-1.21	-23.52	+6.61
8-21-8 (level 8)	Calcite	-5.51	-25.32	+4.75
B-8-23-1 (level 8)	Calcite	-2.67	-22.17	+8.01
B-8-30-2 (level 8)	Calcite	-4.46	-26.31	+3.74

Table 5-9 Trace element contents of purified individual sulfide separated from the Wulong and the Sidaogou gold.deposit

Sample No.	Mineral	Trace element contents (%)										
		Au (ppm)	Ag (ppm)	As	Sb	Bi	Co	Ni	Pb	Zn	Cd	Te
W6	Po.	23.1	2	0.0003	0.00048	0.25	0.025	0.0093	0.0048	0.0130	0.0006	0.0230
W23	Sph.	30.1	38	0.0820	0.00039	0.017	0.012	0.0012	0.1100	50.000	0.2200	0.0100
W21	Py1.	50.7	57	1.3800	0.00027	0.021	0.013	0.0007	0.2800	0.0140	0.0005	0.0019
W29	Py2	88.0	130	0.7200	0.00046	0.120	0.009	0.0013	0.7800	0.0490	0.0009	0.0110
W26	Py2	29.3	15	0.4300	0.00036	0.005	0.018	0.0037	0.0320	0.0180	0.0007	0.0005
W14	Py2	240.0	36	0.5300	0.00084	0.670	0.016	0.0053	0.2300	0.0024	0.0008	0.0460
W9	Py3	20.4	38	0.1800	0.00043	0.078	0.005	0.0140	0.2200	1.1100	0.0047	0.0066
S-3	Py2	124.4	22	0.1400	0.00039	0.005	0.008	0.0220	0.0150	0.8500	0.0041	0.0004

Sample No.	Mineral	Ag/Au	Au/Te	Ag/Te	Co/Ni
W6	Po	0.09	0.10	0.009	2.69
W23	Sph	1.26	1.58	0.38	10.00
W21	Py1	1.12	2.67	3.00	18.57
W29	Py2	1.48	0.80	1.18	7.08
W26	Py2	0.51	5.86	3.0	4.86
W14	Py2	0.15	0.52	0.078	3.02
W9	Py3	1.86	0.31	0.58	0.41
S-3	Py2	0.18	31.1	5.5	3.95

(Samples were analyzed using conventional chemical analysis in the Experiment laboratory at Tianjin Institute of Geology)

Table 5-10- a Compositions of fluids extracted from fluid inclusions in quartz, Wulong deposit (ppm) **(gaseous components are in PPb)**

Sample	Aqueous phase								Gaseous phase						Ratios		
	K^+	Na^+	Mg^{2+}	Ca^{2+}	F^-	Cl^-	NO_3^{2-}	SO_4^{2-}	H_2	N_2	CH_4	CO	CO_2	H_2O	K^+/Na^+	F^-/Cl^-	CO_2/H_2O
L5	1.60	3.50	0.30	-	2.40	5.10	1.00	2.50	0.059	2.375	13.71	2.825	19.171	187.53	0.50	0.47	0.10
L6	2.90	3.50	0.50	-	6.10	12.60	3.00	11.00	0.554	2.500	0.893	2.250	5.590	74.81	0.80	0.48	0.075
L13	3.23	8.10	0.02	-	3.10	8.10	2.00	4.00	0.323	2.425	2.329	2.656	24.671	119.70	0.40	0.38	0.21
L14	0.50	0.10	-	-	1.70	4.25	-	3.00	0.094	2.050	2.529	3.063	10.921	61.84	5.00	0.40	0.18
L35	0.50	1.60	0.01	-	1.65	3.15	-	2.00	0.138	1.900	0.907	2.638	9.114	62.84	0.30	0.52	0.15
L36	0.90	0.50	0.05	-	6.00	15.50	2.00	6.00	0.407	1.875	1.071	2.775	10.410	201.49	1.80	0.39	0.05
L41	1.40	1.70	1.07	-	3.10	7.00	1.00	3.00	0.137	2.275	0.857	3.375	8.123	54.853	0.80	0.44	0.15
L50	1.40	0.80	-	-	6.20	8.60	2.00	10.00	0.096	1.987	1.143	2.600	6.796	193.52	1.80	0.72	0.04

Table 5-10- b Compositions of fluids extracted from fluid inclusions in quartz, Sidaogou deposit

stage	Series	Aqueous phase								Gaseous phase						Ratios		
		K^+	Na^+	Mg^{2+}	Ca^{2+}	F^-	Cl^-	NO_3^{2-}	SO_4^{2-}	H_2	N_2	CH_4	CO	CO_2	H_2O	K^+/Na^+	F^-/Cl^-	CO_2/H_2O
Stage 1	1	4.60	25.00	0.80	80.00	1.58	31.50	5.35	1.11	0.15	1.35	0.81	1.02	37.00	874	0.184	0.05	0.042
	2	5.40	28.00	8.80	217.00	3.07	37.60	7.27	2.80	0.10	1.05	0.78	1.03	35.30	770	0.192	0.082	0.046
	3	10.70	48.00	1.50	77.00	2.00	62.30	6.30	1.10	0.80	1.15	0.72	0.99	29.00	892	0.222	0.032	0.0325
	4	5.40	18.30	2.70	69.90	1.10	20.20	5.40	0.80	0.08	0.57	0.95	1.04	15.90	426	0.295	0.054	0.037
Stage 2	5	5.10	4.60	3.50	71.20	1.70	4.40	4.70	0.30	0.08	0.18	0.69	1.06	10.80	390	1.108	0.386	0.0276
	6	8.60	13.10	4.30	109.00	1.60	15.10	5.70	1.40	0.11	0.40	0.71	1.08	24.60	724	0.656	0.106	0.034
	7	8.20	9.30	2.60	59.90	1.80	6.90	5.00	4.80	0.03	0.34	0.85	1.03	21.00	844	0.882	0.261	0.025
	8	9.30	57.10	0.60	38.50	1.20	74.90	5.10	0.03	0.08	1.21	0.61	1.02	13.00	1030	0.163	0.016	0.013
	9	5.15	6.35	0.18	2.30	2.11	16.12	-	10.00	0.11	1.81	1.85	1.49	26.90	704	0.811	0.131	0.038
	10	11.01	3.00	0.52	1.59	2.55	5.71	-	13.40	0.30	1.98	1.51	1.41	15.46	298	3.67	0.447	0.052
	11	5.60	31.00	1.90	135	1.57	45.20	4.71	0.54	0.09	1.66	0.90	-	14.20	748	0.181	0.035	0.019
3 Stage	12	4.80	23.20	2.40	31.70	1.10	23.50	5.40	4.50	0.09	0.25	0.84	1.05	24.30	1360	0.207	0.047	0.018

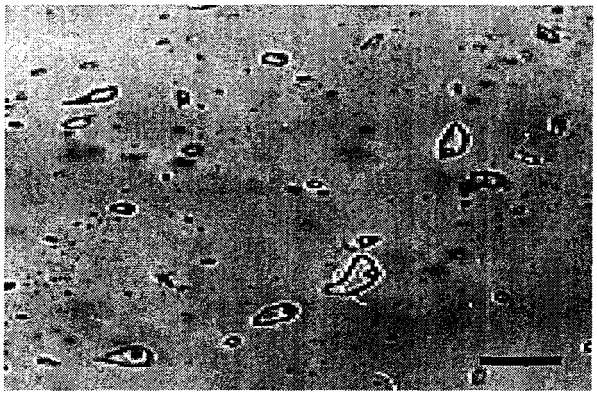

Photo 5-1 Aqueous inclusions with high and steady FD (fill degree) values are easier to be observed in the Sidaogou mine and the Jielishu mine than in ths Wulong mine.(site : Sidaogou mine, x45) (scale bar: 20μm)

Photo 5-2 Fluid inclusion with high ratios of gaseous phase/liquid phase is very common in the Wulong mine, this type of inclusion is characterized by its brown color and large size besides its low first melting temperature at freezing cycle (site : 12 level, Wulong mine , x 45) (scale bar: 15μm)

Photo 5-3 Three phases inclusions (aqueous phase+liquid CO2+gaseous CO2) is occasionaly observed in the Wulong mine (arrow), but not common, this kind of inclusion is not observed in the other two inclusion during this research.
(site : 12 level, Wulong mine, x 45) (scale bar: 25μm)

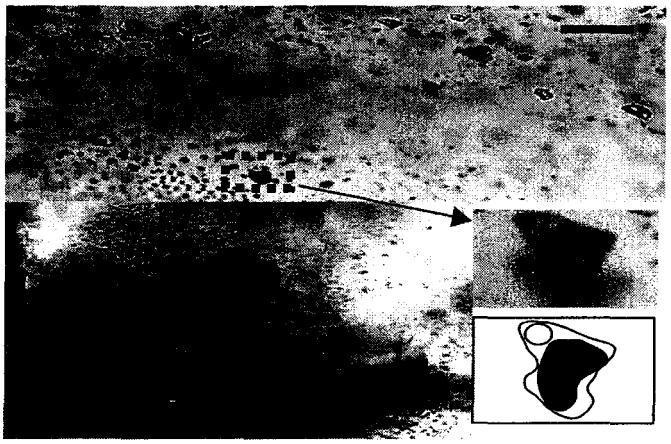

Photo 5-4 Sulfide particles trapped in fluid inclusion is not uncommon in the Wulong mine (upper photo). Such kind of inclusions are usually developed at ending of sulfide vein (lower left photo), under reflect light these black dots are turned to be bright dots indicate their metal behavior. These particles don't melt during heating experiemnt even temperature over 500°C (site : 10 level, Wulong mine) (scale bar: 20μm)

Chapter VI

Discussion

Genetic relationship of the Wulong shear zone, magmatism and gold mineralization

As discussed in the previous chapters, the Wulong shear zone has an intimate spatial relationship with gold deposits and magmatic intrusions with various scales. In this chapter, a comprehensive discussion on the aspects of the spatial and temporal relations among them will be given, especially the possible genetic relationships among the shear zone, magmatism and ore mineralization in the Wulong gold camp.

6.1 Spatial relations of the Wulong shear zone, gold mineralization and intrusions

Numerous papers discussed structural control of shear zone on gold mineralization (Sibson, 1988, Kerrich, 1989, Kerrich and Wyman, 1990, Groves, 1993, Lu et al., 1999). Regional shear zone has been generally considered to be barren of gold, and the importance of subsidiary second and third order splays adjacent to the major structures was often emphasized (Eisenlohor 1987; Groves et al. 1988; Mueller et al. 1988, Witt 1993). Colvine et al., (1988) stressed the significance of regional shear zone as hosts to auriferous structures in Ontario, Canada. In early 1990's, Groves proposed that shear zone controlled gold mineralization world-wide can be formed over a variety of crustal

regimes ranging from 180°C at <1kb to 700°C at 5km (Grove, 1993). And individual deposits, separated by tens to hundreds of kilometers, collectively show transitional variations in structural style of mineralization, vein textures and mineralogy of wall rock alteration related to the P-T conditions.

Structural control of the Wulong shear zones on gold mineralization in the Wulong area mainly show on these aspects:

① On the spatial distribution of mineralization

In the Wulong gold camp, regional geochemical anomaly of Au is exclusively confined in the shear zone (Fig.6-1). All the minable gold mineralization is exclusively controlled by the NE striking Wulong shear zone either in the trunk shear zone or in its splay structures. This is the reason that regional mineral explorations were strictly spotted within the shear zone domain in the past years. In an individual ore deposit, mineralization strictly developed in spaces formed during fault activities. For example, In the quartz-lode dominant Wulong ore deposit, quartz veins, together with various intrusions, were mainly controlled by R shears and T fractures, they usually occur as rhombic grids pattern with grid size of $600*1000m^2$.

② On geometry of ore bodies

Confined by R shears and (or) T fractures, shapes of ore bodies in Wulong shear zone are commonly complex and usually show irregular forms such as pocket-like and hook-like. These irregular shapes of ore-bodies were controlled by the hosting structural spaces of ore bodies; for example, in the Sidaogou deposit, pocket-like ore bodies are confined by the conjunction space of lenses, while the hook-like ore bodies are common

at the ends of lenses. In the Wulong deposit, auriferous quartz lodes filling in R shears demonstrate sinistral pattern on plane (Fig. 3-21).

③ On ore types, ore structure and mineralization stages

Massive, veins (stockworks and veinlets) and disseminated ores are the three dominant ore types developed in the Wulong gold camp. Development of these ore types has an intimate relation with shear features of the shear zone. In the Wulong mine, ore type is characterized by vein type. Auriferous quartz veins commonly occur in R shears or T fractures. Due to the multiple-stage processes of the shear zone, quartz veins usually show laminated structures. In the Sidaogou mine, ore type is dominated by veinlet and disseminated ores. Stockworks and veinlet structures are common. While in the Jielishu deposit, massive ore is the predominant type. Ore structure is characterized by crystal-vug. These ore structure variation features are probably related to spatial variations of lithological rock units and the stress-strain states in the Wulong shear zone.

The activity of the Wulong shear zone also affected mineralization stages developed in individual ore deposits. Field investigations and laboratory observations discussed in chapter four and five indicate that gold mineralization experienced multiple stage processes in the Wulong gold camp. Individual deposit shows different mineralization processes. In the Wulong deposit, four mineralization stages were recognized. In Jielishu deposit, only two mineralization stages were recognized, and strength of mineralization in the Jielishu deposit was much weaker than both the Sidaogou and the Wulong deposit. As discussed later in this chapter, the different stages

and strength of mineralization at different deposit is probably jointly controlled by both the activity of the shear zone and the spatial distance related to the Sanguliu intrusion.

④ On spatial distribution of various magmatic intrusions

The shear zone system controls not only spatial distribution and shapes of ore lodes, but also various magmatic intrusions. The Sanguliu stock directly distributes in the Wulong shear zone, and the reactivity of the Wulong shear zone left structural imprints on the rim of the intrusion. According to Yao et al., (1988), several hundreds of various dykes developed in the Wulong gold camp. 160 ore lodes are directly in contact with dykes among total 190 counted ore lodes in the Wulong gold deposit alone. Most of the dykes are parallel to ore lodes; some dykess may displace ore lodes or vise versa (Fig. 6-2).

6.2 Temporal relations of the Wulong shear zone, gold mineralization and intrusions

Field investigations and microscopic structural interpretations indicate that intrusions can be classified into three episodes based on their temporal and spatial relations to ore lodes in the gold camp: the pre-ore intrusions, the syn-ore intrusions and the post-ore intrusions.

The pre-ore intrusions: Intrusions formed prior to ore mineralization are dominated by diorite dykes. The pre-ore intrusions are characterized by strong alteration and structural deformation developed in these intrusions. Commonly, disseminated

pyritization is visible in pre-ore intrusions. Pre-ore intrusions are especially well developed in the Wulong gold deposit compared with the Sidaogou and the Jielishu gold deposit. In the latter two deposits, diorite dykes are poorly developed. In the Jielishu deposit, altered diorite dykes is only observed in the #8 ore body.

The syn-ore intrusions: the syn-ore intrusions generally refer to those that were formed during the whole ore mineralization processes. Those intrusions were formed either earlier than the ore lodes and experienced hydrothermal alteration or later than the ore lodes but earlier than the last episode of hydrothermal process.

In the Wulong gold camp, the Sanguliu intrusion is the largest syn-ore magmatic intrusion, in addition to the granoporphyre dykes. Several granoporphyre dykes were altered by ore-forming hydrothermal fluids and disseminated pyrites were developed in the dykes, while other granoporphyre dykes were apparently formed after the major ore precipitation stage, since these dykes penetrated ore lodes and, meanwhile, they were altered by carbonatization. In the Sidaogou deposit, the syn-ore dykes are not granoporphyre but lamprophyre, it is the same scenery in the Jielishu deposit.

The post-ore intrusion is formed after the ore-bearing hydrothermal fluid processes. Post-ore intrusions usually penetrate and (or) displace ore lodes and (or) early intrusions (dykes) and no hydrothermal alteration is visible in them. Diabase dykes are the typical post-ore intrusions in the Wulong gold camp. Diabase dykes usually displace not only ore lodes, but also lamprophyre dykes. These diabase dykes are fresh, no alteration was observed in them. In the Wulong gold camp, the temporal relations of intrusions and gold mineralization are chronologically ordered as following: diorite →

granoporphyre (Sanguliu intrusion) → major gold mineralization → granoporphyre + lamprophyre → late stage hydrothermal fluid process → lamprophyre → diabase. The K-Ar isotope ages of the various dykes and tectonites discussed in previous chapter support this conclusion.

On the basis of this time sequence, it is clear that gold mineralization was confined in the whole magmatism processes, the magmatism and the mineralization processes were spatially controlled by the Wulong shear zone. So, from this point, it is natural to raise a question: Is there any geochemical relations among these intrusions and ore lodes? Or in another words, are there any possible genetic relations between them?

6.3 Magmatic genesis or metamorphic genesis?

As mentioned in chapter one, ore genesis regarding the Wulong gold camp has been quite disputable over years. Both the metamorphic genesis hypothesis and the magmatic genesis hypothesis are based on certain geological evidences. Of course, both of them can not be true at the same time and only one of them reveals the possible geological processes occurred in this area. Many researchers studied the geochemical relations of intrusions and gold deposits from different aspects. Peng et al., (1988) analyzed contents of both major and trace elements in several representative magmatic rock types and ores. The analyzed contents of major elements and trace elements are listed in table 6-1 and table 6-2, respectively. Contents of major elements and trace

elements indicate that no obvious differences exist between granitic intrusions and granitic batholith, except the mafic intrusions.

Ore material sources could be derived from any kind of rocks such as magmatic rocks, sediments, metamorphosed rocks ore even pre-existing ore bodies and materials. Tilling et al., (1973) and Boyle (1984) suggested that geochemical abundance of gold could not be used to prospect potential gold target with long term active hydrothermal fluid system and gold mineralization may taken place in low gold background. Keays (1984) proposed that low gold background concentration in greenstone belt could not rule out the possibility of ore source from greenstone belt because geological processes, especially metamorphism, may release ore materials into hydrothermal fluids. They pointed out that the current background concentrations of any ore materials (elements) not essentially represent the proto-background.

Rock and Groves (1988) emphasized the importance of lamprophyre on gold mineralization in Archean gold lodes. They suggested that gold was derived from these co-existing lamprophyre, but new data indicate that proposal is unlikely reasonable since fresh lamprophyre usually contains low gold contents ($<3*10^{-9}$ ppb). Through trace element geochemical study of lamprophyre and ores, Chen (1996) proposed that the co-existing lamprophyre and gold lodes in the Xiaoqinglin orogeny, China, share same tectonic environment and experienced similar tectonic processes, but lamprophyre and gold lodes are not genetically related in terms of material source.

Gold concentration analysis in the Wulong gold camp indicates that gold concentration differences among different intrusions are not obvious, these differences

are less than 1 ppb, except the quartz veins and altered diorites. Contents of gold in intrusions are generally less than 0.5 ppb. Gold concentrations of some intrusions differ slightly within the gold camp and the same type in regional scale, and the variation is not wide. For example, within the Wulong gold camp, the highest gold contents of fine-grained diorite and lamprophyre are 4.5 ppb and 1.4 ppb, respectively, while on regional scale gold contents of the two kinds of intrusions are 0.5 ppb and 0.4 ppb. Concentrations of gold in intrusions and dykes don't provide useful information regarding the source of ore materials in the Wulong gold camp.

Many geologists noticed the intimate spatial relationships of high-grade gold and bismuthinite in the Wulong gold camp (Zhao et al., 1992, Zhen et al., 1993, Liu 1994, Ma et al., 1994). Two kinds of Bi-bearing minerals are identified in this gold camp: bismuthinite and (native) bismuth. These Bi-bearing minerals are mainly distributed in fractures of quartz veins, and free gold is usually coeval with bismuth-bearing minerals and these bismuthinite may contain gold as high as 400-600 ppm according to Zhao et al., (1993). Gold and bismuth usually have a ratio of Bi:Au = 30:1 in contents in the Wulong gold deposit (Li et al., 1988). Listed in table 6-3 are the contents of gold, silver and bismuth in various ores in the Wulong gold deposit. Though no bismuthinite has been identified in the Sidaogou gold deposit, Ma et al., (1994) and Zhen et al., (1993) reported that contents of Au is also proportional to the contents of Bi in the Sidaogou deposit (Table 6-3). And they concluded that Ag-Bi-Cu is a reliable element-association marker for gold exploration in the Sidaogou deposit.

The intimate relationship between gold grade and contents of Bi exists not only in ore deposit, but also in the Sanguliu intrusion. Liu (1993) analyzed contents of trace elements (Au, Ag, Bi, As, Pb) in representative rock types, and study results suggest that contents of Bi is proportional to Au both in the Sanguliu intrusion and in ore lodes (Table 6-4).

Yao et al., (1988) studied REE distribution patterns of different host rocks, intrusions and ores in the Wulong gold camp. They found that various intrusions, though their different contents in major elements, have quite similar REE distribution patterns, and these intrusions have also similar REE patterns to those of ores (Fig. 6-1). But the REE pattern of ores differs to the host rocks in which these deposit is located (Fig.6-2)

Obviously, gold mineralization developed in the Wulong gold camp is unlikely to be metamorphic genesis due to the large time gap between metamorphism event (1150Ma) and the gold mineralization event (about 120Ma), and the geochemical differences between gold deposit and the host rocks (i.e. the different REE between ore and host rocks).

In recent years, a new group of gold deposit-intrusion related gold deposit, has been suggested to compromise a distinct class of magmatic-hydrothermal system (Lang and Baker 2001). Recent research results (Lang et al, 1997, Thompson et al., 1999, Goldfarb et al., 2000, Lang et al., 2000, Newberry 2000) indicate that this group of gold deposit collectively share several features common to most intrusion-related gold deposit and provinces, one of the distinct feature is that gold grade is proportional to Bi, As contents. In addition, this group of gold deposit is featured by low sulfide mineral

contents (mostly <5%) with a reduced ore mineral assemblage that typically comprises arsenopyrite, pyrrhotite, and pyrite, enrich of CO_2 phase in fluid inclusions and typical tectonic settings, which is closely related to convergent plate boundaries, where continental magmatism commonly contains coeval intrusions.

Clearly, isotope signatures extracted from fluid inclusions in the Wulong gold camp didn't disclose convincible information regarding the source of ore-bearing fluids and ore materials. However, mineralogical assemblage feature, types of fluid inclusion, REE pattern and the intimate relation of Bi and Au contents between the Sanguliu intrusion and the gold lodes all together strongly suggest that the Wulong gold camp is likely an type of intrusion-related gold deposit. Most of the geological features we obtained through this study indicate that the Wulong gold camp is much similar to this newly classified gold mineralization type worldwide. We propose that ore genesis of the Wulong gold camp is magmatic genesis, and the gold mineralization is closely related to the convergent belt between the North Pacific plate and the Korea-China plate, which was formed during the Yanshanian orogeny period (Mesozoic age).

As a conclusion of this chapter, we would like to make a summary regarding the genetic relationships among the Wulong shear zone, magmatism and gold mineralization. As a branch of the continental Tancheng-Lujiang deep fault, the Wulong shear zone was probably formed during the Yanshanian movement (Mesozoic age). As the result of plate convergent between the Pacific Ocean plate and the Korea-Sino plate, the Wulong shear zone is a preferential structural belt for the emplacement of magma formed within the subduction zone of the two tectonic plates. Extracted during the

subduction processes, ore materials and fluids were transported upwards accompanying the magma emplacement. Hydrothermal fluids formed in the magamtic system extracted ore-bearing materials. Driven by the magmatic hydrothermal system and differential structural pressures, ore-bearing fluids migrated within the Wulong shear zone and mineral deposition was taken place at favorable structural spaces. Multiple stage activities of the Wulong shear zone contributed the multiple magmatism emplacements of the abundant magmatic dykes and the multiple-stage gold mineralization in the Wulong gold camp. Due to the spatial migrating distance from the Sanguliu intrusion, deposition of ore-bearing materials varies at different structural localities in the shear zone. the closer to the Sanguliu intrusion, the stronger the gold mineralization and more pyrrhotite and arsenopyrite assemblages in ore minerals. This is probably the reason that the Wulong gold deposit and the Sidaogou gold deposit are much larger than the Jielishu deposit in scale and the formal two contain more high temperature mineral assemblages than the latter one since the former two deposits are quite close to the Sanguliu intrusion. Actually, part of the Wulong gold deposit developed within the Sanguliu intrusion, while the Jielishu deposit is 10km away from the Sanguliu intrusion. The spatial distance relative to the Sanguliu intrusion can probably be used to explain the scale variation of gold mineralization among the three gold deposits. Though the three gold deposits are laterally separated in a distance of about 20km, they are probably share the same shear system in the deep, geophysical information disclosed this induction according to Ru (1993). The gold mineralization, magmatism developed in the Wulong shear zone can be conceptually described as Figure 6-5.

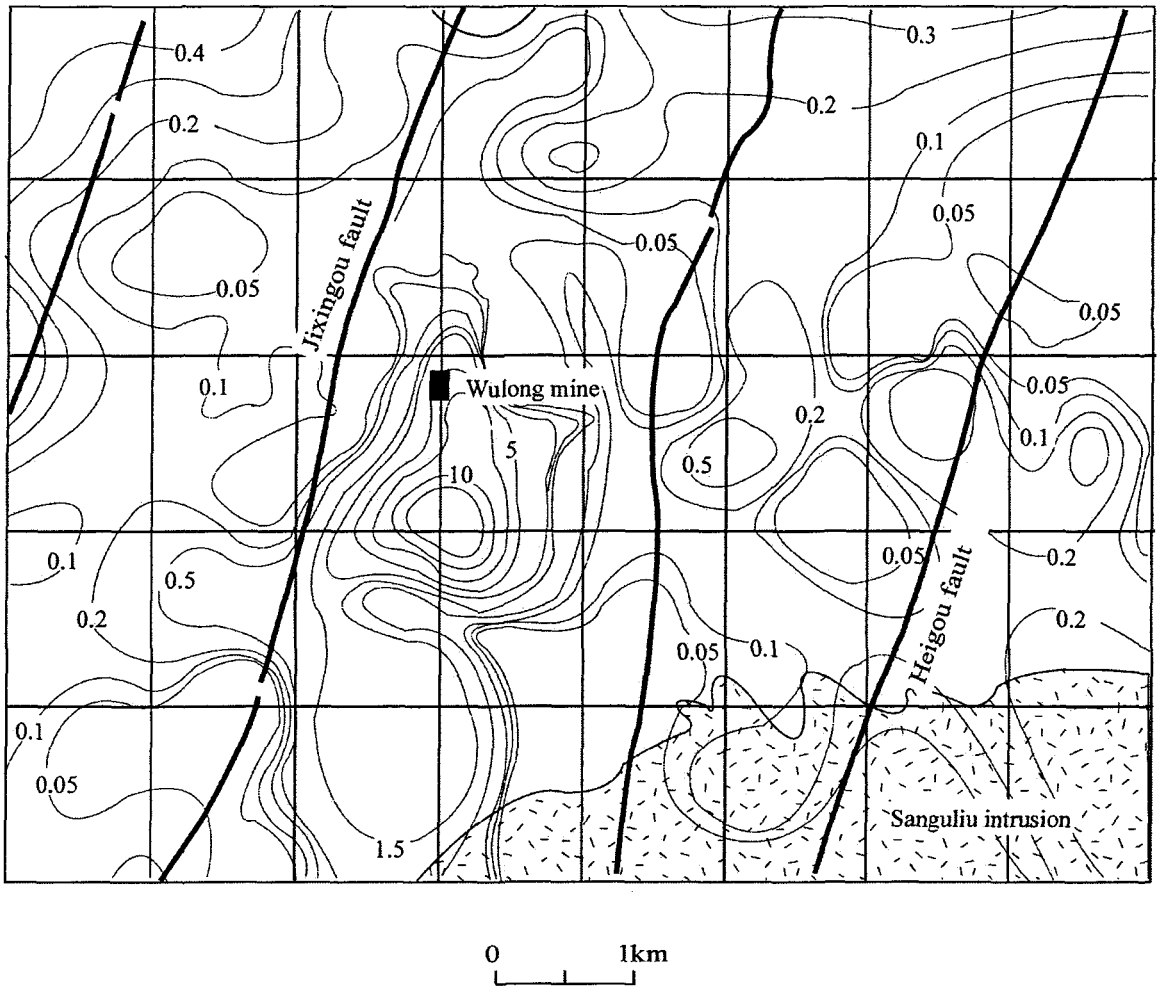

Figure 6-1 Spatial relations of Au concentration contours and the Wulong shear zone in the Wulong gold mine area. (the contours are in ppb unit)

Figure 6-2 Profile demonstrates spatial relations among intrusive dykes, shear zone and gold lodes

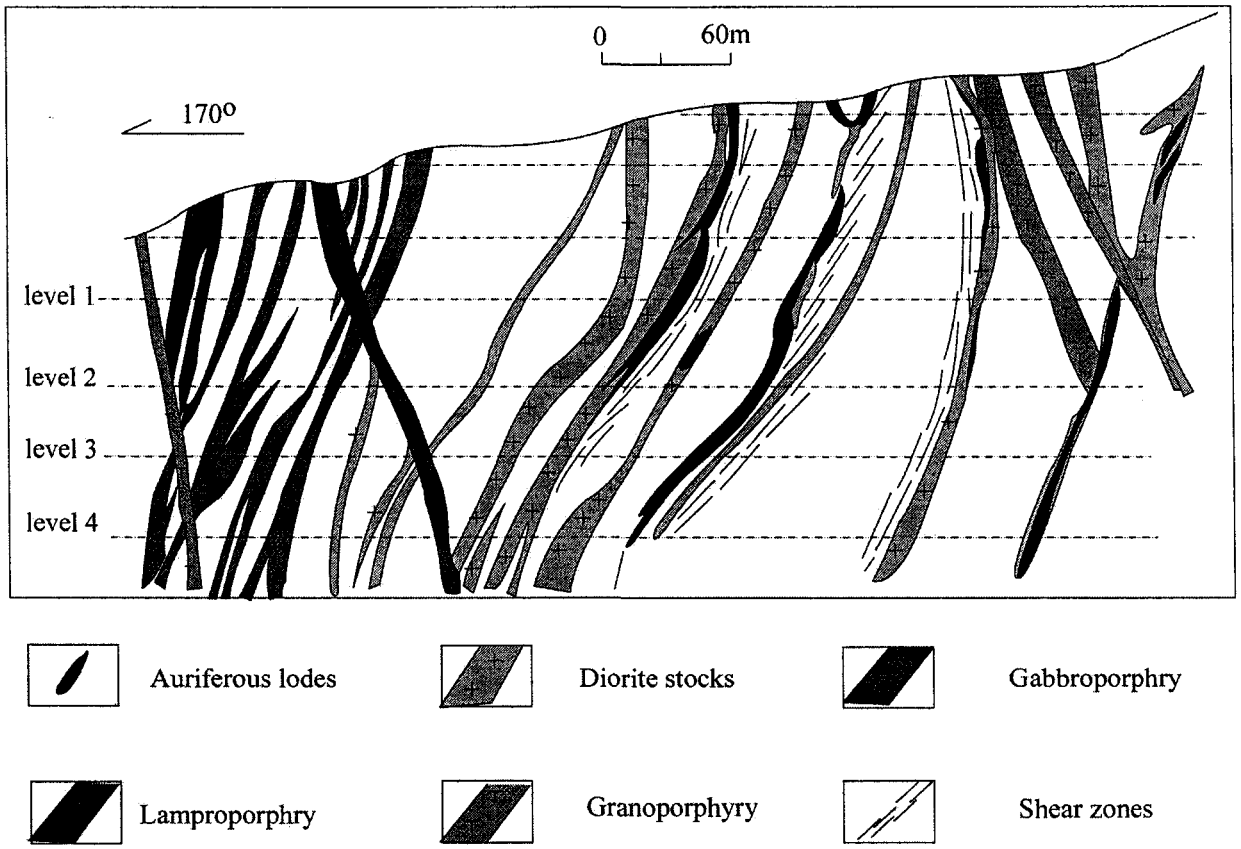

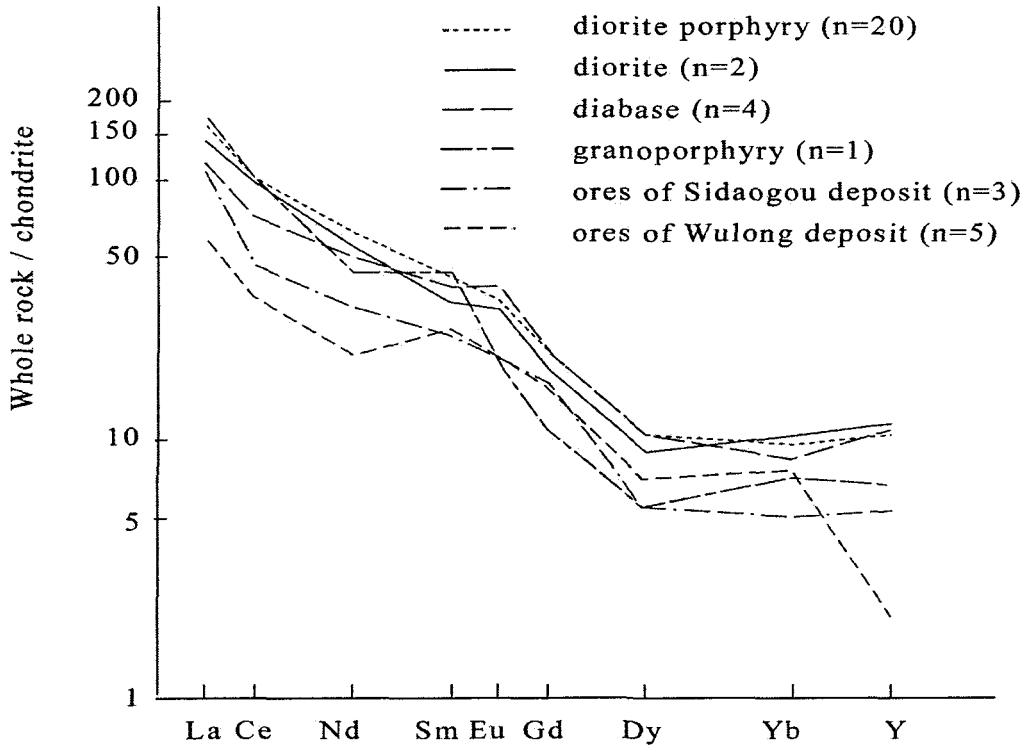

Figure 6-3 : REE patterns of various dykes and ores from the Wulong gold Camp

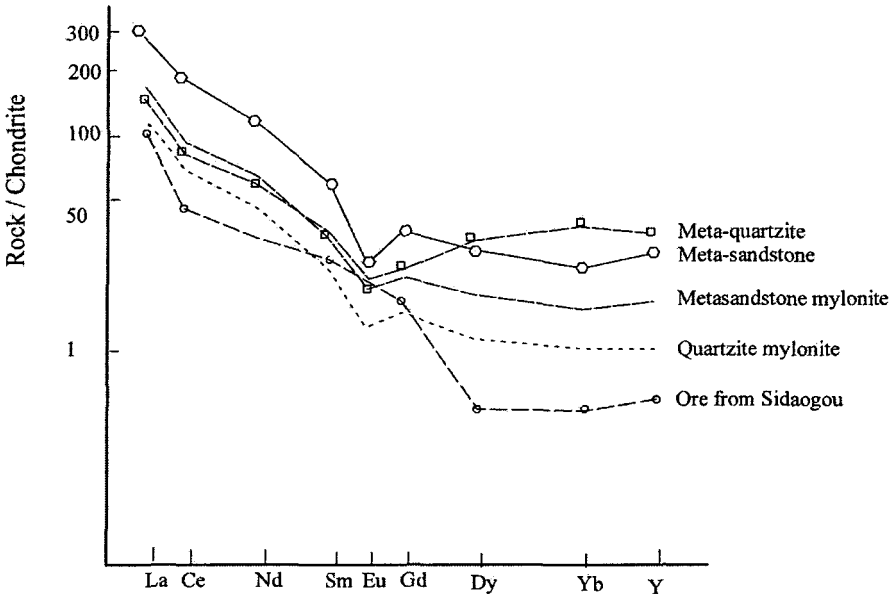

Figure 6-4 Chondrite normalized REE patterns of host rocks and the gold ores from the Sidaogou gold deposit, Wulong gold camp, Liaoning province

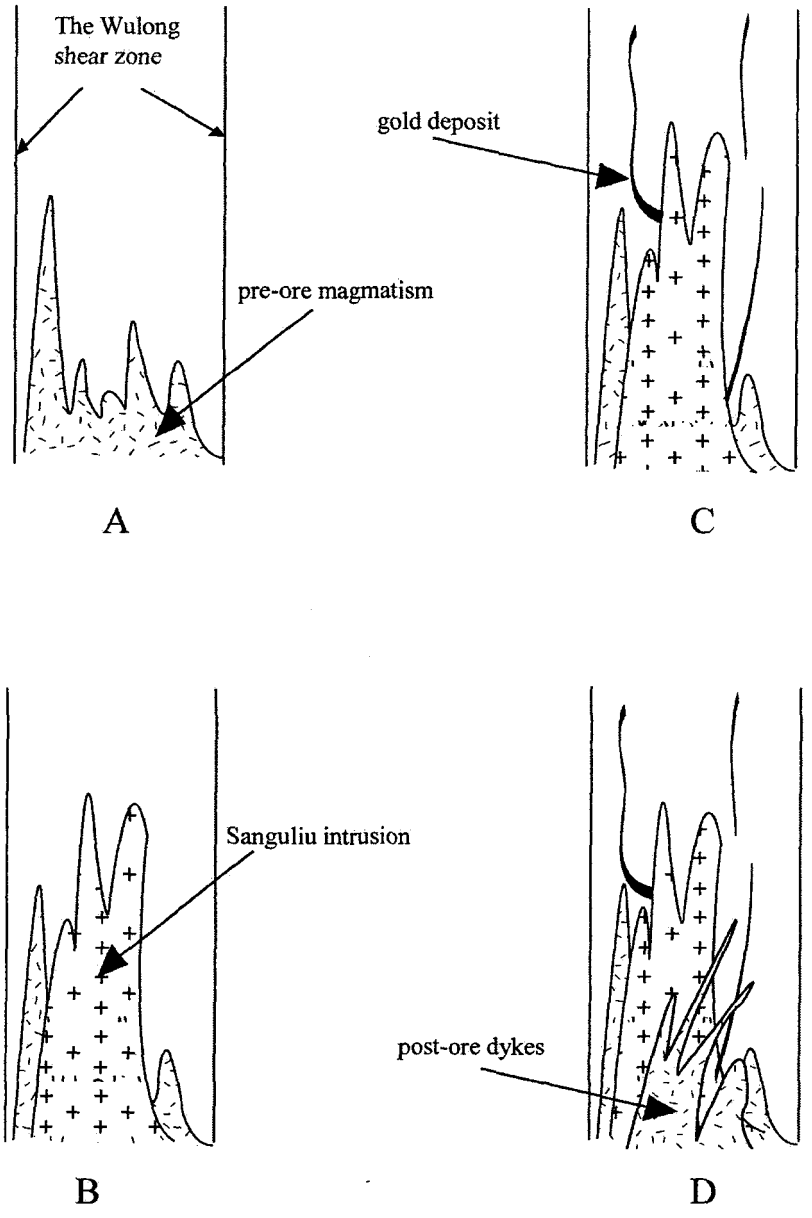

Figure 6-5 An conceptual genetic model of magmatism and gold mineralization in the Wulong gold camp

A : at the initial stage, formation of the Wulong shear zone introduced the emplacement of the early (pre-ore) stage magmatic intrusion;
B : at the peak of the Wulong shear, the Sanguliu intrusion was intruduced;
C : gold mineralization followed the Sanguliu intrusion;
D : post-ore dykes displacedthe early formed gold lode and intrusions.

Table 6-1 Contents of major elements of representaive dykes in the wulong gold camp (unit; %)

Intrusion (dyke)	SiO2	TiO2	Al2O3	Fe2O3	MnO	CaO	MgO	K2O	Na2O	P2O5
Wulongbei instrusion	70.69	0.24	14.86	1.29	0.06	1.21	0.72	4.35	3.28	0.08
Quartz porphyry (dyke)	71.38	0.24	14.88	1.21	0.05	0.76	0.64	4.22	4.00	0.08
Sanguliu intrusion	69.74	0.35	15.05	0.40	0.045	2.41	1.27	4.49	3.47	0.087
Sanguliu intrusion	66.62	0.49	15.15	1.08	0.078	3.21	2.09	4.02	3.39	0.122
Granodioritic porphyry (dyke)	67.32	0.33	14.77	0.49	0.045	1.94	1.59	3.68	3.35	0.087
Quartz diorite(dyke)	65.45	0.49	15.77	0.79	0.045	3.06	1.84	4.19	3.90	0.19
Diorite (dyke)	64.28	0.50	14.50	0.70	0.083	3.32	3.44	3.54	3.96	0.15
Diorite (dyke)	64.84	0.50	14.62	0.95	0.068	3.73	3.65	3.65	4.00	0.11
lamprophyry	52.08	0.73	16.66	0.53	0.09	4.90	4.57	3.86	3.18	-
Fine grained diorite (dyke)	55.64	0.83	15.33	0.24	0.09	5.31	4.86	2.57	3.00	-
Diabase (dyke)	44.76	2.15	14.53	1.47	0.14	6.70	5.67	2.50	2.59	-

Table 6-2: Contents of trace elemens of representai ve magmatic rocks and ores in the wulong gold camp (unit : ppm)

Name of Intrusion or dykes	Cu	Pb	Zn	Rb	Sr	Ba	Li	Zr	Co	Ni
Wulongbei intrusion	12.76	23.66	56.09	142.55	234.13	641.95	9.75	14.91	3.74	5.21
Quartz porphyry (dyke)	9.97	13.65	43.56	109.70	316.40	923.00	14.74	71.84	2.73	4.00
Sanguliu intrusion	9.84	28.29	59.55	159.80	310.70	786.10	18.21	19.00	5.90	9.04
Sanguliu intrusion	13.26	21.22	59.94	151.40	332.90	837.50	18.02	9.08	8.34	13.93
Granodiorite porphyry	25.14	18.77	71.17	126.20	335.20	712.50	12.93	21.95	7.04	19.76
Quartz diorite dyke	11.91	21.57	78.78	114.20	468.47	821.52	13.80	49.93	9.58	15.63
Diorite porphyry	34.88	22.65	89.35	90.00	507.40	707.50	15.11	80.29	14.13	58.14
Diabase dyke	49.42	<13	132.40	38.30	68.77	586.0	9.22	240.90	33.24	82.93
Fine-grained diorite dyke	73.86	<13	61.6	291.40	374.30	637.60	25.99	47.80	18.74	47.98
Ore lode	122.65	1495.00	2801.70	5.35	14.49	5.34	1.55	<1.00	28.70	7.48

(Data are cited from Qui et al., 1988)

Table 6-3 Contents of gold, silver and bismuth in various ore types in the Wulong gold camp (unites : ppm)

Localities	Mineral assemblages Or ore types	Au	Ag	Bi	source
#10 vein (Wulong)	Bis. Bi., Py., Po	134.5	6.0	520.51	1
#2 vein(Wulong)	Py. Po.	0.75	3.0	0.312	1
# 8-2 vein (Wulong)	Po. Py.	90.0	31.0	326.64	1
#76 vein (Wulong)	Po. Cpy. Bis.	90.0	12.0	275.78	1
Pre-ore quart (Wulong)	Py.	0.55	3.0	0.300	1
#32-1(Wulong)	Po. Py. Bis.	143.5	13.0	630.45	1
#32-1(Wulong)	Py. Po.	25.5	38.0	44.25	1
S-1 (Sidaogou)	Massive	10.73	0.19	290.81	2
#4 level (Sidaogou)	Massive	25.79	0.527	652.18	2
#4-5(Sidaogou)	Stockwork	547.08	3.45	1670.21	2
#7-1(Sidaogou)	Massive	138.43	0.33	591.89	3

Abbreviations : Bis : Bismuthinite, Bi. Bismuthinite; Py : pyrite; Po : Pyrrhotite;
Cpy : Chalcopyrite;
1. Zhao et al., 1993; 2. Ma et al., 1994; 3. Zhen et al., 1993.

Table 6-4 Concentrations of Au, Ag, Cu, Bi and As in typical rocks type in the Wulong gold camp (unites: ppm)

Rock type	Au	Ag	Cu	Bi	As
Gneiss	0.022	0.38	40.5	0.33	2.65
Sanguliu intrusion	0.036	0.507	68.91	9.47	41.51
Intermediate-acid dyke	0.039	0.14	65.12	2.50	12.41
Poet-ore basic dyke	0.024	0.016	20.2	0.10	9.68
Early stage auriferous lode	0.53	0.17	71.58	24.91	28.8
Major auriferous lode	5.38	0.51	200.25	142.51	3.32

(data cited from Li G.Z. 1993)

Chapter VII

Conclusions

From the studies and discussions on the Wulong shear zone and the Wulong gold camp in the previous chapters, the following conclusions can be outlined for this project.

1. The Wulong gold Camp is structurally confined by the Wulong shear zone, which is a branch of the continental Tancheng-Lujiang deep fault zone along eastern China. Results of this study indicate that the Wulong shear zone was probably initiated (at least it was active) at Mesozoic period with K-Ar dating ages range from 73 Ma to 165 Ma. Macroscopic and microscale structural measurements suggest that the Wulong shear zone strikes N 41-47 E and dips to NW at an average angle of 55°, the movement of the shear zone shows sinistral shear and the azimuths of the principal regional strain axis are: X : 45/139, Z: 48/310, Sxy : 52/130, based on the strain measurements from the Wulong area.

2. Paleopiezometer calculation results indicate that strain states within the Wulong shear zone is quite variable. These variations of paleopiezometer may suggest the different structural levels on the shear zone section of the three studied areas or the different litho-strain capacity of the different lithological rocks involved in the shear zone. Considering lithological position of the three study areas on the lithological section as shown in Table 2-1, and the facts that the lithological rocks are different in the three areas (marble is the dominant rock type in the Jielishu, while granitic gneiss is

the major rock type involved in the shear zone in the Wulong mine area), the paleopiezometer values may indicate a mixing signature of the two different situations in this area.

3. Field observations and structure studies of the Wulong shear zone, ore lodes and various magmatic intrusions indicate that the Wulong shear zone controls the spatial distribution of ore lodes and intrusions. Fossils and isotope geochronological evidences indicate that the Wulong shear zone was formed at about middle Mesozoic. This period is in agreement with the subduction age of the Pacific Ocean Plate down the Sino-Korean Plate. The Wulong shear zone was initially formed at about 165 Ma. Shear activity contributed to multiple-stage fluid migration and magma intrusions. At its second stage activity, various intrusions and gold mineralization were emplaced in the Wulong gold camp, this stage was the strongest structural event of the shear zone. The evolution of the Wulong shear zone can be summarized in the following lines:

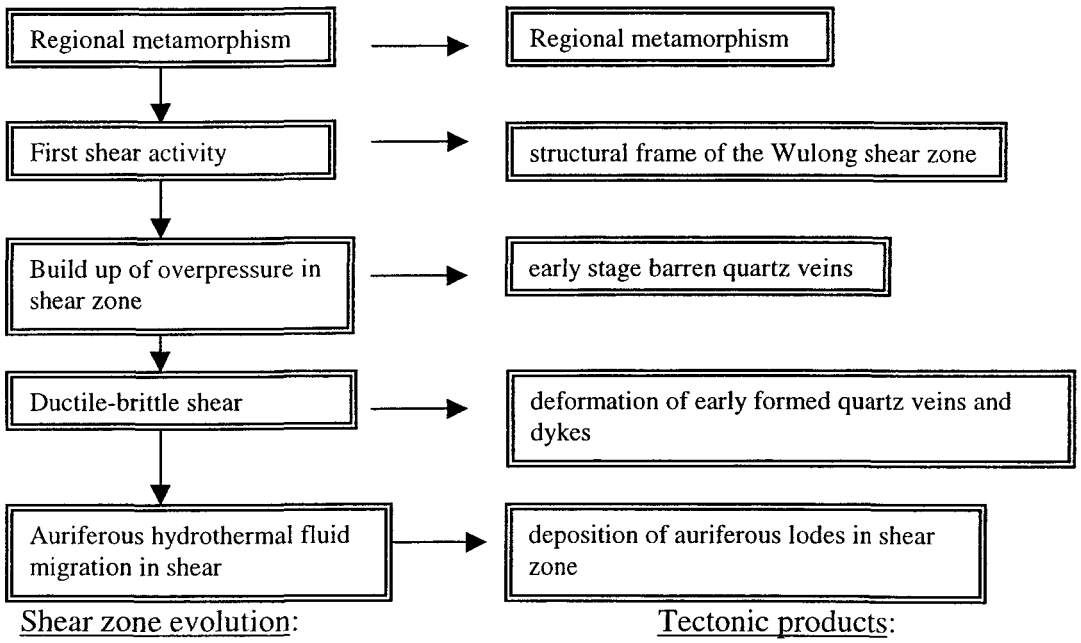

4. Petrological, geochemical and mineralogical studies of the three deposits suggest that the Wulong gold camp is likely magmatic genesis. Though have similar mineralization ages, the Wulong gold deposit and the Sidaogou gold deposit experienced more complex hydrothermal fluid processes and have more complex mineral assemblages as well as mineralization generations than the Jielishu deposit. The reason that mineralogical, geochemical variations among the three deposits may be related with the spatial relations of the three deposits respecting the Sanguliu intrusion, which is proposed providing the ore materials and hydrothermal fluids for these deposits. The closer the deposit to the Sanguliu intrusion, the more complex the mineralogical and geochemical features of the deposit are. This proposal is valid if we check the relative spatial distances of the three gold deposits to the Sanguliu intrusion.

Reference :

Akella, J., 1966. Calculation of material transport in some metasomatic processes : Nues jahrb. Mineralgie Abh., Vol. 104, p316-329.

Appleyard, E.C., 1980. Mass balance computation in metasomatism. Metagabbro / nepheline syenite pegmatite interaction in northern Norway. Contri. Mineralogy Petrology, vol. 73, p131-144.

Boyle, R.W., 1984. Gold, Geochemistry and gold deposit. John Wiley and Sons.

Brown., 1980. The special issue of the Journal of Structural Geology. Vol. 2, No. 1, 2.

Burlinson 1991. Decripitation in gold exploration, A case history from the Cotan prospect, N.T.: J. Geochem. Explor., 42, 143—156.

Bursnall, J.T., 1989. Introduction :Review of mechanical principles, deformation mechanisms and shear zone rocks. *In* mineralization and shear zone. ed. by Bursnall J.T. Geological Association of Canada, short course notes. Vol. 6.

Chen, X.J., 1996. Advance of gold Iodes in metamorphosed terraine. Geo. Sci. Tech. Inf., In Chinese. Vol. 15, No.2, p71-76.

Cheng jirong, Wang yuhua, Gao jianfeng, Fang congyi, 1995, The features of stable isotopes for various types of gold deposits in Liaodong Pennisula. Gold Geology, in Chinese, Vol. 1, No.4. P43-49.

Cheng, J., and Wang, H. N., 1993. Contents and distribution characteristics of REE and trace elements in the fold-bearing Hetai shear zone. Guangdong Mineral Deposit. In Chinese. Vol. 12, No. 3, p

Collins P.L.F., 1979, Gas hydrates in CO2-bearing fluid inclusions and the use of freezing data for estimation of salinity, Econ. Geol., vol.74, p1435-1444.

ConGillen, 1985. Metamorphic geology. An introduction to tectonic and metamorphic processes. George Allen & Unwin Austra. Ltd.

Cox, S.F., Sun, S.S., Etheridge M.A., Wall V.J., and Potter, T.F., 1995. Structural and geochemical controls on the development of turbidite-hosted gold-quartz vein deposits, Wattle gully Mine, Central Victoria, Australia, Econ. Geol. 90, p1722-1746.

Cui, K.Y., Peng, Y.D., Xu, Y.K., 1995. Structural control of the Liaoning shear zone on gold mineralization . Scientific Research Report. In Chinese. Shenyang Institute of Geology.

Curti, E., 1987. Lead and oxygen isotope evidence for the origin of the Monte Rusa gold Iode deposits (Western Alps. Haly) : a comparasion with Archean Iode deposits. Eco. Geol. Vol. 87.

Doe, R.R., and Zartman R.E., 1979. Geochemistry of hydrothermal ore deposits, 1st edition. John Wiley and Sons. P22-26.

Dunnet, D., 1969. A technique of finite-strain analysis using elliptical particles. Tectonophysics. Vol. 7, p2357-2388.

Etheridge, M.A., and Wikie, J. C., 1981.An assessment of dynamically recrystallized grain size as a palepiezometer in quartz-bearing mylonite zones. Tectonophysics, 78, p475-508.

Ferry, J., 1989. Fluid flow, mineral reactions, and metasomatism : a general model. Geol. Soc. Am. Abstr. Program. 21.

Fisher, D., 1987. Structural evolution of underthrusted sediments. Tectonics. 6, p775-793.

Fisher, D., and Byrne, T., 1990. The character and distribution of mineralized fractures in the Kodiak Formation, Alaska : impications for fluid flow in an underthrust sequence, J. Geophys. Res., 95. P9069-9080.

Fisher, D.M., and Susan, L.B., 1992. Models of quartz overgrowth and vein fromation :deformation and episodic fluid flow in an ancient subduction zone. J. Geophy. Res. Vol. 97, No. B13, p20043-20061.

Flinn, D., 1962. On folding during three-dimensional progressive deformation. J. Geol. Soc. London. 118, p385-433.

Fry, N., 1979. Random point distribution and strain measurements in rocks. Tectonophysics. Vol. 60, p

Gary, M., McAfee, R., Jr., and Wolf, C. L., eds., 1974. Glossary of geology : Washington, D.C., Am. Geol. Inst., p860.

Goldfarb R, Hart C., Miller M., Miller L.,Farmer GL., Groves D. 2000, The Tinting gold belt-a global perspective, In: Tucker TL., Smith MT (eds) The Tintina gold belt: concepts, exploration and discoveries, British Columbia and Yukon Chamber of Mines Special Volume 2, pp5-34.

Goldfarb, R., Leach, D.L., Miller, M.L., and Pickthern, W.J., 1986. Turbidite-hosted Iode-gold mineralization within the cretaceous Valdez group south-central Alaska, in

Keppie, J.D., Boyle, R.W., and Haynes, S.J., eds. Geological Association of Canada. Special paper 32, p87-105.

Grant, J.A., 1986. The isocon diagram- a simple solution to Gresens' equation for metasomatic alteration. Econ. Geol. Vol. 81, p1976-1982.

Gresens, R.L., 1967. Composition-volume relationships of metasomatism :Chem. Geology. Vol. 2, p47-55.

Groves, 1993. The crustal continuum model for late-Archean Iode-gold deposits of the Yilgarn Block, western Australia. Mineralium Deposita, 8, p366-374.

Gunning, H.C., and Ambrose, J.W., 1937. Cadillac-Malartic area, Quebec : Canadian Institute of Mining and Metallurgy Transactions. Vol. 40, p341-362.

Holland P.T., Beaty, D.W., and Snow, G.W., 1988, Comparative elemental and oxygen isotope geochemistry of Jasperoid in gold-producing hydrothermal systems, Econ. Geol. Vol.83, p1401-1423.

Hu, S.Y., 1984. The interier texture of the Tan-Lu fault belt, J. Struc. Geol. In Chinese. Vol. 3, p23-32.

Jesen, L.N., 1984. Quartz microfabric of the Laxfordian Canisp shear zone, NW Scotland. J. Struc. Geol.. vol. 6, No. 3, p293-302.

Keays P. R., 1984, Archean gold deposit and their source rocks; the upper mantle connection, Gold'82, A. A. balkema, Rotterdam, p17-51.

Kerrich R . W. 1989. Geodynamic setting and hydraulic regimes: Shear zone hosted Mesothermal gold deposits. *In* : Mineralization and shear zone, Geol. Assoc. Canada, Short course notes, Vol. 6, May 12- 14.

Kerrich, R., and Derek Wyman, 1990. Geodynamic setting of mesothermal gold deposits :an association with accretionary tectonic regimes, Geology, vol. 18, p882-885.

Kohler, A., and Raaz, F., 1951. Uber eine neue Berchnung und graphsche Darstellung von Gesteinscanalyzen. Neu. Jb mineral Mh. Stuttgart. P247-263.

Kumarapeli, S., Huoge, D., Wang, H., and Qi, Q., 1990. Tan-Lu fracture zone east China-An element of an ancient transform belt?in Wiley, T.J., Howell, D.G., and Wang. F.L., eds. Terrane analysis of China and the Pacific rim : circum-Pacific Council for energy and mineral Resources, Earth Science Series, Houston, Texas. Vol. 13, p355-357.

Kuno, H., 1968. Diferentiation of basaltic magmas, in Hess, H. H., and A. Poldervarrt eds. Basalts, vol. 2, New York, p623-688.

Lang JR., Baker T., Hart CJR, and Mortenson JK., 2000, An exploration model for intrusion-related gold systems, Soc. Econ. Geol. News 40(1) : 7-15.

Lang JR., Thompson JFII, Baker T., and Mortenson JK., 1997, Intrusion-related Au mineralization associated with lithophile elements : an under-recognized metallogenic association. Geol. Soc. Am. Prog. Abstr 29 :358.

Li Z.L., Xu W.X, Qing M.Q., Pang W.Z., 1987. Discussion on the genetic mechanism and the geological characteristics of Wulong gold deposit, Liaoning province. *in Chinese* . Weekly Report on Advance in Metallic Geology. Vol. 10, p120-126.

Li, Z.L., 1987. Geological characteristics and genesis of the Wulong gold deposit, Liaoning province, J. Geology and Exploration. In Chinese. Vol. 3, p78-85.

Lister, G.S., 1984. S-C mylonites. J. Struc. Geol. Vol. 6, p716-639.

Lister, G.S., and Snoke A., 1984. S-C mylonites. J. Struc. Geol. Vol. 9, p819-833.

Lister, G.S., and Williams, P.F., 1979. Fabric devevopment in shear zones, theoretical controls and observed phenomena. J. Struct. Geol. 1, p283-297.

Liu G. Z., 1993, Geological characteristics and ore genesis of the Wulong gold deposit, Liaoning province, Liaoning Geology, Vol. 9, No. 22, P134-141.

Liu L.D., Li, Y., and Li, D., 1991. China gold deposit and shear zone. Theory of Metallogeny, in Chinese, No.3, p23-34.

Liu, J.B., You, Z.D., Zhong, Z.Q., Li, N.R., 1993. Mass-balance analysis of mylonites in ductile shear zone-examples from the Shewei shear zone in Qinling, Western Henan province. J. China. Uni. Geosci. Vol. 18, No. 6, p757-764.

Liu, Y.Q.,1982. Structural analysis of the Archean group, NE Liaoning province, China. Proceedings of international pre-cambrian crust evolution.

Lu H. Z., G. Archambault, Y. Li,J. Wei, and N. Chen, 1999, The relation between deformation types and gold mineralization in the Linglong-Jiaojia district, Shandong province, China.

Lu, H.Z., Li, B., Shen, K, Zhao, X., Yu, T., and Wei, J., 1990. Fluid inclusion geochemistry. Geological publishing House. Beijing.

Ma M. T., Zhen T., Shi. C., Yang H.Y., 1994, Geochemical characteristics of the Sidaogou gold deposit, Liaoning province, Liaoning Geology, No. 4, p325-333.,

McKinstry, H.E., 1948. Mining Geology : Prentice-Hall Inc., New York. 680p.

Mercier, J.C., Anderson, D.A., and Corter N.l., 1977. Stress in the lithosphere : inference from steady state flow of rocks. Pure Appli. Geophysics. 115, p210-225.

Miller L.D., Goldfarb R.J., Nie F. J., Hart C. Miller M., Yang Y., Liu Y., 1998. North China gold, a product of multiple orogens, SEG Newsletter. No.33.

Miyashiro, A., 1973. Metamohphism and metamorphic belt. London George Allen & Win.

Morton, R.L., and Nebel, M. L., 1984. Hydrothermal alteration of felsic volcanic rocks at the Helen sederite deposit, Wawa, Ontario. Econ, Geol. Vol.79, p1319-1333.

Mueller, J. Fred., Roger, J.J., Jin, Y., Wang, H., Li, W., Chronic, J., and Mueller Joseph F.,1991. Late carboniferous to permian sedimentation in inner Mongolia, China, and tectonic relationships between North China and Siberia. J. of Geology. Vol.99, p251-263.

Newberry RJ 2000, Mineral deposits and associated Mesozoic and Tertiary igneous rocks within the Interior Alaska and adjacent Yukon portions of the « tintina gold belt », a progress report in : Tucker TL., Smith MT (eds) The Tintina gold belt: concepts, exploration and discoveries, British Columbia and Yukon Chamber of Mines Special Volume 2, pp59-88.

Ni P. and Xu K.Q., 1993 Geological evolution of Liaodong , Liaoning peninsula and genesis of gold deposits . in Chinese, Vol.12, No.3, P231-243.

Nie, F.J., 1997a. Type and distribution of gold deposits along the northern margin of the north China Craton, P.R.C. International Geology Review. Vol. 39, p151-180.

Nie, F.J., 1997b. An overview of gold resources in China. International Geology Review. Vol.39, p55-81.

Niggli, Paul, 1953. Rocks and mineral deposits. English transl. by Robert L. Parker, San Francisco, Freeman.

O'Neil, J. R.,Clayton, R.N. and Mayeda, T.K., 1969. Oxygen isotope fractionation in divalent metal carbonates. J. Chem Phys. 51, p5547-5558.

Ohmoto, H., and M.B. Goldhaber. 1997. Sulfur and carbon isotopes. In : Geochemistry of hydrothermal ore deposits. 3rd ed. Ed. by H. L. Barnes. John Wiley. 552p.

Ohmoto, H., and Rye, D.R., 1979. Isotope of sulfur and cargon. In : Geochemistry of hydrothermal ore deposit. 2nd edition. H. I. Barnes(ed.) New York :Wiley p509-567.

Olsen, S. N., 1985. Mass balance in migmatites, in Ashworth, J.R., ed., Migmatite : Glasgow, Blackie and Son, p145-179.

Opletal, M., 1971. A modified calculation and new graphycal representation of rock analysis. Acta. Uni. Carl. Hejtman. Vol. 1,2 praha p109-122.

Ord, A., and J.M., Christie, 1984. Flow stress in mylonite quarzites of Moine thrust zone. J. Struc. Geol., vol. 6, No. 6, p639-654.

Peltola, E., 1960. On the black schist in the Outokumpu region in eastern Finland. Bull. Comm. Géol. Finl. 192, Helsinki, p1-107.

Peng J.Q. C.Qi, S.Wen and R. Han, 1988, Genetic relationship between granites and gold mineralization and structural control of regional tectonics on gold mineralization. *In* Contributions to the project of regional metallogenetic conditions of main gold deposit types in China, IV Southern Liaoning Province. Ed., the Shengyang Institute of Geology and Mineral Resources.

Peng, J. Q., Qi, S., Luo, S.W., and Han, Y.C., 1988. Controlling of magmatic rocks and regional structures on gold deposits in Southern Liaoning province, in contributions to the project of regional metallogenetic conditions of main gold deposit types in China. IV Southern Liaoning province. Geological Publishing Inc.

Peng, Y.D., 1993. Genesis of the Wulong gold deposit. J. Precious Metallic Geol. In Chinese. Vol. 3, No. 1, p21-28.

Poirier, J.P., and Guillopé, M., 1978. Deformation induce recrystallization of minerals. Bull. Soc. Fr. Minér. Cristallogr. 102, p67-74.

Poirier, J.P., and Nicholas, A., 1975. Deformation induced recrystallization clue to progressive misorientation of subgrains, with special reference to mantle peridotites. J. Geol. 83, P707-720.

Ramsay 1980. Shear zone geometry : a review. J. Struc. Geol. Vol. 2, p83-99.

Ramsay, J.G., and Huber, M.I., 1987. The techniques of modern structural geology. Vol. II, Folds and Fracture. Academic Press. Orlando.

Ramsay. J.T., 1967. Folding and fracturing of rocks : McGraw-Hill. P568.

Rittmann, A., 1957. On the serial character of igneous rocks. Egyptian. J. Geol. 1, p23-48.

Robert, F., and Kelly W.C., 1987, Ore-forming fluids in Archean gold-bearing quartz veins at the Sigma mine, Abitibi greenstone belt, Quebec, canada, Eco. Geol. Vol.82, p1464-1482.

Roberts, R.G., 1987. Ore deposits model, #11, Archean Iode gold deposits. Geoscience Canada, Vol. 76, p37-52.

Robin, P.Y., 1977. Determination of geological strain using strain markers of any shape. Teconophysics. Vol. 42, p1256-1277.

Rock , N .M .S .and Groves, D. J. 1988. Can lamprophyres resolve the genetic controversy over mesothermal gold deposits?, Geology, Vol. 16, P.538—541.

Roedder, E., 1984. Fluid inclusions reviews in mineralogy. Vol.12. Holland.

Ru, Y.F., 1993. Relationship between granitic intrusion and gold Iodes. Examples from the Sanguliu intrusion, Dandong city, Liaoning province. Liaoning Geology. In Chinese. Vol. 2, p120-127.

Shepherd, T.J., Rankin, A.H., and Alderton, D. H.M., 1985. A practical guide to fluid inclusion studies. Blackie & Son Ltd.

Shiro, Y. & Sakai, H., 1972. Calculation of the reduced partition function ratios of alpha-beta quartz and calcite. Japan Chemical Society. Bulletin, 45, p2355-2359.

Sibson, R.H., Roert, F., and Poulsen, H., 1988. High angle faults fluid pressure cycling and mesothermal gold-quartz deposits : Geology. Vol.16, p551-555.

Simonen, A., 1953. Straigraphy and sedimentation of the Svecofennidic early Archean supracrustal rocks in southwestern Finland. Bull. Comm. Geol. Finl. 160. P1-64.

Simpson, C., and Schmidt, S.M., 1983. Microstructural indicators of sense of shear in shear zones. Bull. Geol. Soc. Am. 94, p1281-1288.

Spooner, E.T.C., Bray, C.J., Wood, P.C., Burrows, D.R., and Callan, N. N. J., 1987. Au-quartz vein and Cu-Au-Ag-Mo-anhudrite mineralization, Hollinger-McIntype Mines, Timmis, Ontario : δ13C values (McIntype) fluid inclusion gas chemistry, pressure (depth) estimation, and H2O-CO2 phase separation as a precipitation and dilation mechanism. Ontario Geological Survey Miscellaneous paper. Vol. 136, p 35-56.

Suk, Milos, 1983. Petrology of Metamorphic rocks. Elsevier Scientific publishing company.

Thompson JFII, Sillitoe RH, Baker T., Lang JR., and Mortenson JK., 1999, Intrusion-related gold deposits associated with tungsten-tin provinces, Miner. Deposita, 34 : 34 : 323-334.

Tilling, R.I., Gottfried, D., Row, J.J., 1973. Gold abundance in igneous rocks bearing on gold mineralization. Econo. Geo. 68 (2).

Twiss, R. J., 1977. Theory and applicablility of a recrystallized grain-size paleopiezometer, Pure. Appl. Geophs. Vol. 115, p190-200.

Vrolijk, P.J., 1987. Tectonically-driven fluid flow in the Kodiak accretionary complex, Alaska. Geology 15, p466-469.

Wang Y.M., 1990, Geological features and ore-controlling regularities of dandong ductile shear zone. Msc thesis, Tianjin Geological Academy, MMI.

Wang Y.M., 1990. Geological features of the Dandong shear zone and its control on gold deposits in the Wulong area. Tianjin Institute of Geology, Msc Thesis, (unpublished).

Wang, L.G., Qin, Y.M., McNaughton, N.J., Groves, D.I., Luo, Z.K., Huang, J.Z., Miao, L.C., and Liu, Y.K., 1998. Constrains on crustal evolution and gold metallogeny in the Northwestern Jiaodong Peninsula, China, from SHRIMP U-Pb zircon studies of granitoids. Ore Geology Reviews. 13, p275-291.

Wang, Q. Y., 1996. Fossiles found in the Sidaogou area and their geological signifcance. J.Liaoning Geol. In Chinese. Vol.1, p1-15.

Wang, Y.M., Liu, Y.Q., Zhang, B.H., and Chu, F.X., 1989. Structural contol on Precambrian gold deposits in SE Liaoning province. Scientific Research Report (unpublished).

White, S., 1979. Grain size and subgrain size variation across a shear zone. Contrib. Mineral. Petrol. 70, p139-202.

White, S.H., Burrows, S.E., Carreras, J., Shaw, N.D., and Humpherys, F.J., 1980. On mylonite in ductile shear zone. J. Struc. Geol. Vol. 2, No. 1, 2, p175-187.

Witt, W.K., 1993. Lithological and structural controls on gold mineralizaiton in the Archean Mensies-Kambalda area, western Australia. Australian J. earth Sci. 40, p65-86.

Wood, D.S., 1973. Patterns and magnitudes of natural strain in rocks. Phil. Trans. R. Soc. Lond, A274, P373-382.

Wu C. Y., and Nie, F. J., 1995, Gold deposits related to alkaline igneous rocks in north China craton, P.R.C. *in* Pasava, J., Kribek, B., and Zak, K., eds., Proceedings of the third biennial SGA meeting, 28-31, Aug. 1995. Prague, Czech Repub., p173-176.

Xu J. W., Ru Y., and Wu M., 1989, Shear zone and gold mineralization in the Liaodong region, Liaoning province, Geology and Exploration, in Chinese, No. 4, Vol. 18.p34-43.

Xu, J., and Zhu, G., 1994. Tectonic models of the Tan-Lu fault zone, eastern Chian. International Geology Review. Vol, 36, p771-784.

Xu, J.W., Zhu, G., Tong, W.X., 1987. Formation and evolution of the Tancheng-lujiang wrench fault system : a major shear system to the northwest of the Pacific Ocean. Teconophsics, 134, p273-310.

Yang, Z. S., 1984. Multiple stage defromation in Archean greenstone belt, Hongtou Mountain region, North Liaoning,. J. Changchun College of Geology. Vol.1, p20-32.

Yao F.L., Zou Z.Y., Liu Y.L. Ren H.M., 1988. Evolution of the Mesozoic granites and their relationship to the genesis of gold deposits in South Liaoning province. *In* proceedings of the regional metallogeny environments of main gold mineralization types in China, No.4.

Yin, A., and Nie, S., 1993. An indentation model for the north and south China collision and the development of the Tan-Lu and Hunang fault systems. Eastern Asian : Tectonics. Vol. 12, No.4, p801-813.

Ypma P.J.M., 1963, Rejuvenation of ore deposits as exemplified by the Belledonne metalliferous province, Ph D. dissertation, Uni. Leiden, Leiden, The Netherlands.

Zhang, J. S., 1992. The characteristics of Tancheng-Lujiang ductile shear belt and its significance. Earth Science. J. China Uni. Geoscience. Vol. 17, No. 4, p363-372.

Zhao, Y.S., 1993. Characteristics of typical mineral of quartz and its relationship with gold mineralization in Wulong gold camp. Liaoning province. Liaoning Geology. In Chinese. No. 1, p38-43.

Zhen C.Ma., Yang H.Y., Shi C., 1993, Geological environments of gold mineralization of the Sidaogou gold deposit, Liaoning province, J. Shengyang institute of Gold technology, No.2, Vol.12, p52-68.